# EFFECTS OF MANUFACTURING CONDITIONS, STRESSES, TEMPERATURE AND HUMIDITY ON THE PERFORMANCE OF AN INNOVATIVE FRACTIONAL ORDER CONTROL DEVICE

by

Nachiket Ashok Kulkarni

A thesis submitted in partial fulfillment
of the requirements for the degree

of

Master of Science

in

Mechanical Engineering

MONTANA STATE UNIVERSITY
Bozeman, Montana

November 2005

©COPYRIGHT

by

Nachiket Ashok Kulkarni

2005

All Rights Reserved

APPROVAL
of a thesis submitted by

Nachiket Ashok Kulkarni

This thesis has been read by each member of the thesis committee and has been found to be satisfactory regarding content, English usage, format, citations, bibliographic style, and consistency, and is ready for submission to the College of Graduate Studies.

Dr. Aleksandra Vinogradov

Approved for the Department of Mechanical and Industrial Engineering

Dr. Chris Jenkins

Approved for the Division of Graduate Education

Dr. Joseph J Fedock

## STATEMENT OF PERMISSION TO USE

In presenting this thesis in partial fulfillment of the requirements for a master's degree at Montana State University – Bozeman, I agree that the library shall make it available to borrowers under rules of the Library.

If I have indicated my intention to copyright this thesis by including a copyright notice page, copying is allowable only for scholarly purposes, consistent with "fair use" as prescribed in the U.S. Copyright Law. Requests for permission for extended quotation from or reproduction of this thesis (paper) in whole or in parts may be granted only by the copyright holder.

Nachiket Ashok Kulkarni

November, 2005

# ACKNOWLEDGEMENTS

I would like to thank Dr. Aleksandra Vinogradov for her guidance in my research and thesis work. I would like to express my appreciation to Dr. Gary Bohannan and Dr. Alan George for their work as committee members.

I gratefully acknowledge Dr. Stephanie Hurst for mentoring me throughout this research and Mary Knighton for her staunch support. Without their help this work would not have been possible.

Finally, I would like to appreciate the continued support I received from the staff members of the Department of Mechanical and Industrial Engineering and the fellow graduate students.

TABLE OF CONTENTS

1. INTRODUCTION ..... 1
Fractional Order Calculus ..... 1
Impedance ..... 2
Warburg Impedance ..... 2
The Fractor ..... 6
Goals and Objectives ..... 8

2. INTRODUCTION TO CONTROL SYSTEM ..... 10
Basic Open Loop Control System ..... 10
Close Loop Control System ..... 11
Control Actions ..... 13
Proportional (P) Control Action ..... 13
Integral (I) Control Action ..... 14
Derivative (D) Control Action ..... 14
PID Control Action ..... 15
PID Control Responses ..... 16

3. ELECTROCHEMICAL IMPEDANCE ..... 18
Metal Gel Interface ..... 18
Fractal Surfaces ..... 22

4. POSSIBLE USES OF THE FRACTOR ..... 25

5. SAMPLE MANUFACTURING ..... 29
Abrasion and Sonication ..... 29
Ionic Gel Preparation ..... 30
Dipping and Drawing ..... 32
Encapsulation ..... 35
Experimental Parameters ..... 37
Nomenclature ..... 38

6. GENERAL PHASE - IMPEDANCE ANALYSIS OF VARIOUS FRACTORS ..... 39
Experimental Setup ..... 39
Impedance Analysis Process ..... 40
Conductive Breakthrough ..... 40
Non-Lithium Gel Fractor ..... 41
Steel Fractors Phase Impedance Analysis ..... 44
Aluminum Fractors Phase Impedance Analysis ..... 47
Copper Fractors Phase Impedance Analysis ..... 50

TABLE OF CONTENTS – CONTINUED

Results of Variation in Manufacturing Parameters....53

7. STRESS RELAXATION AGING....55
Concept....55
Aluminum Fractor....56
Copper Fractor....60
Steel Fractor....64
Conclusion....68

8. STRESS RESPONSE ANALYSIS....69
Concept....69
Experimental Setup....69
Process....70
Aluminum Fractor Loading....71
Aluminum Fractor Unloading....76
Steel Fractor Loading....80
Steel Fractor Unloading....82
Copper Fractor Loading....85
Copper Fractor Unloading....87
Conclusion....89

9. VIBRATION RESPONSE ANALYSIS....90
Concept....90
Experimental Setup....90
Vibration Process....92
Aluminum Fractor Vibration....92
Steel Fractor Vibration....94
Copper Fractor Vibration....97
24 Hour Vibration Run....99
Conclusion....101

10. THERMAL RESPONSE ANALYSIS....102
Concept....102
Experimental Setup....102
Thermal variation Process....104
Steel Fractor Cooling....105
Steel Fractor Heating....107
Copper Fractor Cooling....109
Copper Fractor Heating....111
Aluminum Fractor Cooling....114

TABLE OF CONTENTS – CONTINUED

Aluminum Fractor Heating ..... 116
Conclusion ..... 118

11. HUMIDITY RESPONSE ANALYSIS ..... 119
Concept ..... 119
Experimental Setup ..... 119
Process ..... 121
40C Steel Fractor Humidity Variation ..... 121
80C Steel Fractor Humidity Variation ..... 124
Conclusion ..... 126

12. FINAL CONCLUSION ..... 127

13. RECOMMENDATIONS FOR FUTURE WORK ..... 129

14. REFERENCES CITED ..... 130

# LIST OF TABLES

Table Page

1. Baking time according to dipping.....33

2. Temperature variation.....104

# LIST OF FIGURES

Figure Page

1. Bode phase plot ..... 3
2. Bode magnitude plot ..... 4
3. Nyquist plot ..... 5
4. Response of a Fractor on a square wave input ..... 7
5. Open loop Control System (Automobile speed) ..... 11
6. Feedback Control System ..... 12
7. PID control system ..... 15
8. Comparison of PID response with desired response ..... 16
9. Metal – gel interface ..... 18
10. Drift of lithium ions ..... 20
11. Koch fractal surface ..... 23
12. Integrator in a PI controller ..... 25
13. Fractional order integrator in a $PI^{\alpha}$ controller ..... 26
14. Responses of a PI and $PI^{\alpha}$ controllers ..... 28
15. Abrasion path pattern ..... 29
16. Silicate matrix with lithium ion dispersed ..... 32
17. The dipping process ..... 33
18. Copper samples before abrasion, after abrasion and after dip baking ..... 34
19. Block diagram of a Fractor ..... 35

LIST OF FIGURES - CONTINUED

Figure Page

20. Encapsulation of the Fractor .....36

21. The Fractor .....37

22. Setup of impedance analysis .....39

23. Conductive Breakthrough .....41

24. Non lithium Fractors – phase plot .....42

25. Non lithium Fractors – impedance plot .....43

26. Steel Fractors comparison – phase plot .....45

27. Steel Fractors comparison – impedance plot .....46

28. Aluminum Fractors comparison – phase plot .....47

29. Aluminum Fractors comparison – impedance plot .....49

30. Copper Fractors comparison – phase plot .....51

31. Copper Fractors comparison – impedance plot .....52

32. Aluminum Fractor stress tightening comparison – phase plot .....56

33. Aluminum Fractor stress tightening comparison – impedance plot .....57

34. Aluminum Fractor stress relaxation comparison – phase plot .....58

35. Aluminum Fractor stress relaxation comparison – impedance plot .....59

36. Copper Fractor stress tightening comparison – phase plot .....60

37. Copper Fractor stress tightening comparison – impedance plot .....61

38. Copper Fractor stress relaxation comparison – phase plot .....62

LIST OF FIGURES - CONTINUED

Figure Page

39. Copper Fractor stress relaxation comparison – impedance plot .....63

40. Steel Fractor stress tightening comparison – phase plot .....64

41. Steel Fractor stress tightening comparison – impedance plot.....65

42. Steel Fractor stress relaxation comparison – phase plot .....66

43. Steel Fractor stress relaxation comparison – impedance plot .....67

44. Block diagram of the loading system.....70

45. Aluminum Fractor stress loading comparison – phase plot.....71

46. Aluminum Fractor stress loading comparison – impedance plot.....73

47. Nyquist plots at different loading .....75

48. Aluminum Fractor stress unloading comparison – phase plot.....76

49. Aluminum Fractor stress unloading comparison – impedance plot.....77

50. Nyquist plots at different unloading .....79

51. Steel Fractor stress loading comparison – phase plot .....80

52. Steel Fractor stress loading comparison – impedance plot .....81

53. Steel Fractor stress unloading comparison – phase plot .....83

54. Steel Fractor stress unloading comparison – impedance plot .....84

55. Copper Fractor stress loading comparison – phase plot .....85

56. Copper Fractor stress loading comparison – impedance plot .....86

57. Copper Fractor stress unloading comparison – phase plot .....87

LIST OF FIGURES - CONTINUED

Figure Page

58. Copper Fractor stress unloading comparison – impedance plot .....88

59. Block diagram of vibration setup.....92

60. Aluminum Fractor vibration comparison – phase plot .....93

61. Aluminum Fractor vibration comparison – impedance plot.....94

62. Steel Fractor vibration comparison – phase plot.....95

63. Steel Fractor vibration comparison – impedance plot .....96

64. Copper Fractor vibration comparison – phase plot.....97

65. Copper Fractor vibration comparison – impedance plot.....98

66. Copper Fractor 24 hour vibration comparison – phase plot .....100

67. Copper Fractor 24 hour vibration comparison – impedance plot .....101

68. Thermal test setup .....103

69. Steel Fractor cooling comparison – phase plot .....105

70. Steel Fractor cooling comparison – impedance plot.....106

71. Steel Fractor heating comparison – phase plot .....108

72. Steel Fractor heating comparison – impedance plot.....109

73. Copper Fractor cooling comparison – phase plot .....110

74. Copper Fractor cooling comparison – impedance plot.....111

75. Copper Fractor heating comparison – phase plot .....112

76. Copper Fractor heating comparison – impedance plot .....113

LIST OF FIGURES - CONTINUED

Figure Page

77. Aluminum Fractor cooling comparison – phase plot.....114

78. Aluminum Fractor cooling comparison – impedance plot .....115

79. Aluminum Fractor heating comparison – phase plot.....116

80. Aluminum Fractor heating comparison – impedance plot.....117

81. Humidity analysis setup.....120

82. Steel Fractor (40C) humidity variation comparison – phase plot.....122

83. Steel Fractor (40C) humidity variation comparison – impedance plot.....123

84. Steel Fractor (80C) humidity variation comparison – phase plot.....124

85. Steel Fractor (80C) humidity variation comparison – impedance plot.....125

# ABSTRACT

An innovative fractional order control device (Fractor) has been developed. The principal characteristic of the Fractor is a non-integer order power law relationship between the impedance and frequency. The exponent or the order in this power law is the Constant Phase Element (CPE). Warburg impedance is the ideal goal for the optimal performance of the Fractor which is intended for applications in feedback control systems. The Fractor is based on a specially developed material system which involves a synthesized polymer gel interfaced with metal electrodes. The roughness of the electrode is inversely correlated to the CPE.

The main objective of this study is to determine the effectiveness of the Fractor depending on the manufacturing, loading and environmental conditions over a wide range of frequencies from 20 Hz to 500 kHz. A consistent experimental study has been performed to investigate the performance and response characteristics of the Fractor. Various material compositions of the Fractor have been investigated. The study has been performed for a wide range of parameters, including pressure, temperature, and humidity.

The results of this investigation provide important information and guidelines for optimizing the performance and properties of the Fractor for feedback control of mechanical and electrical systems.

# INTRODUCTION

The fraction order control device (Fractor) is a novel, brand new electronic device exhibiting non-integer order power law relationship between impedance and frequency. This device is based on the principle of generalized Warburg impedance which states impedance varies proportional to square root of the frequency.

The Warburg impedance has been known since the end of 19$^{th}$ century but unfortunately was something that people wanted to eliminate. But it is this very phenomenon that allows us to carry out fraction order calculus operations if a single power law is isolated. The following section gives a brief description of fraction order calculus.

## Fractional Order Calculus

A generalized fraction order derivative over the interval [a,t] is given as follows,

$$ {}_0D_t^{\alpha} f(t) = \lim_{N\to\infty}\left\{\left(\frac{t-a}{N}\right)^{-\alpha}\sum_{k=0}^{N-1} w_k f\left(t-k\left[\tfrac{t-a}{N}\right]\right)\right\} \quad \text{..... (1)} $$

where $\alpha$ is any real number,

$w_k$ = weight function consisting of ratio of gamma functions,

N = step size.

As $N \to \infty$, $(t-a)/N \to dt$

A derivative of negative order is a generalized integral. The order α in the above equation is the same exponent as in the power law relationship of the impedance to the frequency in the Warburg impedance called as the constant phase angle element (CPE).

## Impedance

Impedance is defined as the measure of the ability of an electrical circuit to resist the flow of current through it. In an ideal resistance case, the current and the voltage are in phase with each other where as for impedance the current lags behind the voltage by a phase angle θ.

Impedance can be expressed as a combination of a real and imaginary part i.e. as a complex number by,

$Z(\omega) = Z_0(\omega) (\cos \theta(\omega) - j \sin \theta(\omega))$……...(2)

at any frequency ω.

## Warburg Impedance

The Warburg impedance tries to represent the diffusion process by stating a power law relation ship between impedance and frequency by,

$Z(\omega) = Z_0 \omega^{-0.5} (\cos \theta - j \sin \theta)$……(3)

Note that the CPE (η) equals 0.5 for perfect diffusion modeling. The Warburg also states equal relation ship between the real and imaginary components of the impedance over a range of frequencies. This effect is generally observed on a corroded or roughened electrode with a surface film or coating.

The Warburg is well defined on the Bode plots

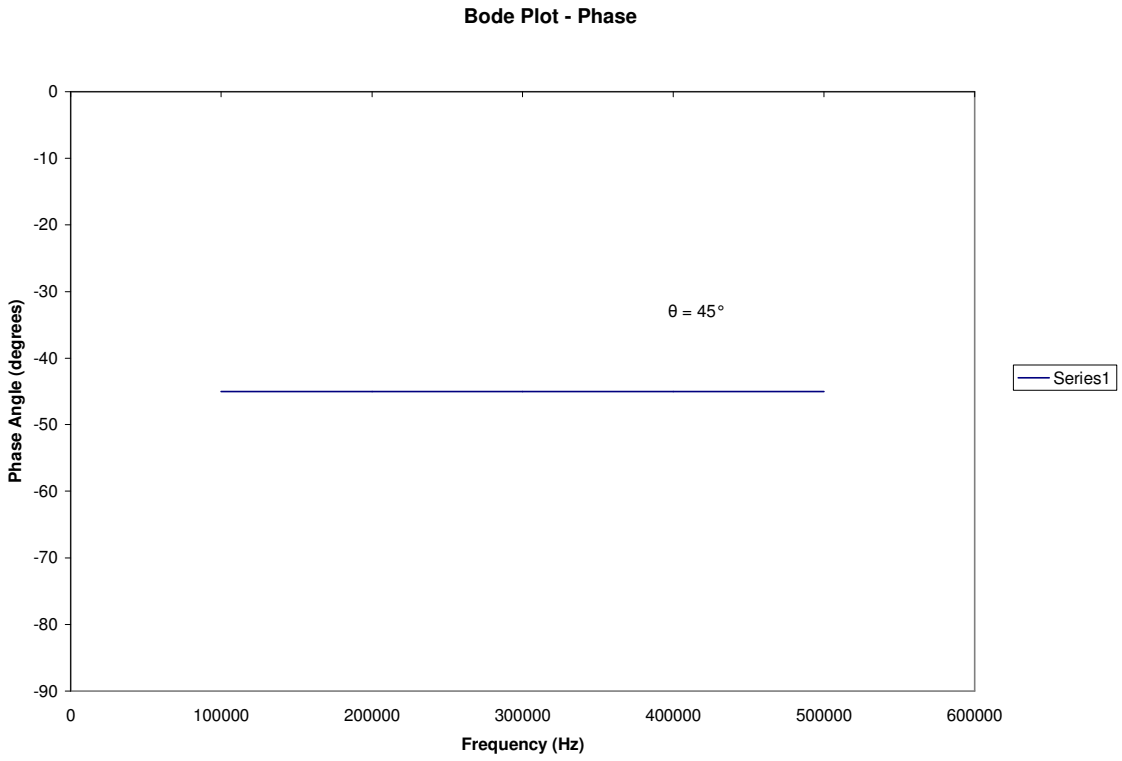



Figure 1. Bode phase plot.

The Bode phase plot gives the variation of the phase angle of the Fractor at different frequencies. For an ideal Warburg effect the Bode phase plot shows that on a phase angle v/s frequency plot the phase ideally stays at 45° for all frequencies.

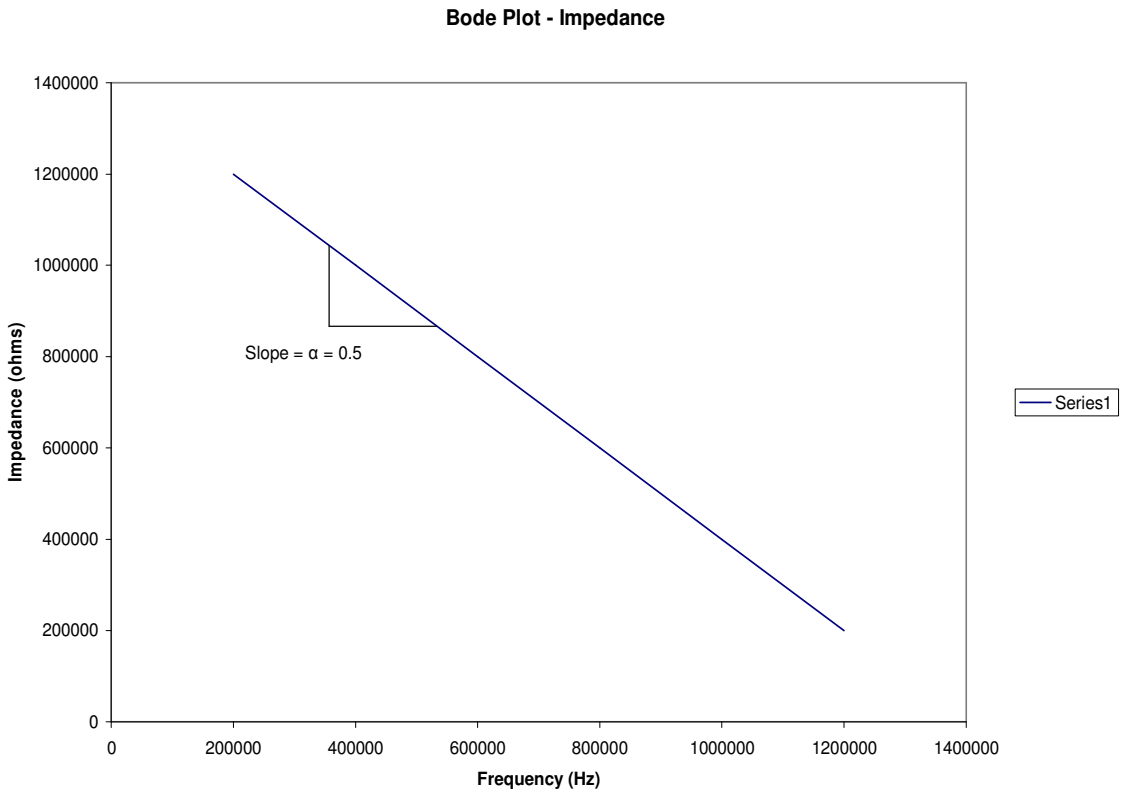



Figure 2. Bode magnitude Plot.

The Bode impedance plot gives the variation of the impedance of the Fractor at different frequencies. For an ideal Warburg case, it suggests that the slope of the line on an impedance magnitude v/s frequency plot stays at 0.5. It is corresponding to this slope that the phase angle becomes 45° on the Bode phase plot. The slope of 0.5 is particularly dominant in the lower frequency ranges. As the frequency increases, pure resistance due to charge transfers becomes significant instead of the Warburg impedance.

The Nyquist plot gives the relation between the real and imaginary components of the Fractor. The Nyquist plot suggests equal components on the imaginary and real parts which gives rise to the Warburg effect. For ideal Warburg impedance all the Nyquist plots show a 45° line.

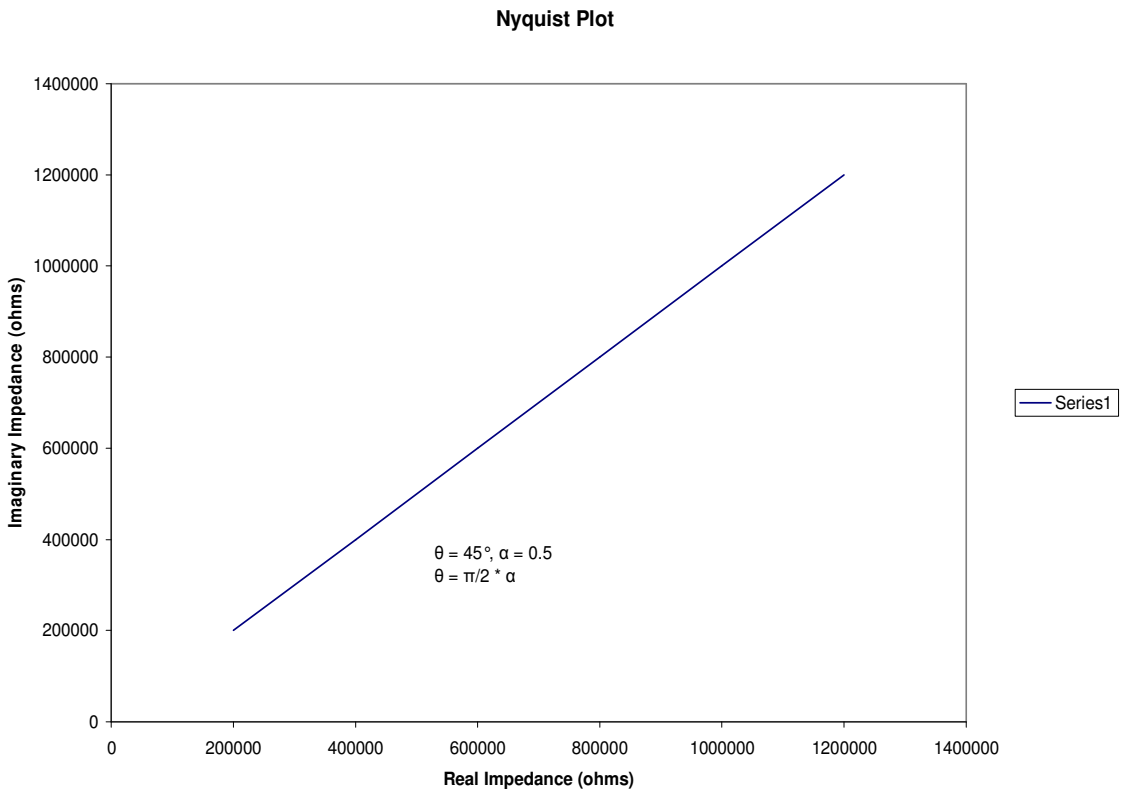



Figure 3. Nyquist plot.

In the following sections of this thesis, the Bode phase and impedance plots are more commonly used as they provide more comprehensive information than Nyquist plots.

## The Fractor

A Fractor is an electrical element non integer order power law impedance over a frequency range and ideally models the Warburg effect (define later). The power law impedance behavior of the Fractor is given as[3],

$$Z(\omega) = K/(j\omega\tau)^{\alpha} \quad \ldots\ldots(4)$$

where K is the impedance magnitude at frequency $\omega_c = 1/\tau$,

$\tau$ = time constant,

$\alpha$ is the non integer exponent and $0 < \alpha < 1$

The phase is related to exponent by $\theta = 90 \times \alpha$ ($\alpha$ is later mentioned in the electrochemistry as constant phase element or exponent, CPE). As $\alpha \rightarrow 0$, the Fractor becomes resistive and as $\alpha \rightarrow 1$, the Fractor becomes capacitive.

The gain of an inverting amplifier is the ratio of the feedback impedance to the input impedance. As observed from above controller definitions, the gains of an integer and derivative controller are proportional to a specific time constant. The Fractor on the other hand allows non integer order operators. This is because the fractional order feedback impedance divided by constant input impedance value will provide fraction order gain. This fractional response allows the control system to tackle non linearity whereas the integer order control fails do this. This results into over integration or actuator saturation.

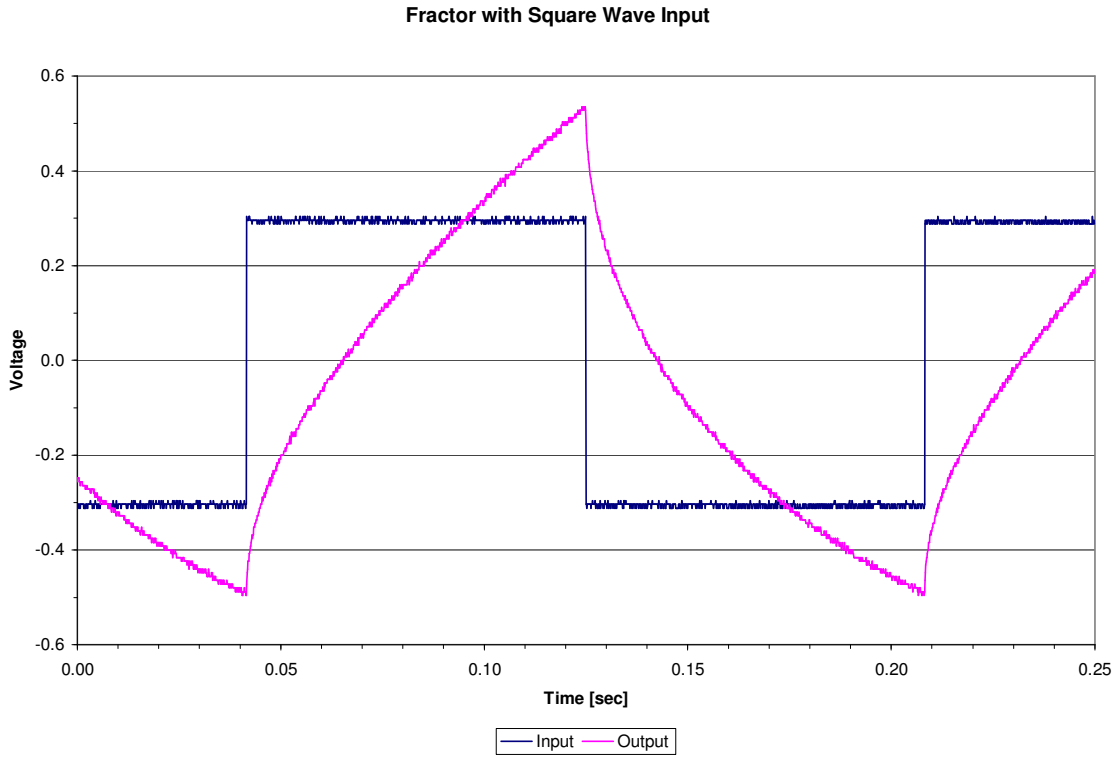



Figure 4. Response of a Fractor on a square wave input.

(Figure provided by Dr. Gary Bohannan)

For example for a fraction order integral controller as shown in above figure, the fraction order gain is $G/(\tau s)^{\alpha}$

where $s = j\omega$

and G = gain magnitude.

The inverse Laplace transform of $1/(\tau s)^{\alpha}$ is $\frac{1}{\tau^{\alpha}} {}_{o}I_{t}^{\alpha}$, which is the fractional order integral of order $\alpha$.

In the figure 4, the fraction order integer controller gives response proportional to $\sqrt{t}$ on a square wave input whereas an integer order controller would have produced a ramp and a proportional controller would have produced a square wave.

The Fractor performance is totally due to the electrochemical impedance and frequency relationship. This is explained in detail on the chapter on impedance spectroscopy.

## Goals and Objectives

This concept raised an important question. Could a single power law be isolated so that it could later be converted into an electronic device? After a significant amount of review on impedance spectroscopy and experimental trials Dr. Stephanie Hurst, Department of Chemistry, Montana State University, Bozeman, MT managed to develop a recipe for a near perfect power law relationship.

Once this was done, an engineer (the author) was required to design a device out of the recipe. The objectives of the were,

- How to laboratory manufacture the device in a repeatable way? Addressed in the chapter ‘Sample manufacturing’.
- What parameters make difference in the Fractor response? Addressed in the chapter ‘General phase – impedance response analysis’.
- Does the Fractor response vary under stress issues like pressure or vibration? Addressed in the chapters ‘Stress response analysis’ and ‘Vibration response analysis’.

- Is the Fractor response affected by changes in temperature? Addressed in the chapters ‘Thermal response analysis’ and ‘Humidity response analysis’.

# INTRODUCTION TO CONTROL SYSTEM

The Fractor is used in feedback systems for electrical circuits for more precise responses. This section addresses the functioning of control systems and its components.

## Basic Open Loop Control System

A control system is the means by which a parameter under consideration in a system is maintained or altered according to the requirement. In a basic control system the output of the system has no effect on the controlling action. The output is neither measured nor fed back for comparison with the input. Consider, for example, an automobile in motion whose control system is shown by the figure 5. The speed of the automobile is the controlled variable and is a function of the position of the accelerator (the control element). An increase in the pressure (input actuating signal) on the accelerator pedal will force it down thus giving a signal to the engine (plant), which results into increase in the speed. Thus the set point or the input is the pressure on the accelerator pedal while the controlled output variable is the speed. Note that this system has no means of monitoring the change in the speed or the current speed of the automobile as the speed is not being measured or fed back to the system for comparison. Due to the absence of the feedback this system is known as the open loop control system.

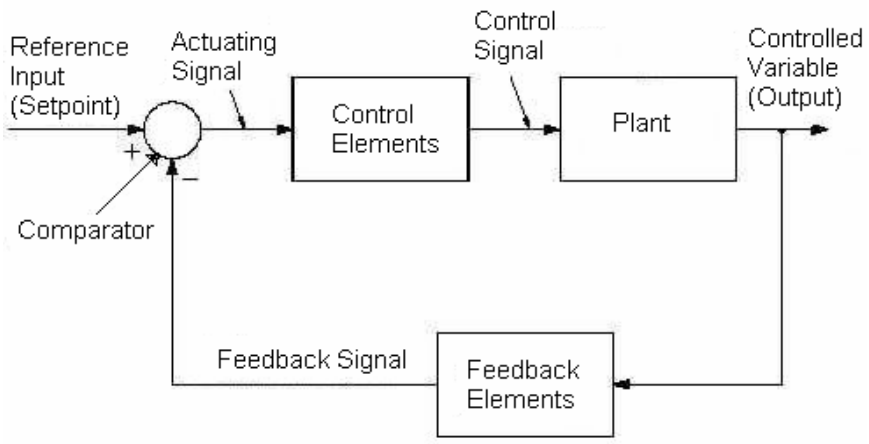



Figure 5. Open loop Control System (Automobile speed).

## Close Loop Control System

Consider the same case of an automobile in motion. Suppose the driver wants to maintain a speed of 'x' miles per hour on the road. He applies a specific force on the accelerator to achieve the specific speed of 'x' miles and holds it steady at that position to maintain the speed. The speed remains uniform unless there are disturbances caused by the road surface. But as the slope of the road changes or becomes uneven, the speed varies. The speed is reflected on the speedometer. This enables the driver to compare the current and the desired speed mentally and calculate the difference. Accordingly he executes the corrective action to increase or decrease the speed by varying the pressure on the accelerator pedal.

This system is called as the closed loop control system as the information about the instantaneous state of the output is fed back to the controller for comparison with the

input signal. This helps in correcting the input signal to give the desired output. The block diagram of an ideal control system is shown in the figure 6.

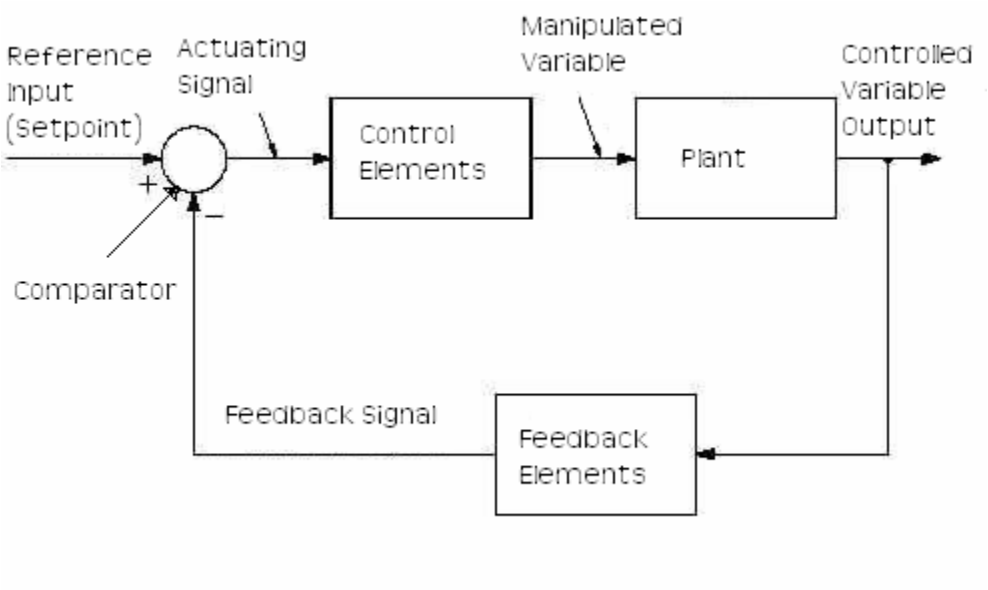



Figure 6. Feedback Control System.

The error comparator compares the feedback signal which is a function of the output signal with the reference input signal. Any difference between these two signals results in an error signal which actuates the control elements. The control elements in turn manipulate the plant parameters resulting in the plant performing the necessary corrective actions, for example the furnace heats up more to provide increase in temperature in a temperature control system. Thus the error in the system is narrowed down to the minimum.

## Control Actions

The controlling actions of the control elements are of three distinct types.

### Proportional (P) Control Action

Steady process operation with absence of disturbances is possible only when the controlled variable is the continuous function of the error. Thus the P type of control action is widely preferred continuous controller modes as it establishes a smooth, linear relationship between the controlled output and the error.

The control relationship is given as,

$P(t) = K_p\, e(t)$ ……(5)

where P(t) = controller output at any time 't' with error in consideration

e(t) = error signal at any time 't'

$K_p$ = proportional controller gain or proportional constant

Proportional control is characterized by a permanent residual error in operating point of the controlled variable called as the offset error.

Proportional control action deals with the present or current error by providing a response proportional to the error. Typically it gives a large gain and reduces a large part of the error.

Integrator (I) Control Action

The integral control deals with the past or history of the process by integrating the error over a span of time. The integral action has no offset as the output keeps on changing as long as any error persists.

The control relationship is given as,

$P(t) = K_i \int e(t)\, dt + P(0)$……..…..(6)

where P(t) = controller output at any time 't' with error in consideration

e(t) = error signal at any time 't'

P(0) = controller output at without any error

$K_i$ = integration controller gain or inverse of the "integral time constant"

Due to capacitor charging the initial response to any error is slow.

Derivative (D) Control Action

The derivative control handles the future with giving the controller output proportional to the rate of change of error at any instant of time. The response to the error variation is quick.

The control relationship is given as,

$P(t) = K_d\, d(e(t))/dt$ ……(7)

where P(t) = controller output at any time 't' with error in consideration

e(t) = error signal at any time 't'

$K_d$ = derivative controller gain or derivative "time constant".

If the error is constant, the derivative control produces no change in the output.

The P-I-D control action

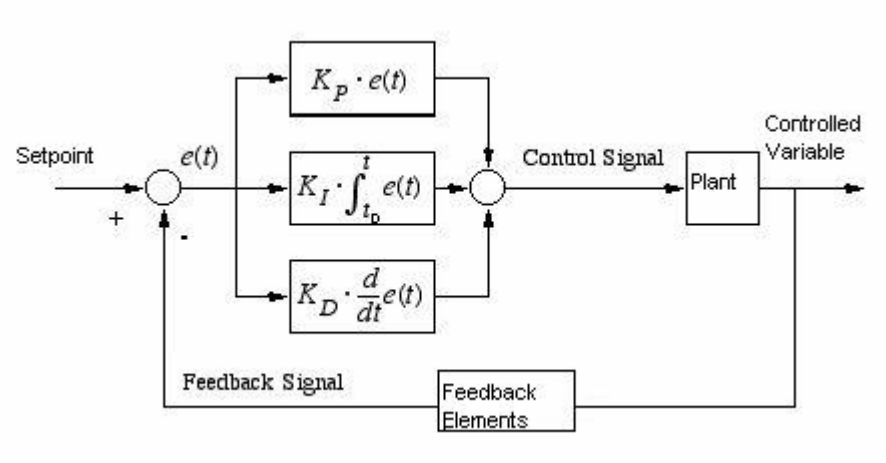



Figure 7. PID control system.

The figure 7 shows the combined PID control system. The proportional system reduces the variation in the system and increases the closed loop gain. The integral system corrects the offset error that besieges the proportional system by resetting the set point after each load change. The addition of a derivative system to the above reduces the deviation from set point and the stabilizing time. The equation of the whole system is given as,

$P(t) = K_p\, e(t) + K_p\, K_i \int e(t)\, dt + K_p\, K_d\, d(e(t))/dt + P(0)$……(8)

where P(t) = controller output at any time 't' with error in consideration

e(t) = error signal at any time 't'

P(0) = controller output at without any error

$K_d$ = derivative constant

$K_i$ = integration controller gain or integral constant

$K_p$ = proportional controller gain or proportional constant

Thus, this system combines the advantages of the individual P, I and D controllers and hence is used extensively in many process environment. Together the PID system can narrow down a large margin of error but not eradicate it completely.

PID Control Responses

Though the PID system combines the best of all the three individual systems, it does not exactly cure all the problems. There exist some inherent problems with the PID controllers that make it difficult to use them in sensitive electrical systems. Deviation of the responses with respect to the ideal may create circuit burnouts or other problems in these systems.

The figure 8 below compares the ideal and PID responses and shows the differences between them over a time scale.

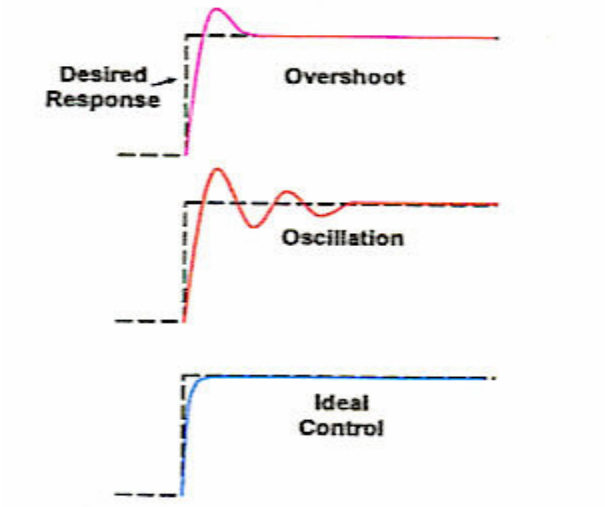



Figure 8.Comparison of PID response with desired response (provided by Dr. Bohannan).

It can be seen that the PID response suffers from

a) Overshoot: The response crosses the desired response due to lack of control precision.
b) Oscillations: The response shows narrowing positive and negative variations about the desired response due to overshoot and undershoot of the control variable. It settles down when the error signal eventually becomes zero.

The last graph in the figure shows an idea response which faithfully follows the desired response. This can be modeled by designing a $PI^{\alpha}D^{\beta}$ by using a Fractional Order Device (Fractor) in the circuit. The Fractor is currently being patented by the Department of Chemistry, Montana State University (MSU), Bozeman and Wavelength Electronics, Inc. (WEI). The behaviour of the Fractor is currently being researched at MSU, Bozeman.

# ELECTROCHEMICAL IMPEDANCE

## Metal Gel Interface

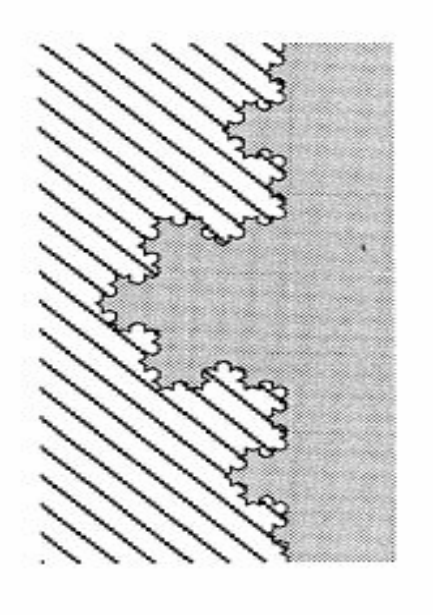


Figure 9. Metal – gel interface. [2] (Metal – white, gel –gray).

The Fractor is an electrochemical cell made up of a solid electrolyte between two metal electrodes. The basic process in a Fractor is the electric charge transfer across the interface of an electrode and a solid electrolyte in the form of baked gel as shown in figure 9. The impedance of this system is ideally denoted by resistance and capacitance in series.

$Z(\omega) = R - j / (\omega C)$ ……(9)

where C = the interfacial or double layer capacitance,

R = the ionic or double layer resistance,

and $\omega$ = the angular frequency.

The first term on the right is called the resistive or real impedance and the last term is the capacitive or imaginary part of the impedance.

It has been shown that the capacitance of such a system with a rough electrode is dependent on more frequency rather that a similar system with smooth electrode.[5] This dependence is often observed to take the power law form as follows,

$C \sim \omega^{-\alpha}$,

$\alpha$ being any positive index.

This tendency of power law relationship to frequency was found out to be effective when material was removed from the surface. Where as etching led to more systematic material removal and thus more prominence in the above effect. [4] This showed that the frequency dependence of the capacitance of the metal electrode – ionic gel interface may have originated from the electrode roughness but ions may also have played an important part.[5]

The metal-gel interface can be modeled as space charge capacitor and double layer capacitor connected in series in which the resulting capacitance is the mostly space charged if both the metal surface and metal gel interface are constant at all frequencies. [6] This happens when the surfaces are ideally smooth. But real surfaces are not smooth and capacitance being directly proportional to area is largely influenced by variation in area.

The rough surface capacitance can be explained as follows. The metal gel system has ions on the gel side and electrons on the metal side. The ions being heavier and more charged than the electrons have lower mobility. Hence ions have much slower response

to the applied AC signal than the electrons. The distance that the ion can travel at any given frequency is called as drift (X) of the ion at that frequency and is given by,

$X \sim \mu / \omega$ ……(10)

where $\mu$ is the mobility of the ions,

and $\omega$ is the frequency.

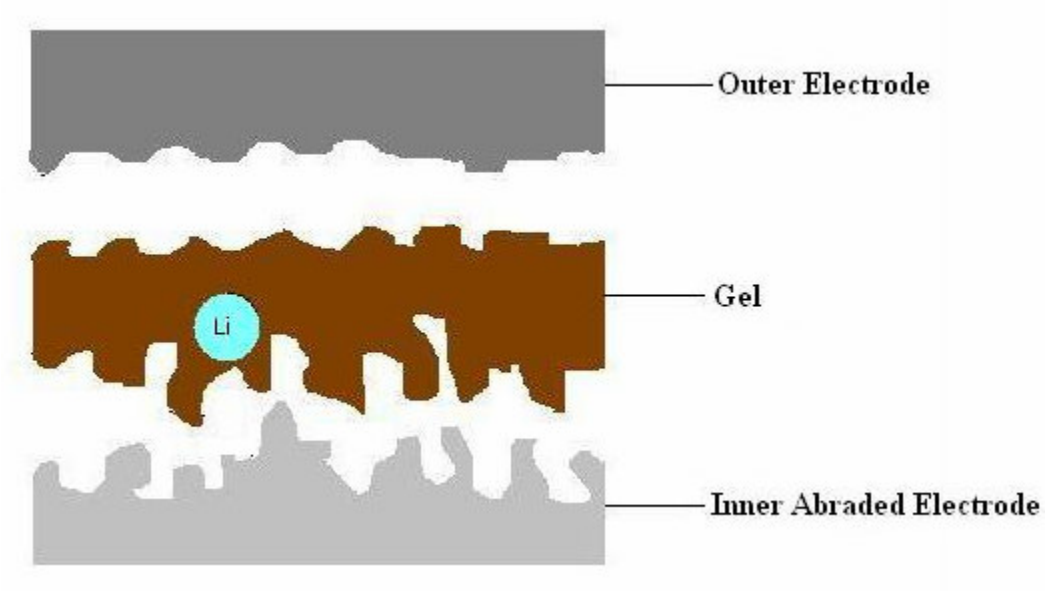



Figure 10. Drift of lithium ions.

At higher frequencies, the ions get less time for drifting between the polarized electrodes and thus end up vibrating about their mean position.

At lower frequencies the ions can have more drift and hence access the depths of the roughened electrode. At lower frequencies, the area accessed by the ions increases. Figure 10 shows the drift of lithium ion in the gel matrix. This results in making the

double layer capacitance more influential in the above equation. So the capacitance of the rough metal -gel system is dominated by double layer capacitance.

The impedance of the double layer is given by Sapoval [10] as,

$Z(\omega) = Z_0(j\omega)^{-\eta}$ ……..(11)

So, converting to polar form,

$Z(\omega) = Z_0\omega^{-\eta} (\cos\theta - j \sin\theta)$, ……(12)

The above impedance is called as the constant phase angle (CPA) impedance. $\eta$ is the constant phase angle exponent (CPE) and its related to the phase angle by $\theta = \eta (\pi/2)$.

$\eta$ lies between 0 and 1 and is negatively related to the surface roughness.[2]

Now, from the definition of real and imaginary impedances,

$Z_0 \cos\theta = R_0$

$(Z_0 \sin\theta)^{-1} = C_0$

where $R_0$ and $C_0$ are the initial resistance and capacitance of the system.

So,

$Z(\omega) = R_0\omega^{-\eta} - j /( C_0 \omega^{-\eta})$……(13)

Thus comparing with equation 9,

$R = R_0\omega^{-\eta}$

$C = C_0 \omega^{-(1-\eta)}$

Thus it can be shown that the capacitance and the resistance of the system depend upon the constant phase angle exponent.

But these equations are trying to model a real system on the principles of combination of two ideal systems (i.e. resistance and capacitance). To perfectly model

the metal gel interface, infinite amount of resistors and capacitors will de required. It has been noticed from the Warburg Nyquist plot that the real and imaginary components of the system seem to scale together on being subjected to different frequencies. This cannot happen with the above case as we are speaking of coupling together two independent processes.

Thus we can only conclude that the extremities of the metal gel film interface are pure resistance and pure capacitance. The Fractor cannot be modeled as a combination of resistance and capacitance. But, the point that impedance is related to the frequency by the above equations makes sense.

The metal gel interface is also modeled by the same Fractor equation introduced by Dr. Gary Bohannan as given before,

$$Z(\omega) = K/(j\omega\tau)^{\alpha} \quad \text{.....(15)}$$

K depends upon the mobility and amount of the charge carriers

$\alpha$ depends upon the gel chemistry and fractal surface. The meaning of fractal surfaces is explained in the following section.

## Fractal Surfaces

From the above part it can be noticed that the degree of the roughness or fractality matters significantly in the frequency dependence of the metal gel system. Rough surfaces can be described by the factor "D" called the fractal dimension of the surface.[7] As mentioned from above, $\eta$ is inversely proportional to the surface roughness.

The fractal dimension "D" is acquired from a structure function. The structure function obtained by measuring the surface profile of the electrode. The dimensionality is related to the characteristic exponent of this function.[1]

For a smooth electrode, $\eta = 1$. Putting this in equation (12) leads to pure capacitive or imaginary impedance.

$Z(\omega) \approx Z_0 / (j\omega)$

For a very rough electrode, $\eta = 0$. Putting this in equation (12) leads to pure resistive or real impedance.

$Z(\omega) \approx Z_0 / \omega$

CPE is directly related to the fractal dimension D by,

$\eta = 3 - D$. [9]…… (16)

For a very smooth electrode, D = 2 and for a ideal fractal electrode D = 3.

An ideal fractal surface repeats its structure on magnification as shown in figure 11.

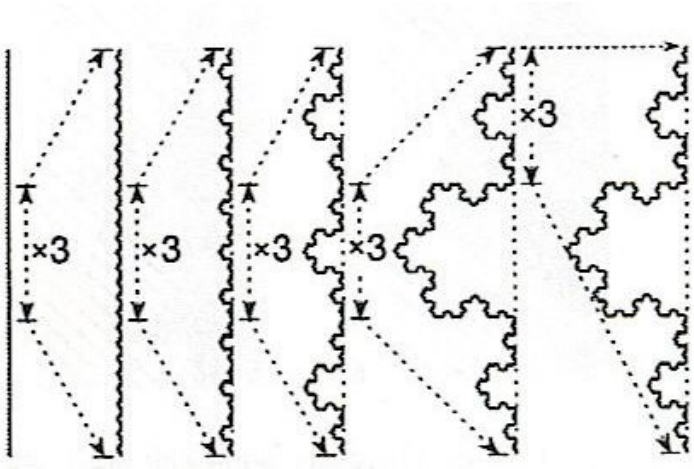



Figure 11. Koch fractal surface.[2]

The impedance depends on the CPE and the CPE depends upon the fractal roughness. For a Fractor to give response equal to a series circuit between capacitance and resistance the fractal dimension D must be equal to 2.5.

So we need to abrade the middle electrode in a Fractor to achieve a good degree of roughness.

## POSSIBLE USES OF THE FRACTOR

1) Temperature Controllers:

A Fractor can be implemented in a PI controller to make it an $PI^{\alpha}$ controller thus giving better control by getting rid of the overshoots and oscillations. One such experiment was conducted by Dr. Gary Bohannan to compare the response of the PI and $PI^{\alpha}$ controllers.

This was done by mounting a thermoelectric cooler on an aluminum block (14cm x 7.5cm x 0.5cm) and using 10KΩ negative temperature coefficient thermistor as temperature sensor.

The aluminum block was subjected to thermal loading on one side and cooling on the other side via the thermoelectric cooler. The current through the thermoelectric cooler was controlled by a PI and $PI^{\alpha}$ controller separately.

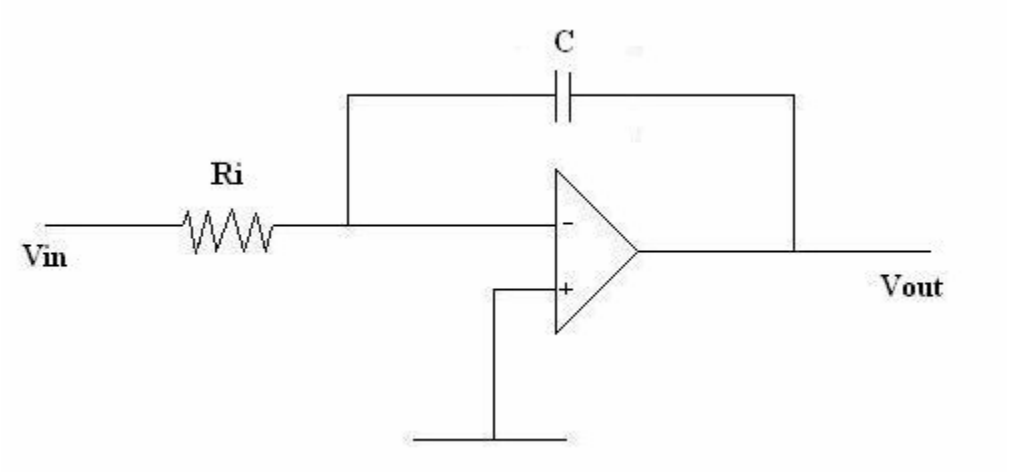



Figure 12. Integrator in a PI controller.

Figure 12 shows the integrator of a PI controller. The feedback gain is the ratio on the feedback impedance to the input impedance. This is given by,

$V_{out} / V_{in} = -1/ R_i (j\omega C)$…….. (17)

Where $R_i$ = input impedance

C = feedback capacitance.

Note that the feedback gain is integer ordered.

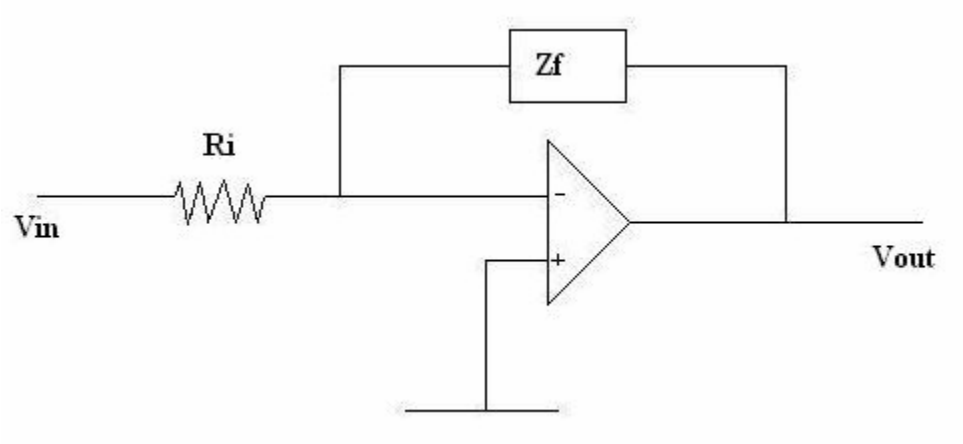


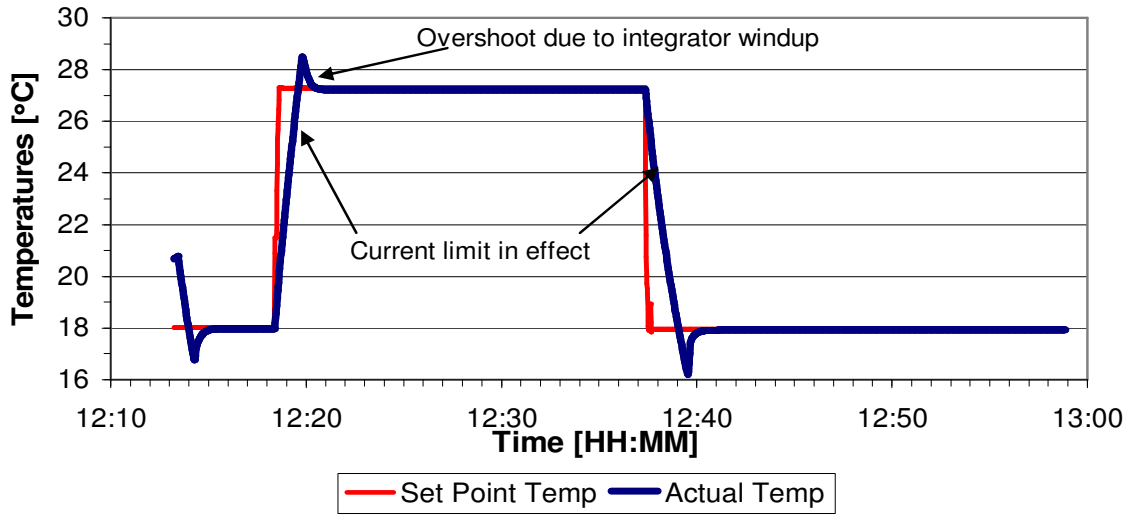

Figure 13. Fractional order integrator in a $PI^{\alpha}$ controller.

Figure 13 shows the integrator in a $PI^{\alpha}$ controller obtained by replacing the capacitor in feedback of a traditional integrator by a Fractor. The feedback gain in this case is given by,

$V_{out}/ V_{in} = -K / R_i (j\omega\tau)^{\alpha}$ ……..(18)

Note that the feedback gain is of non integer order $\alpha$.

The inverse Laplace transform of this function gives an integral of the order α. This provides fractional order control in the feedback control circuit



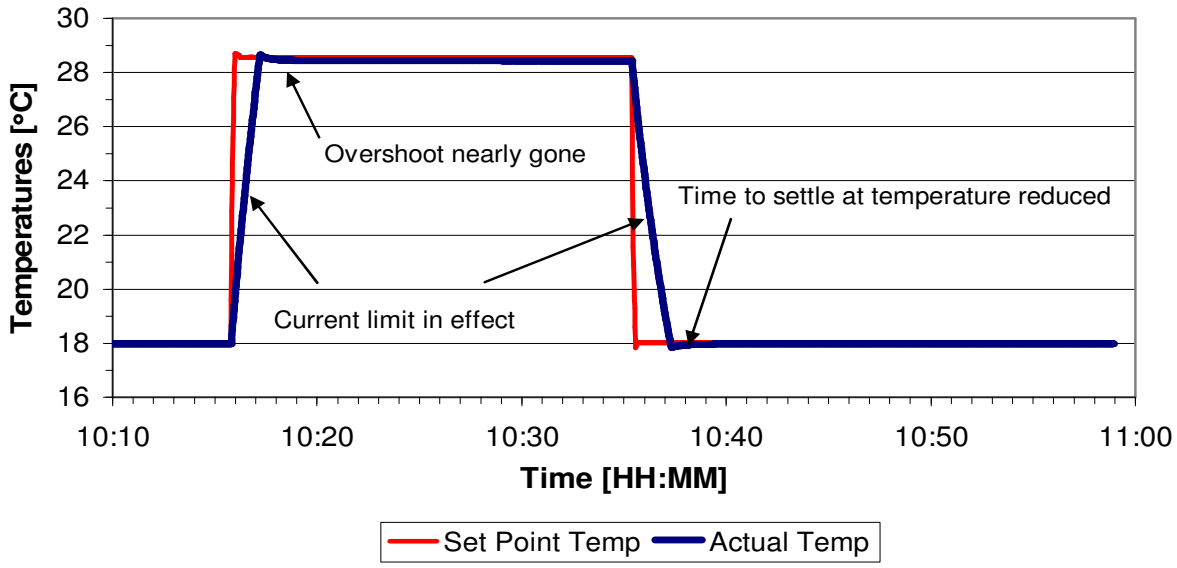




Figure 14. Responses of a PI and PI$^{\alpha}$ controllers.

(Figure provided by Dr. Gary Bohannan)

It can be seen from comparing the PI response graph with the $PI^{\alpha}$ response graph in the figure 14 that the overshoot has disappeared and the stabilizing time has been reduced upon using a fractional order control system as to integer order one. (Figure provided by Dr. Gary Bohannan)

2) Robot arms:

Fractors can be used in robot arm controllers to give them human like flexible motions. This will provide fluency for the positioning and motion from one coordinate point to other in welding robots, assembly line robots, etc. This will also provide preceding results for the later experiments of integrating the Fractor with prosthetic devices for better pseudo human response

3) Hard disk drive heads:

Integrating Fractors in the circuit will reduce the overshoots that occur when the hard disk head moves from one address to another to read the data. The stabilizing time when narrowing down at one address is also reduced.

4) Powered wheelchairs:

The Fractor can help the controller give better response for the motor powered wheelchairs by providing instantaneous adaptation towards changing ground conditions.

# SAMPLE MANUFACTURING

## Abrasion and Sonication

A 1mm thick sheet of the desired metal was cut into square pieces of size 1 inch x 1 inch. The square plates were washed with acetone to cleansing of the unwanted dust particles. Then the plates were dried on clean paper for approximately 5 minutes on each side at room temperature (23°C ~ 25°C). The plates were always handled with tweezers and gloved hands to minimize any chance of contamination.

The plates were then abraded with silicon carbide of different grits using compressed nitrogen in the EconOline abrasion machine. Different pressures were used for different samples. Each side of the plate was abraded three times using the following zigzag patterns of spraying as shown in figure 15.

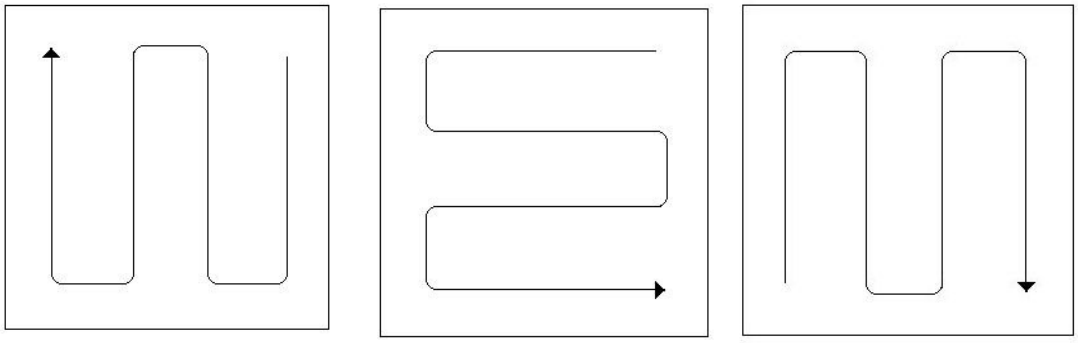


Figure 15. Abrasion path pattern.

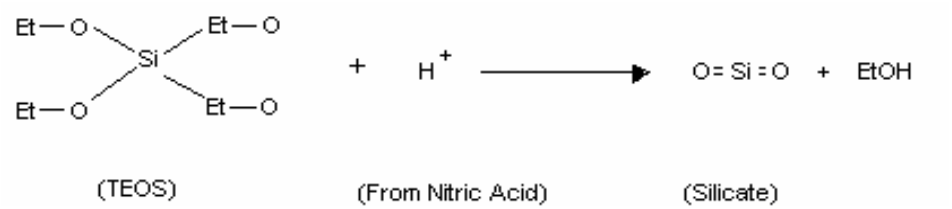
The metal plates were observed to lose their metallic luster and gain a dull, rough

surface. The plates were then immersed completely in plastic petri dishes filled with distilled de-ionized water. These petri dishes were then placed in a sonication bath, also filled with distilled de-ionized water to reduce contamination. The plates were sonicated for approximately 45 seconds. During sonication black silicon carbide were observed rising from the metal surface. The plates were then turned over for the other side to sonicate. The whole idea of the process of sonication was to get rid of the silicon carbide particles lodged in the roughened surface of the plates. The sonicated plates were held under gently flowing distilled de-ionized water for added cleaning and dried at room temperature.

## Ionic Gel Preparation

28 ml of distilled de-ionized water was mixed with 28 ml of 95% ethanol in a clean beaker with a stirring bar. Both of these were initially washed with distilled de-ionized water. 2.8 g of lithium nitrate ($LiNO_3$) was weighed and added to this mixture. The beaker was mounted on a stirrer and stirred for 30 minutes at room temperature. During this time the beaker was covered with a petri dish cover to prevent evaporation. 14 ml of tetraethylorthosilicate (TEOS, $Si(OEt)_4$ ) was added to the above solution. The solution became hazy as TEOS is insoluble in the above solution. One drop of concentrated nitric acid ($HNO_3$) was added to the solution with the use of a pipette. The solution was returned to the stirrer and stirred for about 2 hours with the cover on.

Within few minutes of stirring the hazy solution gradually changed into a clear one. This happened as the TEOS which was insoluble in the above solution was hydrolyzed to soluble silicate $Si(OH)_4$ on the addition of nitric acid. The chemical equation below gives the reaction between TEOS and hydrogen ion from the nitric acid to give am silicate matrix and ethyl alcohol as the by product.




Eight drops of polyaniline sulphonic acid (5% wt/wt solution in water) was added to the solution using a pipette. During this process the stirring continued for about 15 minutes with the beaker cover replaced to ensure proper homogeneity. The colour of the solution progressively changed from clear to dark brown. The amount of polyaniline sulphonic acid is used to determine the approximate impedance values and phase angle. It is a conductive polymer and penetrates the silicate matrix leading to easy flow of ions. The amount of 8 drops was experimentally found to be suited for optimal results[8]. The above procedure was developed by Dr. Stephanie Hurst of the Chemistry department of MSU during isolation of the single power law relationship between the impedance and the frequency .

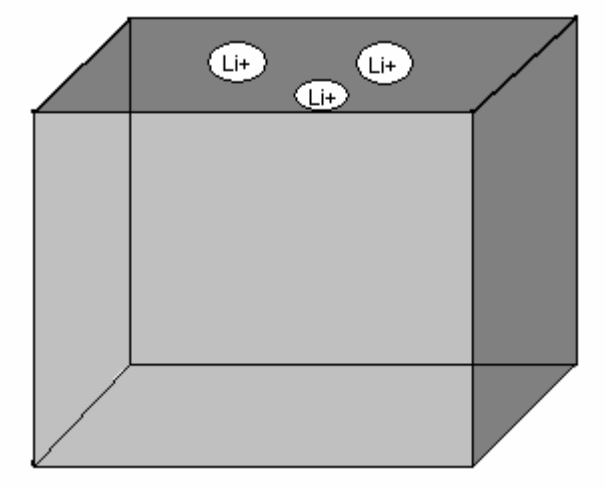



Figure 16. Silicate matrix with lithium ion dispersed.

## Dipping and Drawing Process

The abraded metal plates were held by tweezers and dipped into the gel solution. They were held there for about 10 seconds and were slightly shaken from side to side to allow the gel to penetrate the cavities in the roughened metal surface. The plates were then drawn out at the speed of 10 mm/sec so that the gel would not adhere to the surface in form of droplets. These plates were placed on a glass apparatus in an almost vertical position. The plates were baked for the solidification of the coated gel. They were placed in an over at 150 C for a span of 10 minutes initially as excessive heating in the initial stage might result in the formation of an oxide layer over the surface. The plates were then allowed to cool at room temperature for about 20 ~ 30 minutes after each dipping.

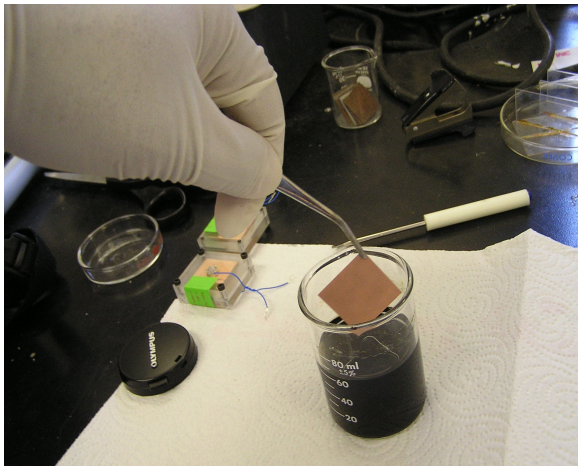


Figure 17. The dipping process.

The dipping continued to make the gel layer thicker. Along with the thickness the baking time was also increased. The plates were then allowed to cool at room temperature for about 20 ~ 30 minutes after each dipping. The figure 15 shows the dipping process.

| Dipping no. | Time for baking (minutes) |
|---|---|
| 1st | 10 |
| 2nd | 12 |
| 3rd | 16 |
| 4th | 18 |
| 5th | 140 |

Table 1: Baking time according to dipping.

Before each dipping apart from the first the plates were rotated by 90 so as to allow uniform gel coating. This also meant that the location were the tweezers held the plates were changed warranting an evenness the coat.

After the final dipping the colour of the plates was observed to have changed distinctly as compared to the abraded plates. This indicated that the surface texture had been modified. Figure 18 shows the variations in the plates at different stages.

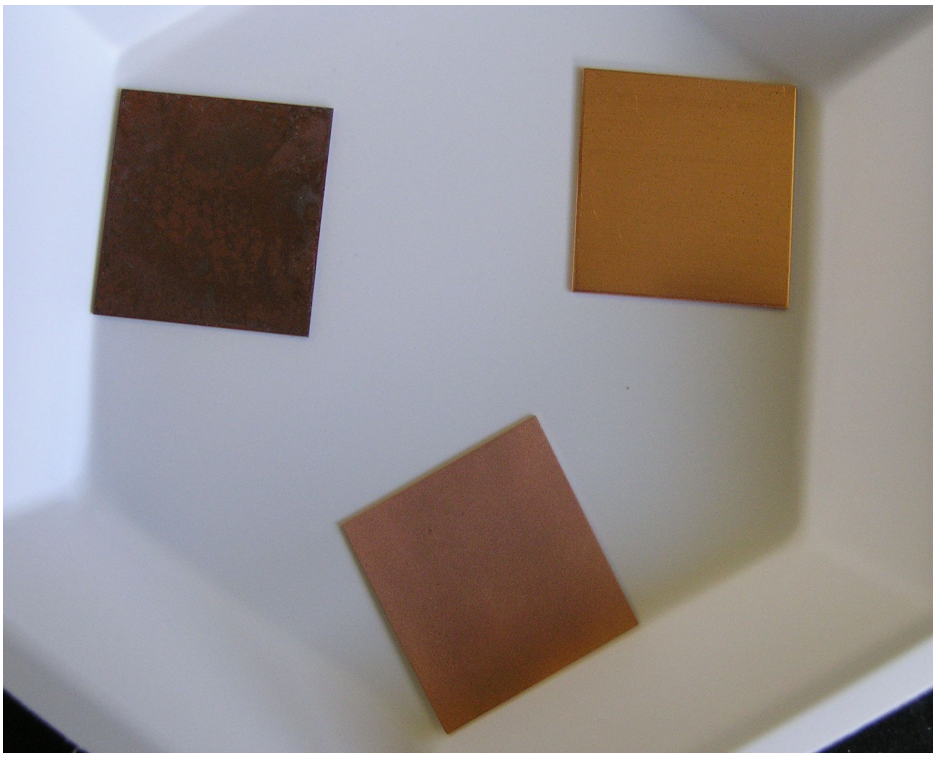


Figure 18. Copper samples before abrasion (right), after abrasion (center) and after dip baking (left).

## Encapsulation

Two plexiglass plates 1.5 inch x 1.5 inch x 0.15 inch were used for clamping the Fractor. These plates had one 0.2 inch in diameter in the center for allowing electrical connection. The upper plate had 4 untapped while the lower plate had 4 tapped threaded holes 0.15 inches in diameter at the four corners inserting screws. Two plain copper plates 1 inch x 1inch were glued to the plexiglass plates and were given electrical contact by connecting copper wires to them using conductive epoxy.

After final baking the abraded and coated plate was placed between the assembled plates and the screws were tightened diagonally to ensure equal pressure. A plastic stick tape was wrapped around the open edges of the assembly to ensure enclosure. Figure 19 shows the block diagram of the Fractor. Figures 20 and 21 show the encapsulation and the end product of a Fractor.

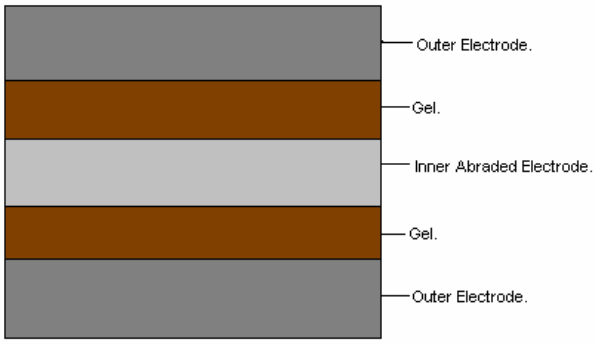



Figure 19. Block diagram of a Fractor.

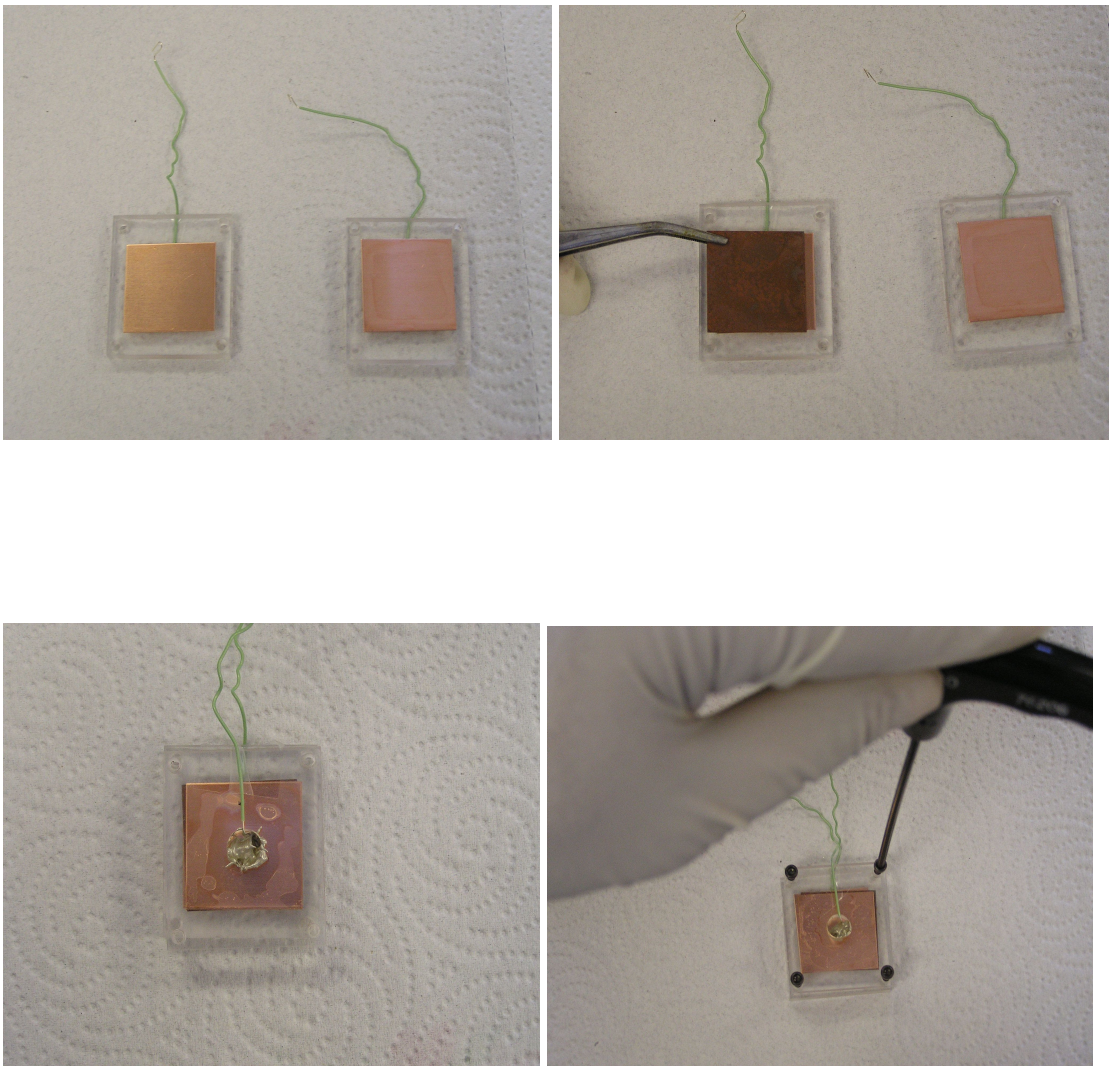


Figure 20. Encapsulation of the Fractor.

Two plain copper electrodes were glued on to a plexiglas plate to act as electrodes. The baked fractal plate was placed between the two electrodes and was assembled using screws to develop the “Fractor” device shown below (figure 19).

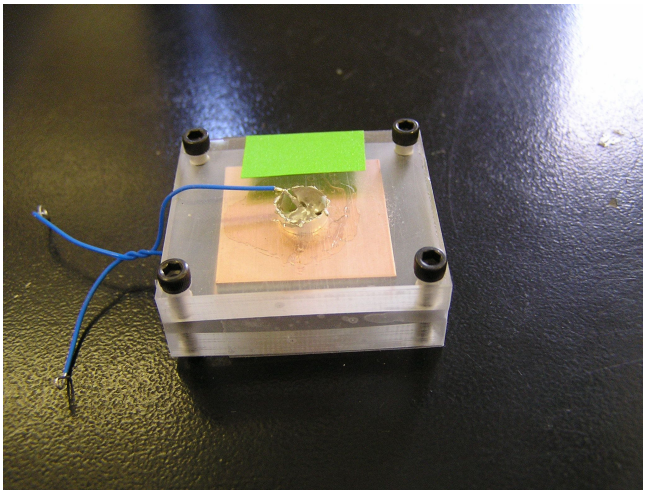


Figure 21. The Fractor.

## Experimental Parameters

During manufacture of the Fractor, a select set of parameters were experimented with.

a) Different metals: Copper (Cu) 110 alloy, Aluminum (Al) 3003 alloy and Stainless Steel (St) 430 alloy were the different metals used for the middle abraded electrode. The main intention behind this variation was to produce surfaces with different roughness and observe their effect on the Fractor response.

b) Different grit size: Grits of 80(coarse), 120(medium) and 180 (fine) mesh were used to produce different roughness structures on the metals.

c) Different grit blasting pressures: The pressure of the compressed nitrogen used for blasting was varied between 40 psi and 80 psi. This assured different indentations on the metal surfaces.

## Nomenclature

The Fractors were named according to their manufacturing parameters for easy identification.

The format used was PPS-MMNN

where

PP- Grit blasting pressure in psi (40 psi or 80 psi)

S – Grit size (C-coarse, M- medium, F – fine)

MM- Metal (Cu- copper, Al- aluminum, St- steel)

NN – Sample number (01, 02, 03 or 04)

E.g. NK-40C-Al01 means a Fractor prepared by blasting aluminum at 40 psi with coarse grit and is sample number 01.

## GENERAL PHASE IMPEDANCE ANALYSIS OF VARIOUS FRACTORS

Fractors were manufactured using different experimental variables mentioned in the sample preparation. The response of these Fractors was analyzed using the Bode phase (Phase angle vs. Log frequency) and Bode impedance plots (Log impedance magnitude vs. Log frequency) which can fully characterize the Fractor.

### Experimental Setup

The Fractor was connected to an impedance analyzer (m/c name: Wayne Kerr precision component analyzer 6430B). An impedance analyzer is used to conduct electrochemical impedance spectroscopy measurements by applying sinusoidal potential frequencies across the Fractor electrodes. The response from the Fractor (of impedance and phase angle) was computed by the analyzer. The analyzer was connected to a computer for data storage and display via a General Purpose Interface Bus (GPIB). A software program has been used to acquire the data, display it and store it in the form of an excel spreadsheet. Figure 22 shows the impedance analysis setup of the Fractor.




Figure 22. Setup of impedance analysis.

## Impedance Analysis Process

The frequency of analysis was varied, starting from 500 kHz and stepping down to 20Hz with a constant amplitude peak to peak voltage of 0.2V. Before displaying the result at any frequency, the Fractor was automatically analyzed 8 times and the data gained was averaged by the instrument. This was done for frequencies from 500 kHz to 20Hz decreasing in logarithmically spaced steps. The resulting data was impedance magnitude and phase angle at each frequency.

## The Conductive Breakthrough

This phenomenon is seen in the Fractor when the two metal electrodes, the smooth and the abraded, of the Fractor break through the gel in between to touch each other. This results in direct metal to metal conduction making the impedance go really low and the Fractor totally resistive. This happens when the Fractor is subjected to loading or extreme thermal variation which makes the gel in between crack resulting in contact of the metal surfaces. Figure 23 shows how conductive breakthrough takes place. This also happens when the surface is abraded by relatively fine SiC particles. Thus there is not much space for the gel to seep into. So during the drawing, the gel gets off the surface resulting in metal - metal contact in the Fractor upon encapsulation. Conductive renders the Fractor ineffective by turning it into a pure resistor.

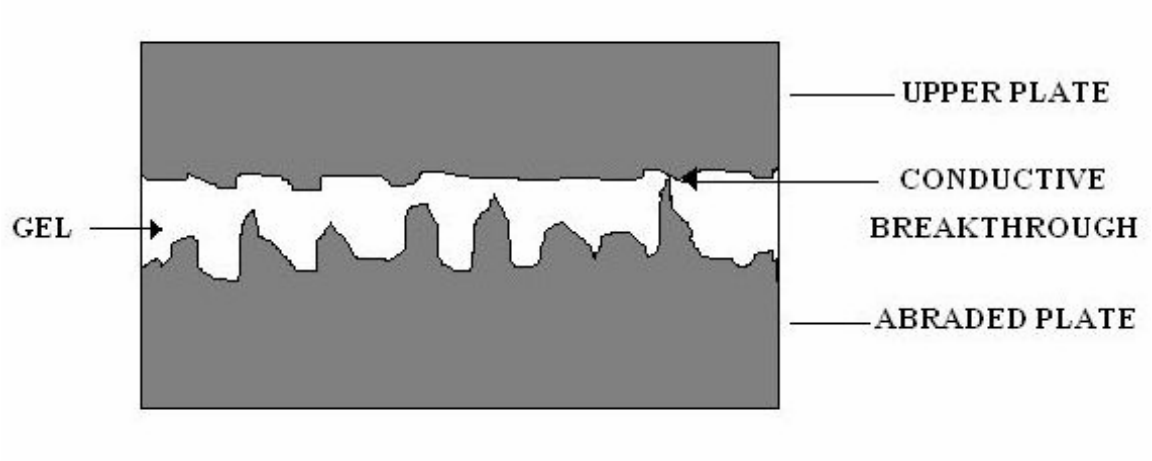



Figure 23. Conductive Breakthrough.

Non-Lithium Gel Fractor

Lithium (Li) is the most consequential chemical in the Fractor performance. The Lithium ions constitute to the ionic flow in the Fractor. They act as charge carriers and flow from the flat electrode plate to the rough one and vice versa on application of AC current.

In the absence of Li ions, there will be no charge flow. This will be lead to very low resistance and very high capacitance. On the whole, in the absence of Li ions, the phase angle should drop to about 90° indicating capacitive nature and the impedance should rise very high.

To test this theory, three non- lithium samples were manufactured. One from aluminum, copper and steel each. The manufacturing combination used was fine grit

blasting at 40 psi. The gel used for this process was made using the same technique described before but this time no lithium nitrate was added to the solution. This made the gel Li ion free. The roughened plates were dipped in this gel and baked using the normal process. They were then encapsulated between two copper electrodes to create a Fractor.

The steel Fractor showed breakthrough due to the reasons mention before. The other two Fractors exhibited interesting results.

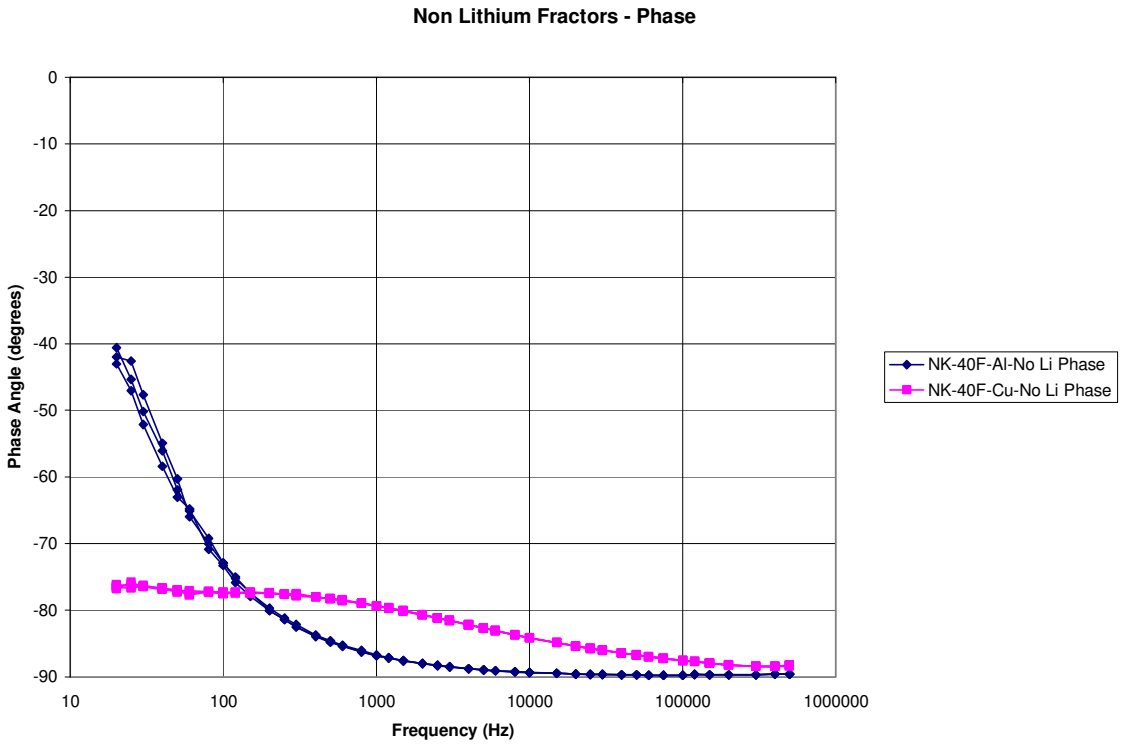



Figure 24. Non lithium Fractors – phase plot.

The figure 24 shows the phase of the two non-lithium Fractors over a frequency range from 20 Hz to 500 kHz.

The NK-40F-Al-No Li Fractor shows phase angle of about 41° to 43° at the frequency of 20 Hz and starts to drop steeply as the frequency increases. This indicates that its not capacitive in nature at lower frequencies but tends to be capacitive. As it gets past 100 Hz, it becomes more capacitive with phase angle getting closer to 90°. After 1000 Hz, the phase angle becomes 90° till the highest frequency of 500 kHz. This indicates that the Fractor has turned totally capacitive.

The NK-40F-Cu-No Li Fractor demonstrates an angle of 77° at 20 Hz suggesting its capacitive nature at low frequencies. As frequency increases it becomes increasingly capacitive element. At higher frequencies between 100 kHz to 500 kHz, the Fractor touches a phase of about 88°.

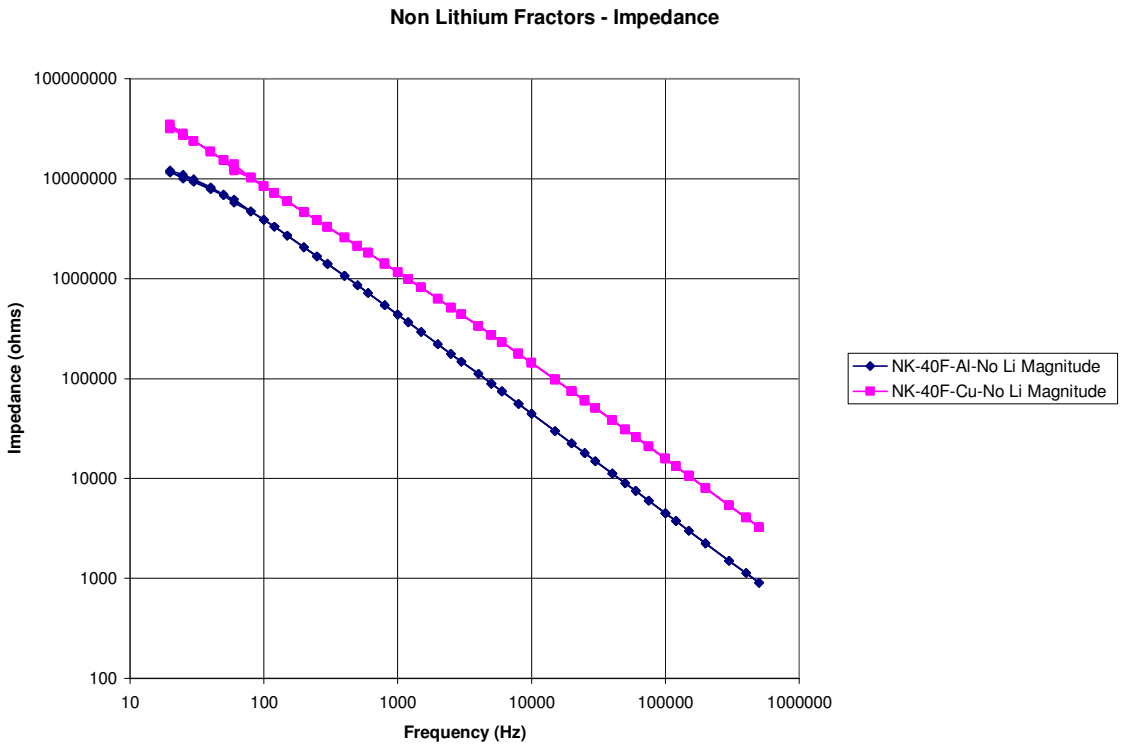



Figure 25. Non lithium Fractors – impedance plot.

Figure 25 shows the impedance of the two non-lithium Fractors over a frequency range from 20 Hz to 500 kHz.

The NK-40F-Cu-No Li displays extremely high impedance of 34.98 x $10^6$ ohms at low frequency of 20 Hz. Its impedance of 3248 ohms at 500 kHz is also termed very high for a Fractor at that frequency.

The NK-40F-Al-No Li impedance is slightly beneath the NK-40F-Cu-NoLi impedance. It has an impedance of 11.782 x $10^6$ ohms at 20 Hz and of 900 ohms at 500 kHz.

The above capacitive phase angle and high impedance behaviour at different frequencies can be rationalized by the absence of Li ions. This supports the theory constructed above that the Li ions are responsible for the ideal behaviour of the Fractor.

## Steel Fractors Phase Impedance Analysis

Steel Fractors of different manufacturing combinations were used for this data analysis.

Figure 26 shows the phase angle V/S the frequency for variation in the experimental parameters for steel Fractors. The NK-40F-St02 shows breakthrough at all frequencies. It becomes totally resistive. The fine grit doesn't seem to have inflicted sufficient roughness in the steel surface for the Li gel to seep into. Thus on baking the gel solidified only on the surface and then, on tightening the screws broke apart giving the breakthrough.

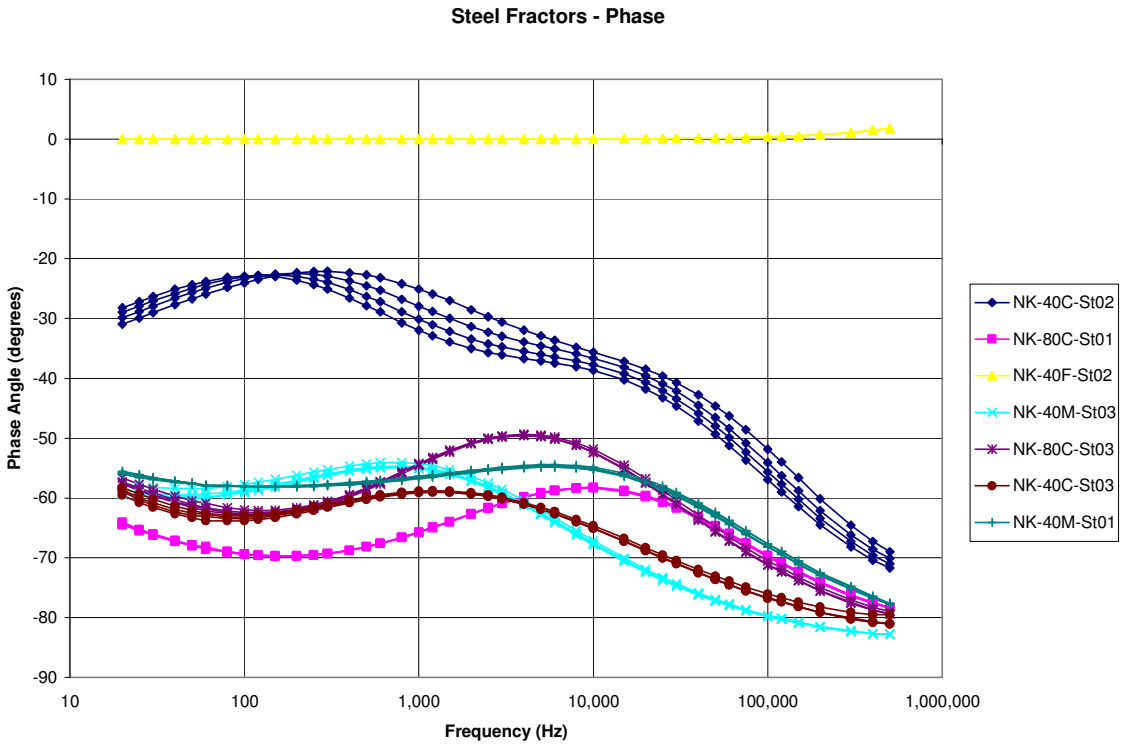



Figure 26. Steel Fractors comparison – phase plot.

All the 3 Fractors manufactured using these parameters showed resistive breakthrough behaviour.

The NK-40C-St02 phase line stands out due to its higher phase compared to others. But the NK-40C-St03, made using the same parameters lies with the others in the range of -55° to -65° at frequency of 20Hz and -75° to -85° at the higher frequency of 500 kHz.

The Fractors manufactured using other parametric combinations also lie in the same range and do not show any distinct difference. There is fluctuation in the phase

angle in the mid frequencies of 1000 Hz to 100 kHz but none can be identified as a trend of any specific parametric combination mentioned before .

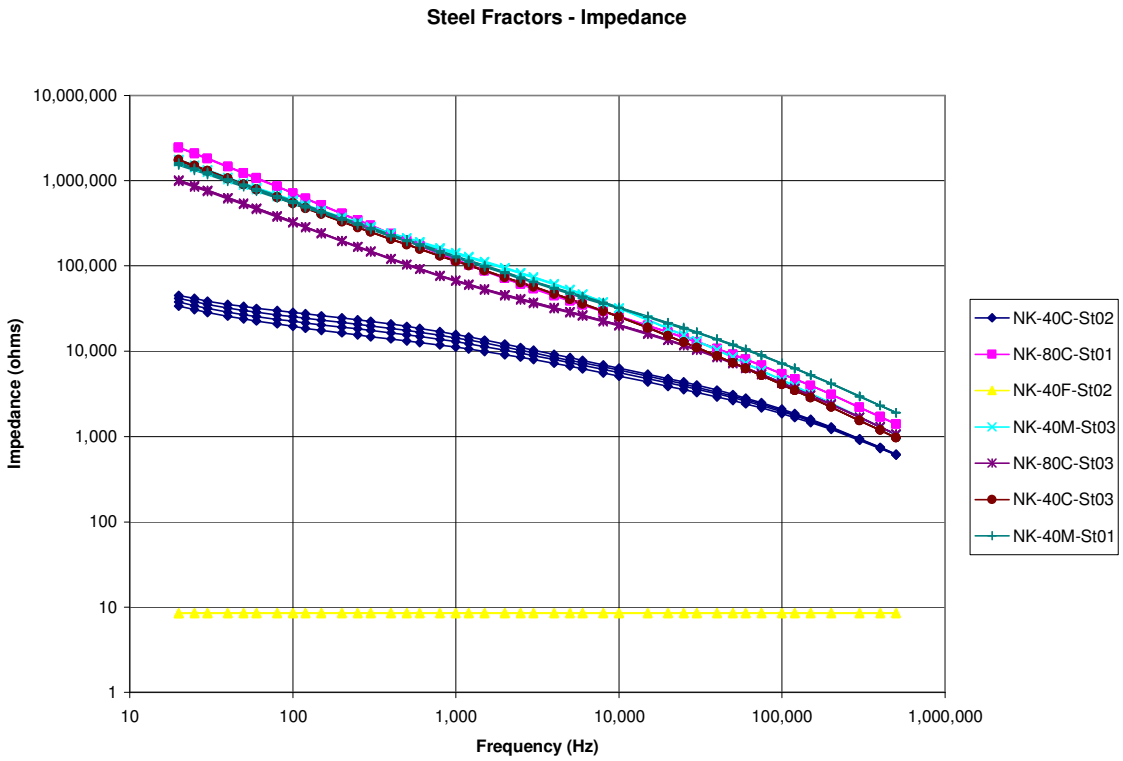



Figure 27. Steel Fractors comparison – impedance plot.

Figure 27 shows the impedances of steel Fractors manufactured using varying combinations at various frequencies.

The NK-40F-St02 shows same impedance for all frequencies because of breakthrough. Thus, this impedance is purely resistive.

The NK-40C-St02 exhibits much lower impedance than other Fractors. At 20 Hz, it shows impedance of 42000 ohms and at 500 kHz, of 620 ohms. In contrast, NK-40C-St03 of the same parametric combination shows impedance of 1561000 ohms at 20Hz

and 960 ohms at 500 kHz. Thus it can't be conclusively said that the 40C-St combination reduces the impedance.

The rest of the Fractors with different manufacturing combinations closely follow the NK-40C-St03 impedance line.

## Aluminum Fractors Phase Impedance Analysis

Aluminum Fractors with variations in manufacturing parameters were compared to evaluate the effect on the electronic response.

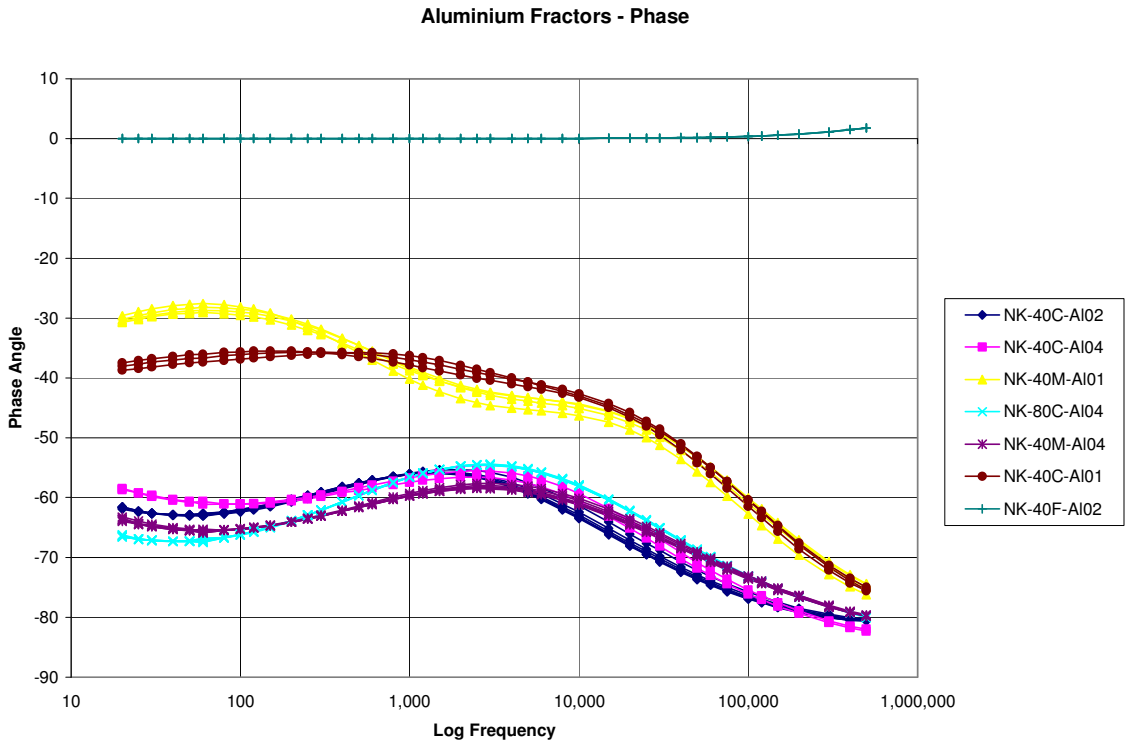



Figure 28. Aluminum Fractors comparison – phase plot.

Figure 28 shows the phase angle V/S the frequency for variation in the experimental parameters for aluminum Fractors. The NK-40F-Al02 shows breakthrough at all frequencies and becomes totally resistive. The fine grit doesn't seem to have inflicted sufficient roughness on the steel surface for the Li gel to penetrate into. Thus on baking the gel solidified only on the surface and then, on tightening the screws broke apart. This gave the breakthrough. All the 3 Fractors manufactured using these parameters showed resistive breakthrough behaviour.

The NK-40C-Al01 and NK-40M-Al01 phase lines stand out due to their higher phase compared to others. This may be due to excessive tightening of the Fractor screws leading to the compression effect (addressed later in the thesis) which results in lifting the phase angle up. But the NK-40C-Al02 and NK-40C-Al04, made using the same parameters as NK-40C-Al01 lie in the range of -58° to -62° at frequency of 20Hz and -78° to -82° at the higher frequency of 500 kHz. This seems to suggest that the experimental parameters don't produce any specific trend.

The Fractors manufactured using other parametric combinations also lie in the same range and do not show any distinct difference. There is negligible fluctuation in the phase angle in the mid frequencies of 1000 Hz to 100 kHz but none can be identified as a trend of any specific parametric combination. Thus the phase of the aluminum Fractors was in the required range when the indentations made by the various combinations were sufficient.

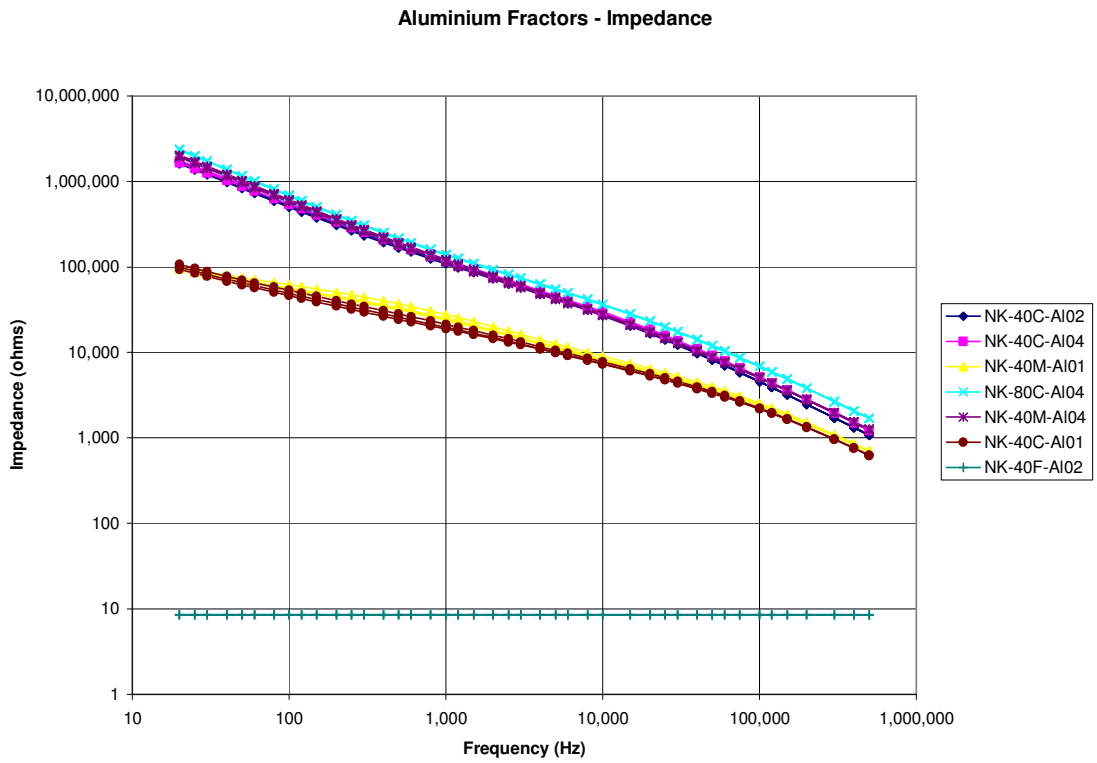



Figure 29. Aluminum Fractors comparison – impedance plot.

Figure 29 shows the impedances of aluminum Fractors manufactured using varying combinations at various frequencies.

The NK-40F-Al02 shows same impedance for all frequencies because of breakthrough. Thus, this impedance is purely resistive.

The NK-40M-Al01 and NK-40C-Al01 exhibits much lower impedance than other Fractors possibly due to accidental excessive tightening of screws more than other samples (as the tightening of the screws is manual and might results in some error). At 20 Hz, NK-40M-Al01 shows impedance of about 99310 ohms and at 500 kHz, of 690

ohms. In contrast, NK-40M-Al04 of the same parametric combination shows impedance of 2027750 ohms at 20Hz and of 1257 ohms at 500 kHz.

The impedances of NK-40C-Al01 are 93098 ohms at 20 Hz and 625 ohms at 500 kHz. The NK-40C-Al02 and NK-40C-Al04 have impedances of 1649600 ohms and 1755850 ohms respectively. Whereas at 20 Hz the impedances are 1056 ohms and 1257 ohms Thus it can't be conclusively said that the 40C-Al or the 40M-Al combination reduces the impedance.

The rest of the Fractors with different manufacturing combinations closely follow the NK-40C-Al02 and NK-40C-Al04 impedance line.

## Copper Fractors Phase Impedance Analysis

Copper Fractors with variations in manufacturing parameters were compared to evaluate the effect on the electronic response

Figure 30 shows the phase angle V/S the frequency for variation in the experimental parameters for copper Fractors. The NK-40F-Cu02 shows the highest phase till 1000 Hz and then dips down. This is very different than the other medium grit blasted metal Fractors as they all show breakthrough at all frequencies and becomes totally resistive. The fine grit seems to have abraded the copper surface with sufficient roughness for the Li gel to seep into. Thus on baking the gel solidified inside the rough crests to give the current response. Out of the 3 Fractors manufactured using these parameters, one showed resistive breakthrough behaviour.

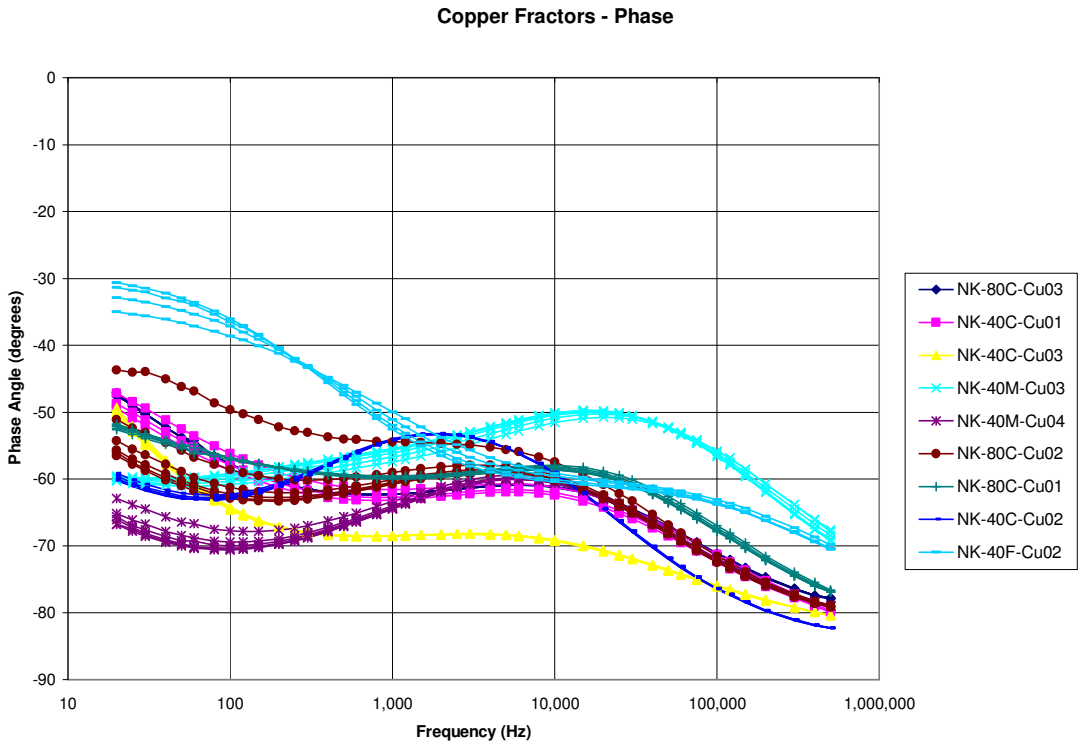



Figure 30. Copper Fractors comparison – phase plot.

As can be seen from the graph, the 80C-Cu Fractors have slightly different frequencies at 20 Hz and narrow down to nearly the same frequency at 500 kHz. However they are consistently close to each other in the mid frequencies of 1000 Hz to 100 kHz.

The 40C – Cu Fractors show a different trend. They start off at different frequencies and divert substantially at mid frequency range. The NK-40C-Cu02 phase bumps up, the NK-40C-Cu03 falls down while the NK-40C-Cu01 remains reasonably flat. The phases narrow down at 500 kHz with a difference of 6° to 8°.

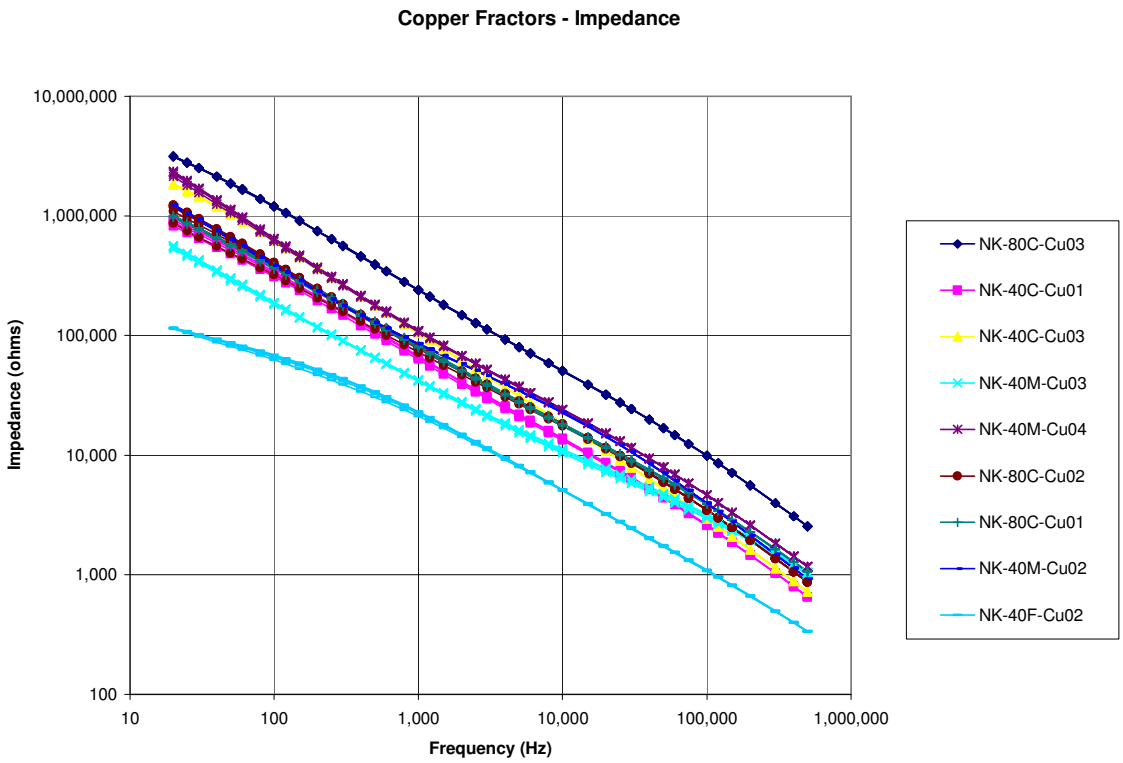



Figure 31. Copper Fractors comparison – impedance plot.

Figure 31 shows the impedances of copper Fractors manufactured using varying combinations at various frequencies.

The NK-40F-Cu02 shows the lowest impedance for all frequencies. The NK-80C-Cu03 impedance is the highest at all frequencies.

NK-40M-Cu04 impedance is the second highest closely followed by NK-40M-Cu02. The NK-40M-Cu03 impedance is the second lowest at all frequencies. Thus we can't claim that 40M-Cu combination reduces the impedance.

The other NK-80C-Cu Fractors nearly overlap from the lowest to highest frequency and lie in the middle part of the impedance lines. So the 80C-Cu combination doesn't set a trend either.

The impedance of NK-40C-Cu Fractors lies below the NK-80C ones. They are consistent with each other throughout the frequency range.

## Results of Variation in Manufacturing Parameters of the Fractor

It can be seen for each of the steel, aluminum and copper Fractors that the 80C, 40C or 40M manufacturing variations do not have any specific effect on the electronic response. In some cases, a single Fractor with a specific manufacturing configuration shows some rise or fall in phase or impedance but the hypothesis that this configuration sets forth a trend doesn't hold true as a Fractor made of similar configuration contradicts it. For example NK-40C-St03 proves that the phase rise in NK-40C-St02 is not due to its manufacturing parameters by displaying much lower phase.

Thus we can conclude that one specific combination of the above mentioned parameters does not show any rise or fall in the phase angle or the impedance.

It can also be seen that for the above combinations, the phase angles and impedances of the three different metals are not very different. In fact, it can be said that the phase angle and impedance are not related to the metal types once sufficient indentations are achieved. So, coarse and medium grit SiC at the pressure of 40 psi to 80 psi can indent sufficiently deep abrasions in the three metals to make the electronic response similar.

In case of the 40-F manufacturing parameters, the case is a bit different. 2 out of 3 40F-copper Fractors provided some response whereas all the 3 Fractors made from aluminum and steel each showed breakthrough. This happens as the copper turns out to be a relatively softer metal than the other two. The 40F creates deeper crests and prominent peaks in copper into which the gel can penetrate before baking. Thus it can display better response than steel or aluminum. Whereas for the other two metals, due to finer grit and increase in hardness, indentations are less. So there is not much space for the gel to seep into during the manufacture. So during the drawing of the abraded plate from the gel, it gets off the surface resulting in metal - metal contact in the Fractor.

So, we conclude that at fine grit SiC abrasion at 40M may not make enough indentations in each case of aluminum and steel metals to give electronic responses.

# STRESS RELAXATION AGING

The effect of stress and aging was tested on the Fractor. The 4 screws on the Fractor were tightened by one rotation each. The tightening was done diagonally to assure equal distribution of the stress. This ensured that the Fractor was under compressive stress. Readings were taken before tightening and after tightening. To monitor the relaxation effect of the Fractor, its response was monitored after 7 days and 14 days. The process of degradation of the Fractor response over a span to time due to relaxation is termed as “Aging”.

## Concept

The tightening of the screws reduced the interfacial gap between the gel and the abraded electrode. This leads to increase in the exposed area and decrease in interfacial distance between the metal gel. This results in the overall impedance. Over a period of time, the reaction forces of gel- electrode relax the magnitude of compression on the system thus lowering the pressure and increasing the gap between the interfaces. This leads to increase of the impedance back to near normal and recovery near to the phase angle.

Apart from this, there are some changes that cannot be explained and can be associated to the over relaxation and microstructure of the material.

This test was performed on three Fractors of different metals and configuration.

Aluminum Fractor

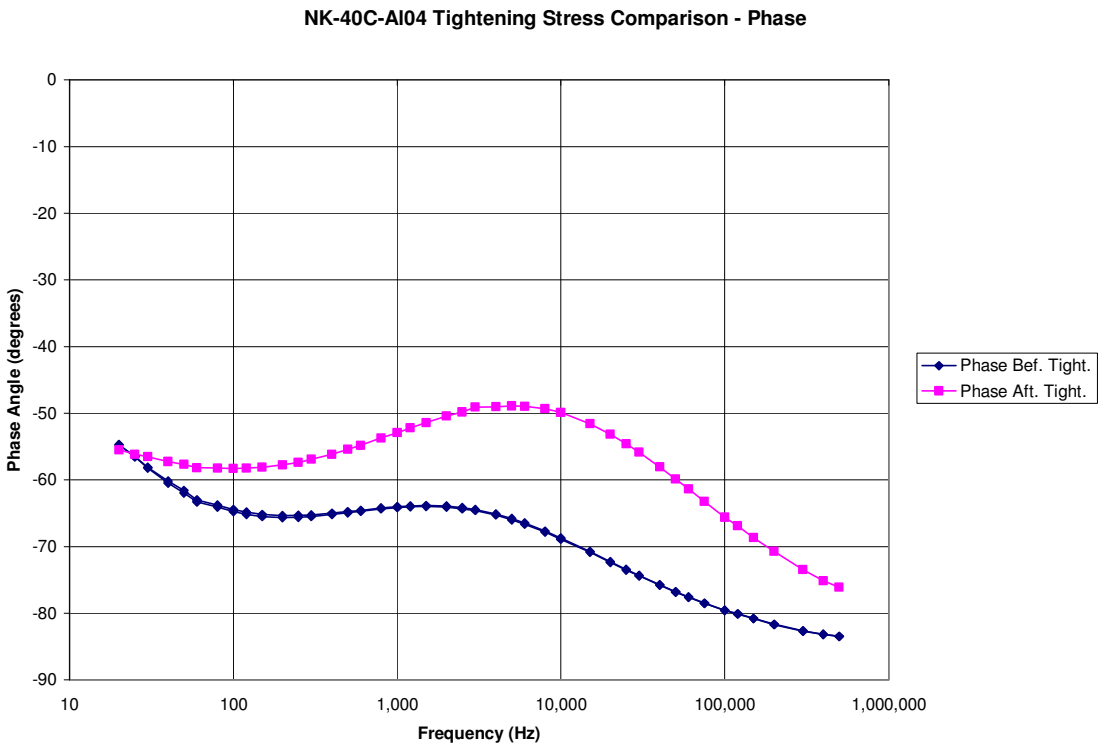



Figure 32. Aluminum Fractor stress tightening comparison – phase plot.

Figure 32 shows the variation in the phase angle upon application of stress over a frequency range for the Fractor NK-40C-Al04 by tightening the screws.

The phase after tightening seemed to have lifted up from the phase before tightening (the initial phase). Both curves coincide at 20 Hz, but drift apart as the frequency increases. At 500 kHz, the after tightening phase drifts above the initial by about 9°. The maximum deviation of 18° is at 10 kHz.

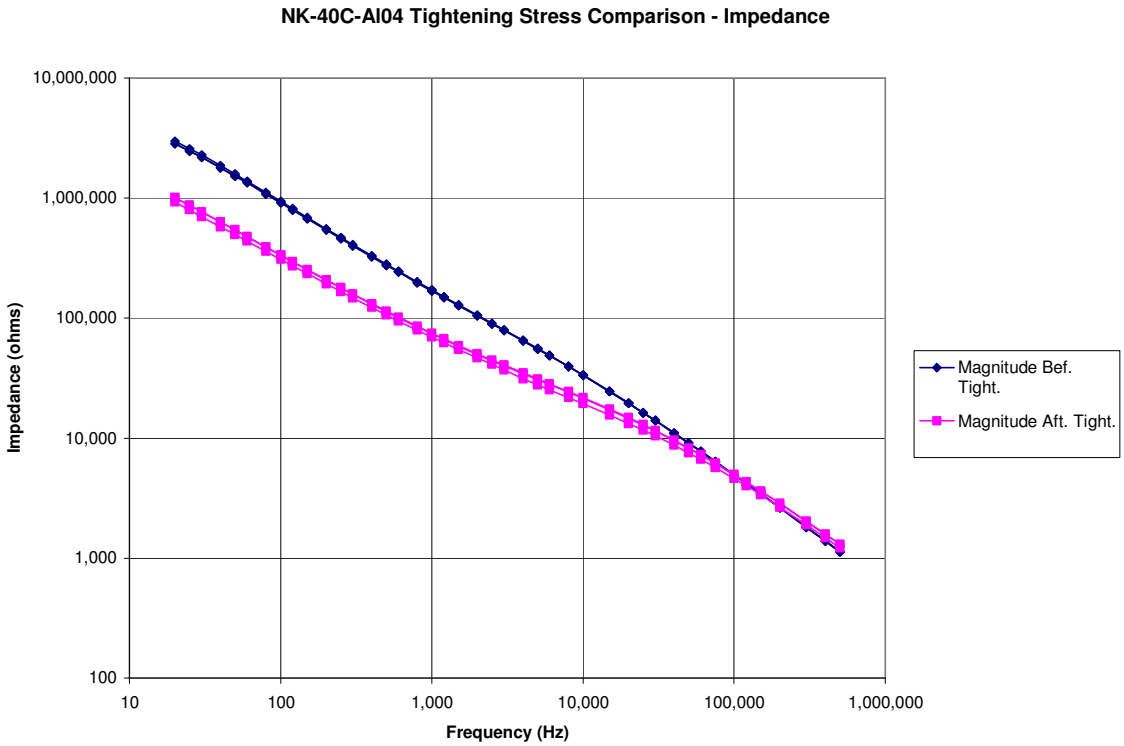



Figure 33. Aluminum Fractor stress tightening comparison – impedance plot.

Figure 33 shows the variation in the impedance upon application of stress over a frequency range for the Fractor NK-40C-Al04.

The after tightening impedance drops below the initial at a frequency of 20Hz and continues this behaviour till about 100 kHz where it coincides with the other till 500 kHz. The maximum deviation of $1.83 \times 10^6$ ohms is at 20 Hz.

Thus we can see that in this particular case, the general effect of stress due to tightening is to lift up the phase and to lower the impedance.

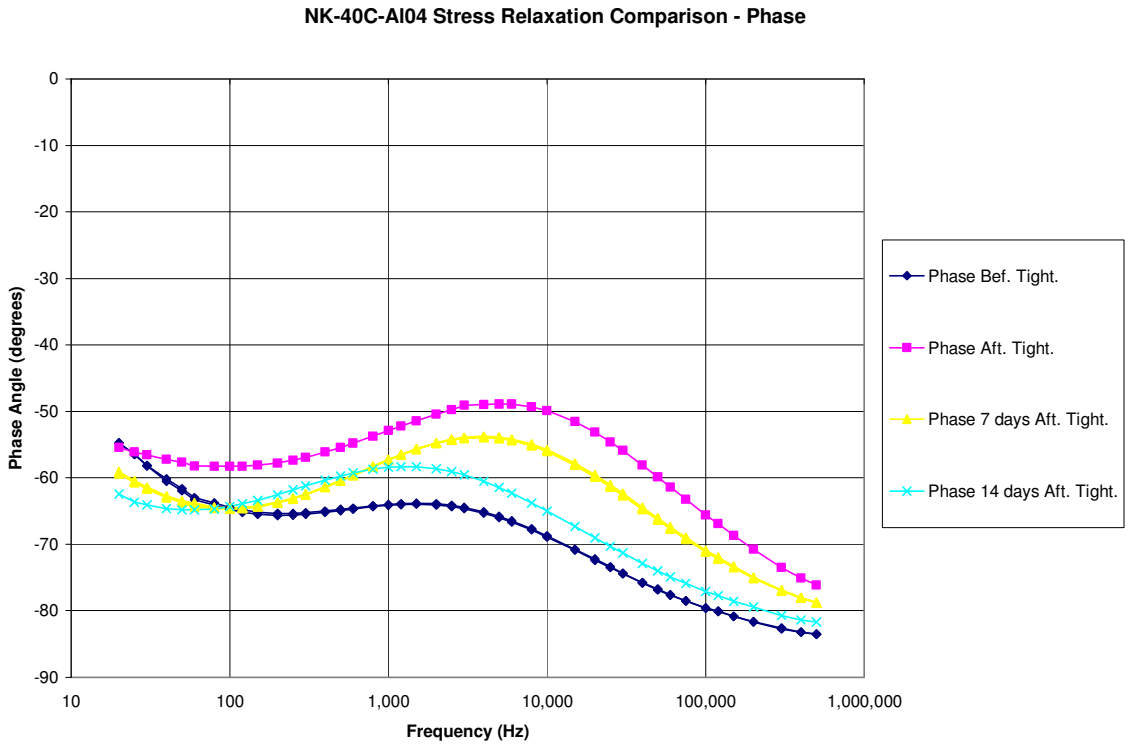



Figure 34. Aluminum Fractor stress relaxation comparison – phase plot.

Figure 34 shows the variation in the phase for different time spans over a frequency range for the Fractor NK-40C-Al04. This is the effect of relaxation- aging on the phase angle.

The after 7 days phase seems to drops the after tightened phase indicating that the tension in the Fractor is relaxing gradually. The after 14 days phase seems to drop even lower than the after 7 days one especially in the higher frequency range indicating its tendency to revert to the original phase. At the 20 Hz to 100 Hz range though, the phase seems to be slipping below the initial phase which can be attributed to slight change in the material chemistry

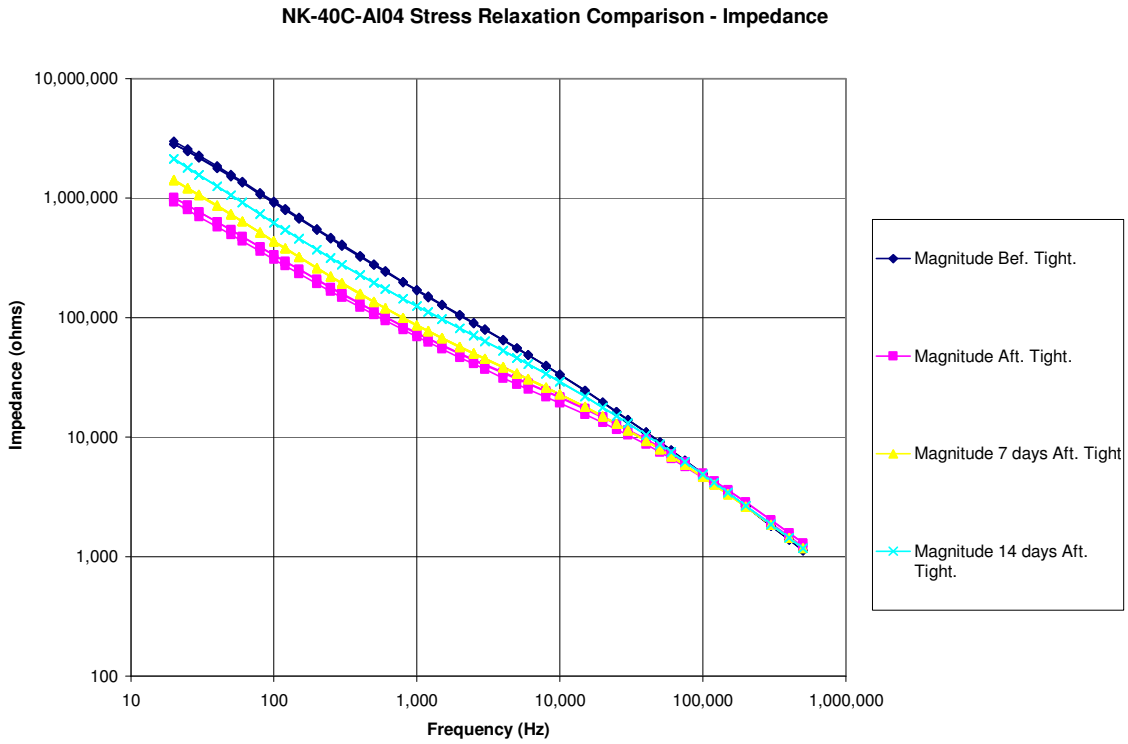



Figure 35. Aluminum Fractor stress relaxation comparison – impedance plot.

Figure 35 shows the variation in the impedance for different time spans over a frequency range for the Fractor NK-40C-Al04. This is the effect of relaxation aging on the magnitude of impedance.

The graph shows that the impedance after tightening drops below the initial before tightening one at lower frequencies and remains the same at higher frequencies. The impedance after 7 days rises a bit above the impedance after tightening. While the impedance after 14 days rises significantly, heading towards the initial impedance. There is not a noticeable variation in the impedances in the electronic high frequency range.

Copper Fractor

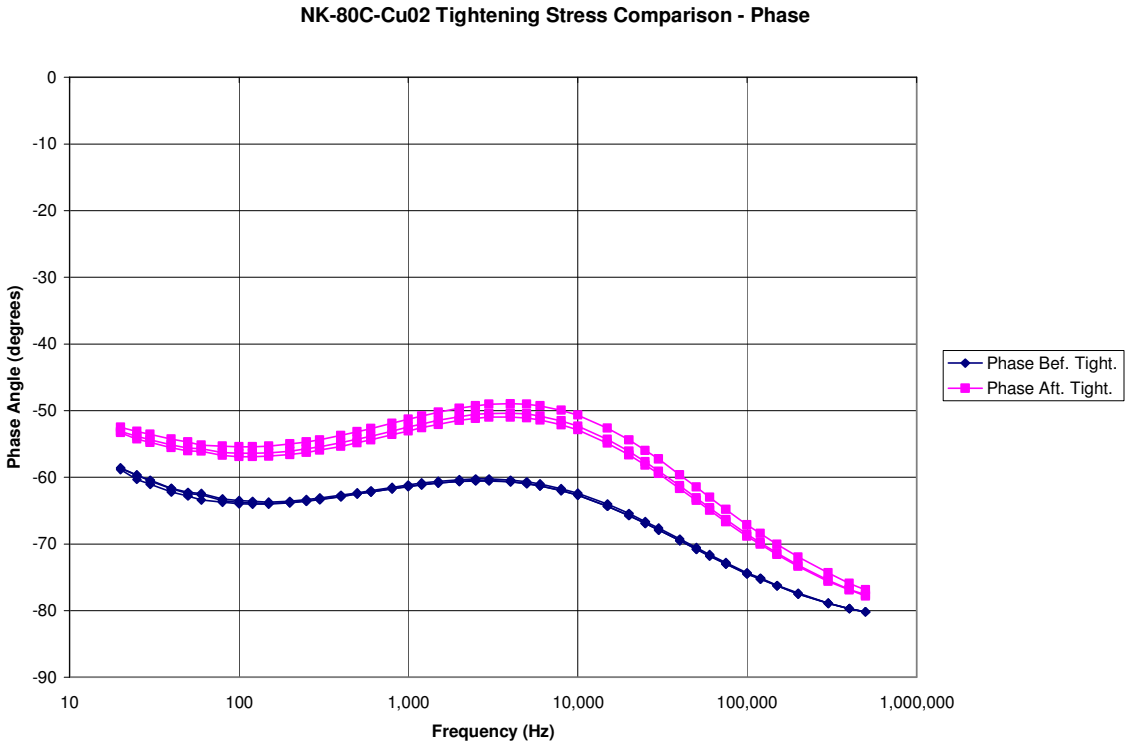



Figure 36. Copper Fractor stress tightening comparison – phase plot.

Figure 36 shows the variation in the phase angle upon application of stress over a frequency range for the Fractor NK-80C-Cu02.

The phase after tightening has lifted up from the phase before tightening (the initial phase). At 20 Hz the phase change is about 5° while at 500 kHz, the after tightening phase drifts above the initial by about 3°. There is a steady phase gap of about 10° between 100 Hz and 100 kHz.

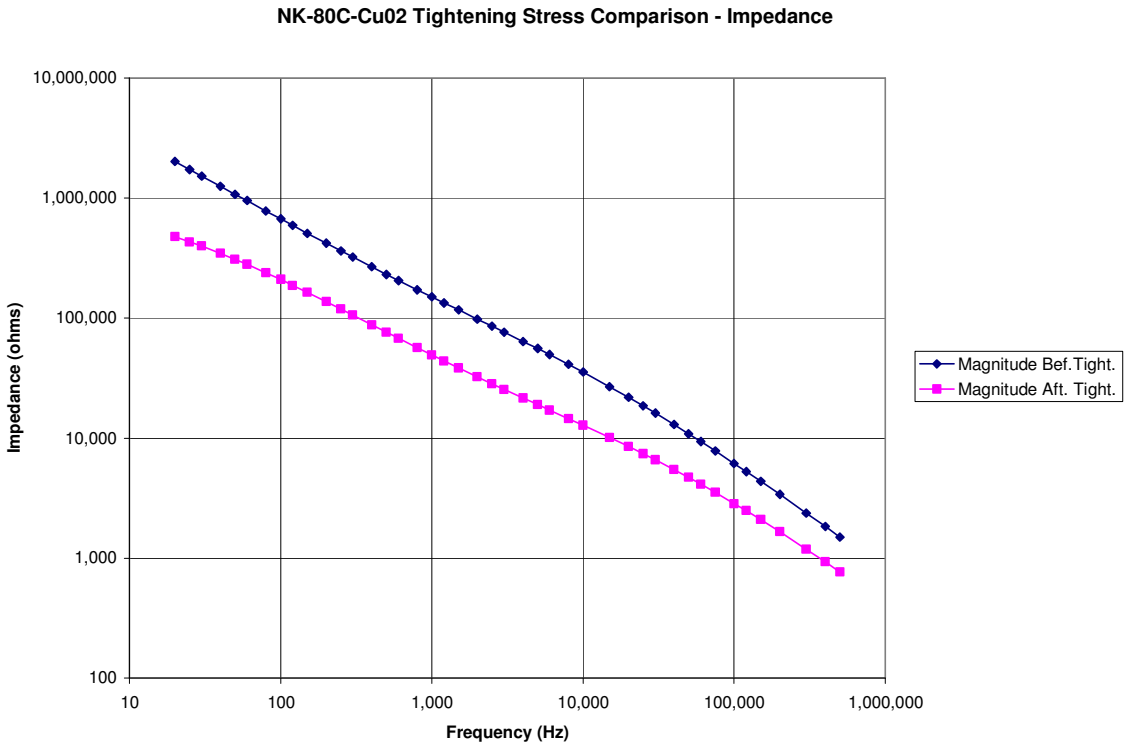



Figure 37. Copper Fractor stress tightening comparison – impedance plot.

Figure 37 shows the variation in the impedance upon application of stress over a frequency range for the Fractor NK-80C-Cu02.

As can be seen, there is a drop in the after tightening impedance, with the maximum drop of 1,500,000 ohms being at 20Hz and the minimum of 700 ohms at 500 kHz.

Thus, we can conclude for this particular case that tightening stress raises the phase above the initial and lowers the impedance below the initial. This is consistent with our hypothesis.

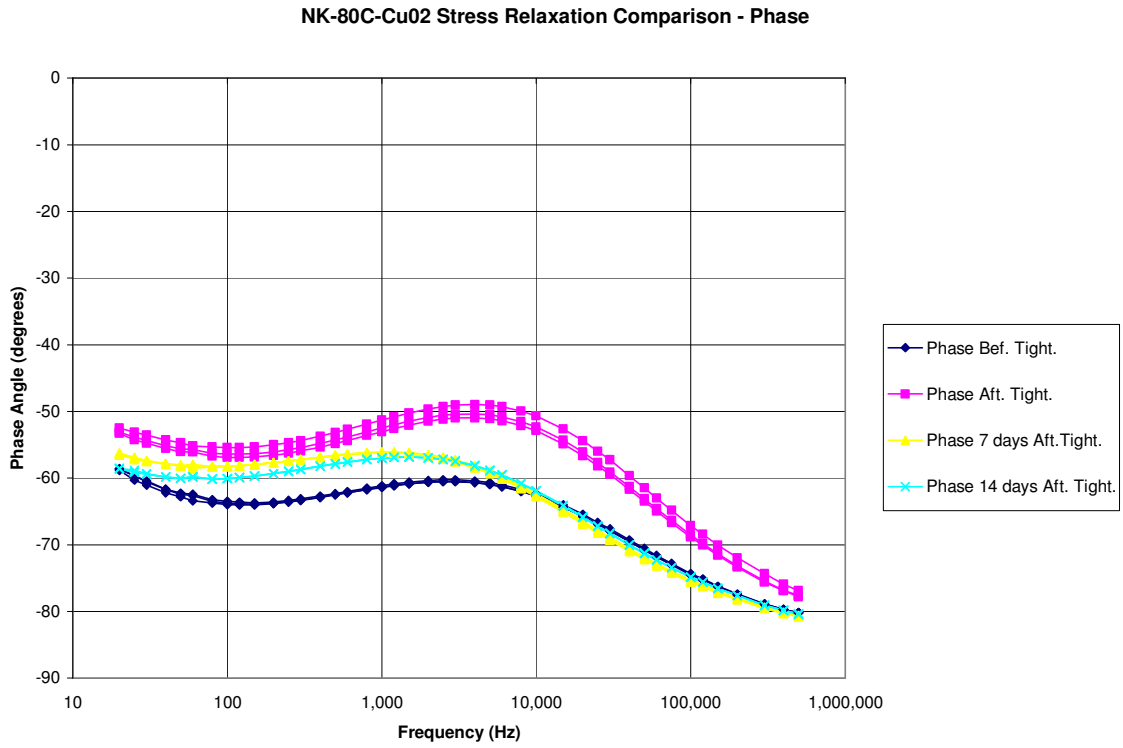



Figure 38. Copper Fractor stress relaxation comparison – phase plot.

Figure 38 shows the variation in the phase for different time spans over a frequency range for the Fractor NK-80C-Cu02. This is the effect of aging on the phase angle.

The phase after tightening shoots up above the phase before tightening as a result of the effect of stress. The Fractor was then allowed to relax over a span of time and its response was monitored. The phase after 7 days and 14 days seems to be dropping back to the initial gradually. In the higher frequency range of 10 kHz to 500 kHz, the phase seems to drop even lower than the initial. This can be plausibly explained as over relaxation in the material chemistry.

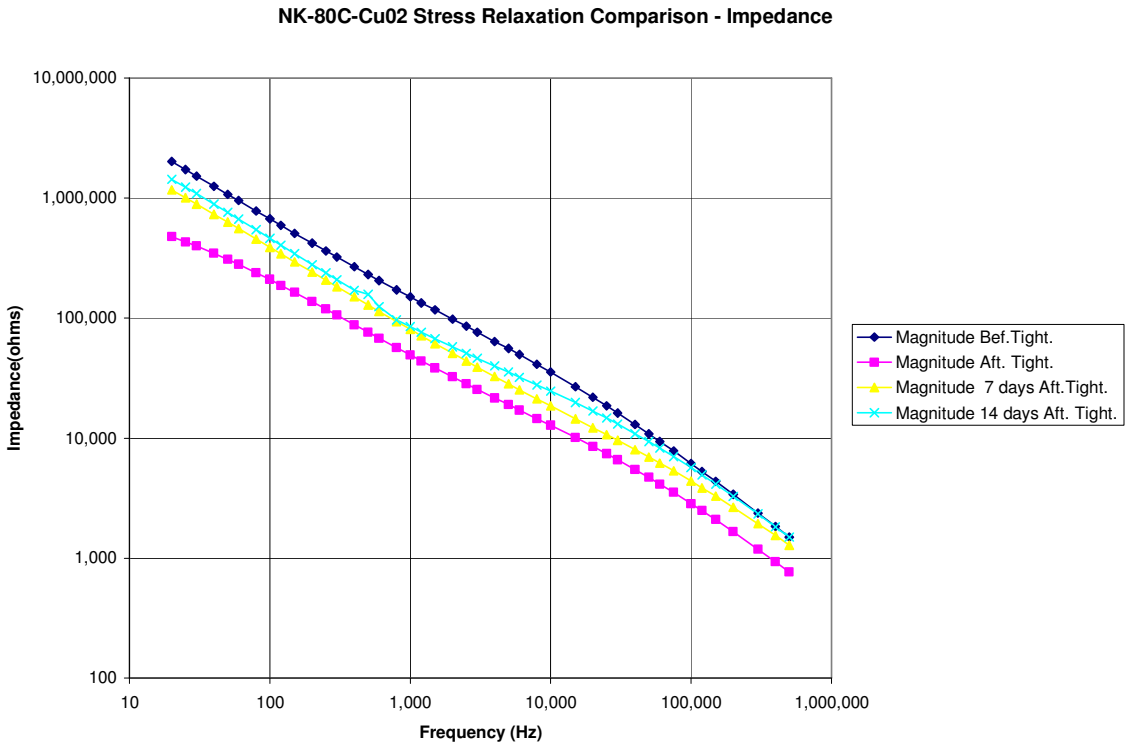



Figure 39. Copper Fractor stress relaxation comparison – impedance plot.

Figure 39 shows the variation in the impedance for different time spans over a frequency range for the Fractor NK-80C-Cu02. This is the effect of relaxation aging on the magnitude of impedance

Unlike the aluminum Fractor, there is lowering of the impedance after tightening in the lower frequency range as well as the higher frequency range. But the Fractor shows gradual recovery from 7 days to 14 days supporting our hypothesis.

Steel Fractor

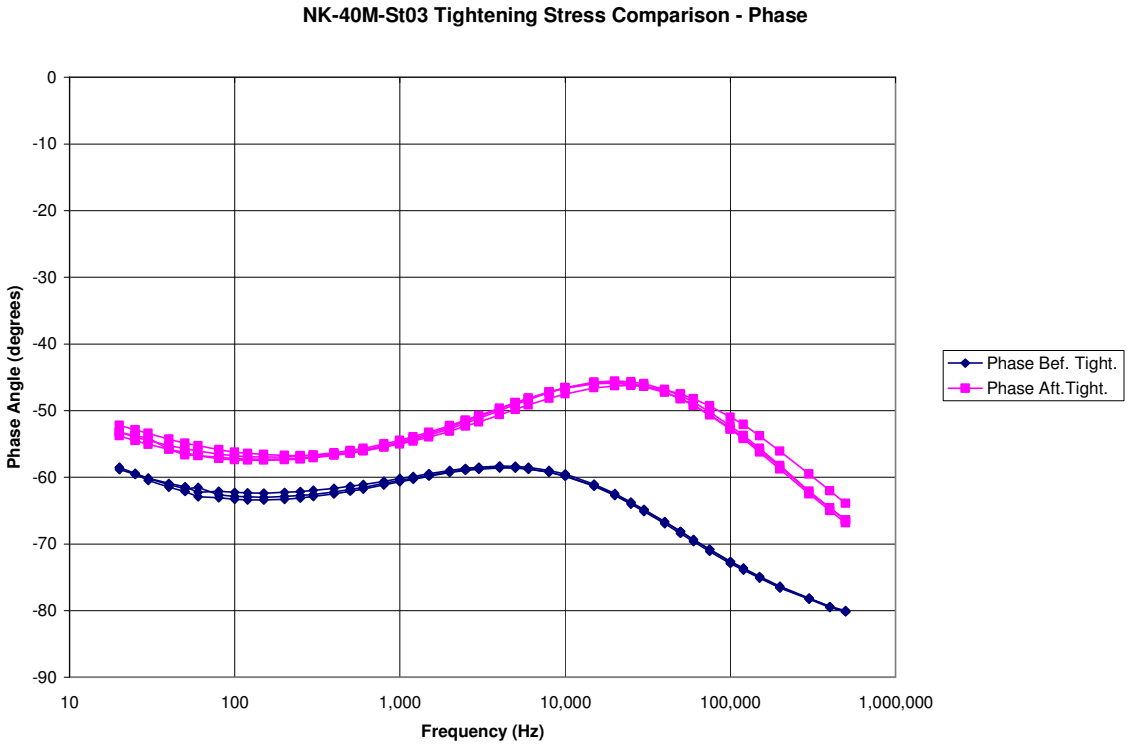



Figure 40. Steel Fractor stress tightening comparison – phase plot.

Figure 40 shows the variation in the phase angle upon application of stress over a frequency range for the Fractor NK-40M-St01.

The phase after tightening has lifted up from the phase before tightening (the initial phase). At 20 Hz the phase change is about 5° while at 500 kHz, the after tightening phase drifts above the initial by about 18°. The maximum phase gap is at 75 kHz and is of 20°.

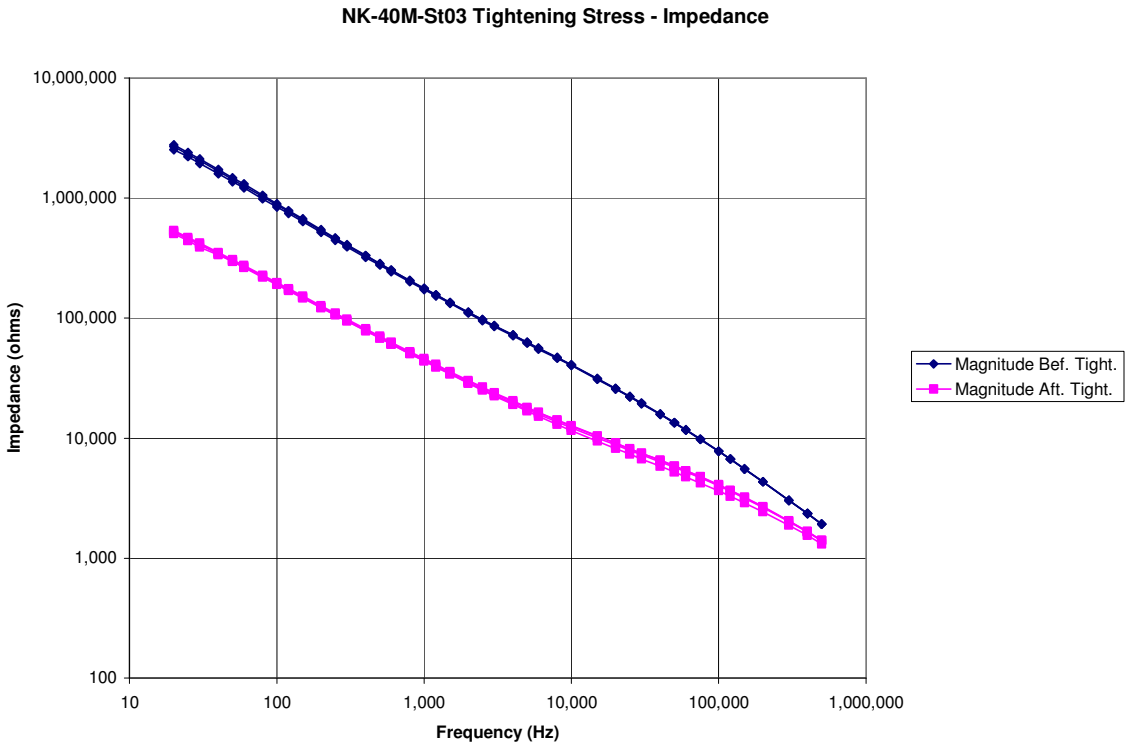



Figure 41. Steel Fractor stress tightening comparison – impedance plot.

Figure 41 shows the variation in the impedance upon application of stress over a frequency range for the Fractor NK-40M-St01.

The after tightening impedance drops below the initial at a frequency of 20Hz and continues this behaviour till the higher frequency extreme of 500 kHz. The maximum deviation of 2.04 x $10^6$ ohms is at 20 Hz while the least variation of about 525 ohms is at 500 kHz.

Thus we can observe that in this particular case, the general effect of stress due to tightening is to lift up the phase and to lower the impedance. This result matches with the results of the other Fractors tested above.

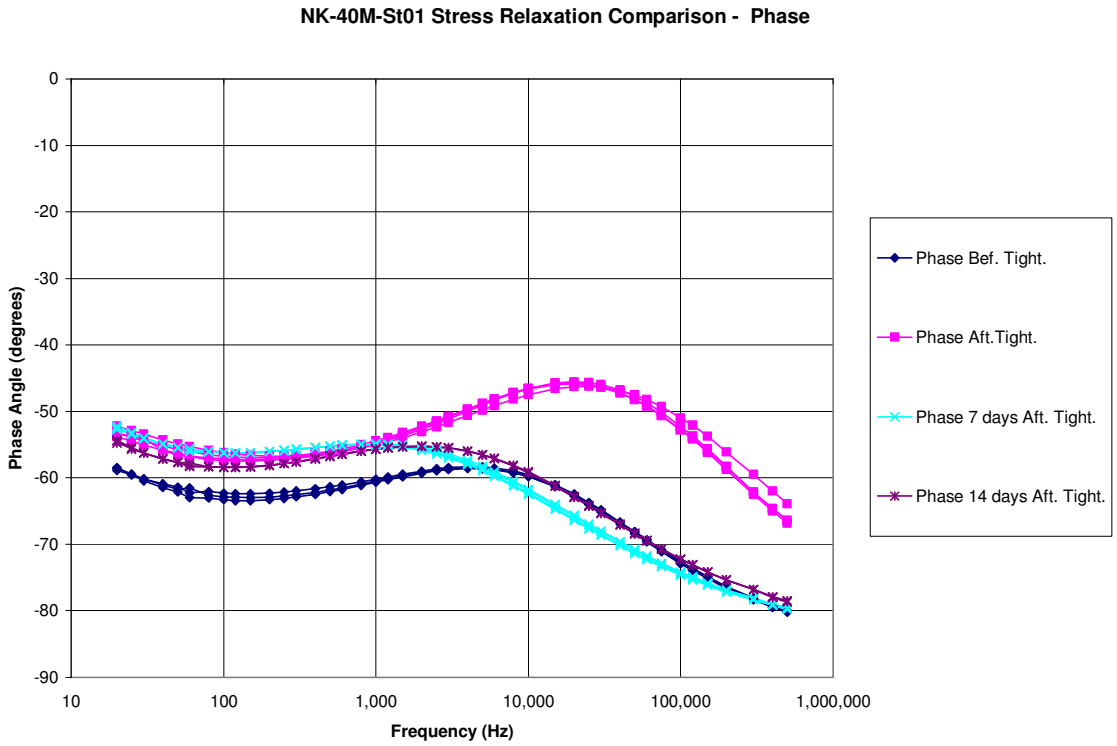



Figure 42. Steel Fractor stress relaxation comparison – phase plot.

Figure 42 shows the variation in the phase for different time spans over a frequency range for the Fractor NK-40M-St01.

The phase after tightening shoots up above the phase before tightening as a result of the effect of stress. The Fractor was then allowed to relax over a span of time and its response was monitored. The phase after 7 days drops from near tightened phase at 20 Hz to below the initial at 500 kHz. The phase after 14 days on the other hand drops slightly below the phase after 7 days at lower frequencies and rises slightly above it at frequencies from 10 kHz to 500 kHz. This effect cannot be justly explained by the

relaxation theory and possibly has to do with the micro chemical changes that took place due to relaxation over the span of 14 days.

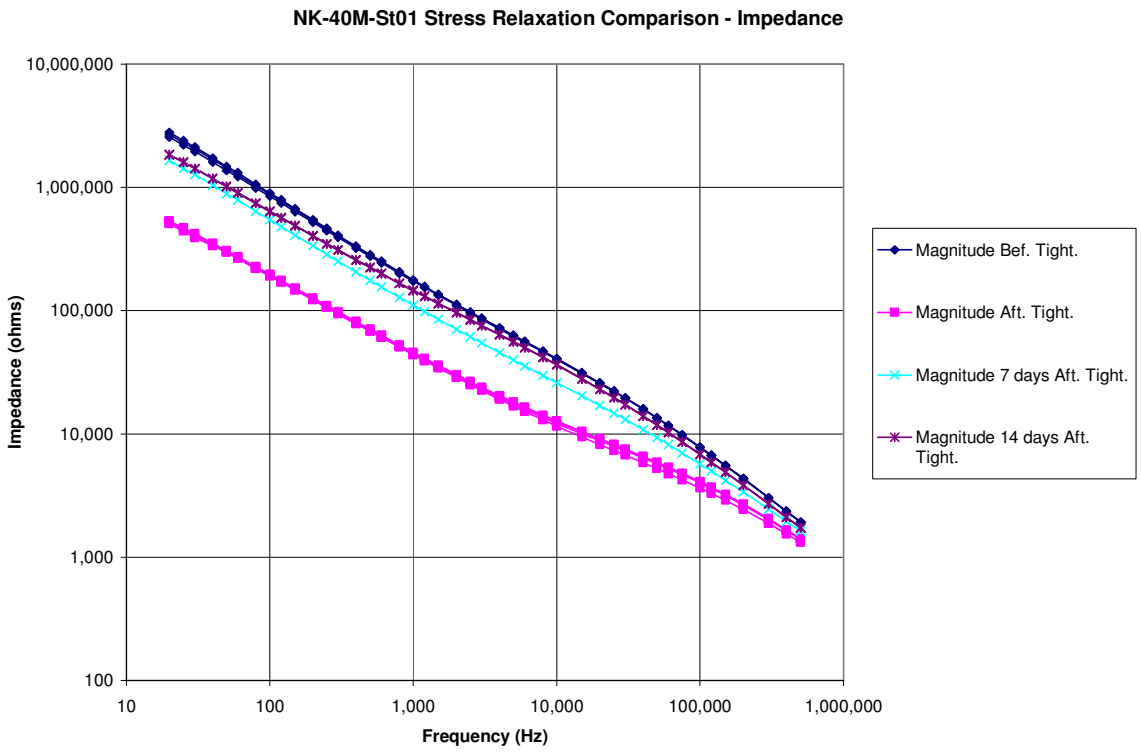



Figure 43. Steel Fractor stress relaxation comparison – impedance plot.

Figure 43 shows the variation in the impedance for different time spans over a frequency range for the Fractor NK-40M-St01. This is the effect of relaxation aging on the magnitude of impedance

There is lowering of the impedance after tightening in the lower frequency range as well as the higher frequency range. But the Fractor shows gradual recovery towards

the initial impedance from 7 days to 14 days indicating relaxation of the metal gel interface.

## Conclusion

For all the different Fractors, the overall results seem to ensure the initial hypothesis.

1) The increase in stress lowers the impedance and raises the phase angle.
2) The aging leads to relaxation. The impedance tries to get back to initial by rising up and the phase angle tries to recover itself by lowering towards the initial phase.
3) Some of the effects like lowering of the phase angle below the initial might be due to over- relaxation or its effect on the microstructure of the material.

# STRESS REPONSE ANALYSIS

It has been initially seen that stress induced by tightening the screws on the Fractor has had a considerable effect on the electronic properties. Hence, the Fractor response was tested under increasing loading conditions in the MSU Bozeman's materials lab using an Instron 4206 automated testing material testing machine.

## Concept

When compressive stress is applied to the Fractor, the interfacial distance between the gel and the abraded electrode decreases. This results in giving a greater drift to the ions at the same frequencies. So the ions flow more freely at the same frequencies. This lowers the overall impedance as an effect. As the Fractor is unloaded the interfacial distance widens and area accessible to the ions reduces resulting in increase in impedance.

## Experimental Setup

The Fractor was placed between the jaws of the Instron compression machine with grooved plexiglass plates above and below it. The copper leads of the Fractor were protected and guided by the grooved plates out of the jaws. These leads were connected to the Wayne Kerr impedance analyzer which in turn was connected to the data acquisition computer. The loading machine had an electronic interface to input the

loading rate and a digital display showing the output load. The experimental setup is shown in the figure 44.

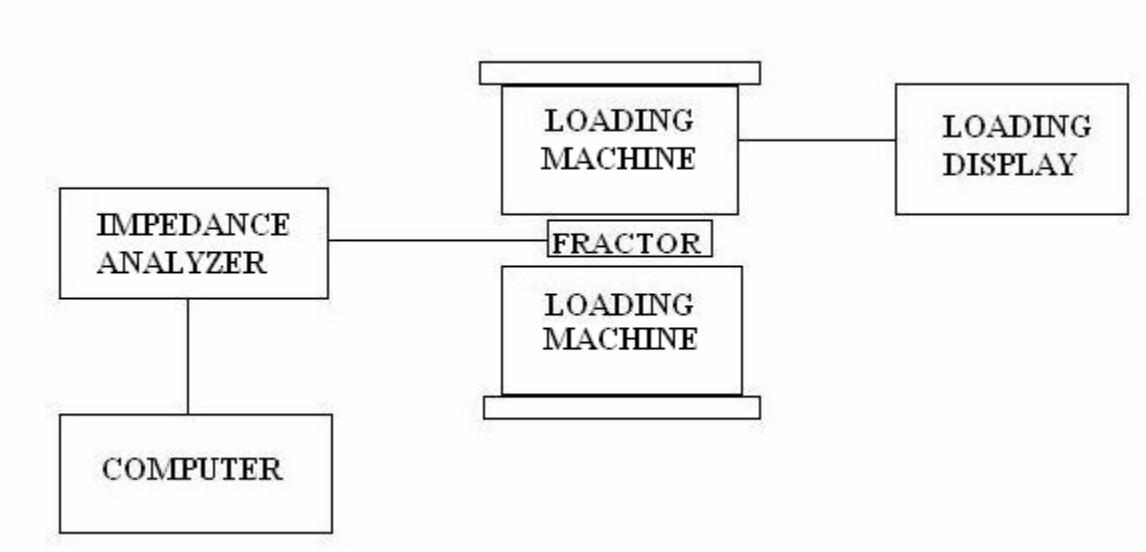



Figure 44: Block diagram of the loading system.

Process

Loading Process: The samples were loaded approximately up to 170 pounds in the unequal steps as the accuracy of the machine wouldn't allow reaching any precise loading point. After each loading step, the sample response was checked for about 25 minutes.

Unloading process: The samples were unloaded the same way they were loaded, trying to match the unloading step with the loading within the limit of the machine's precision. After each unloading step, the sample response was checked for about 25 minutes. The loading and unloading were done at the feed rate of 0.002 inches/minute.

Out of the samples tested, results of three samples of different materials are presented here.

Aluminum Fractor Loading

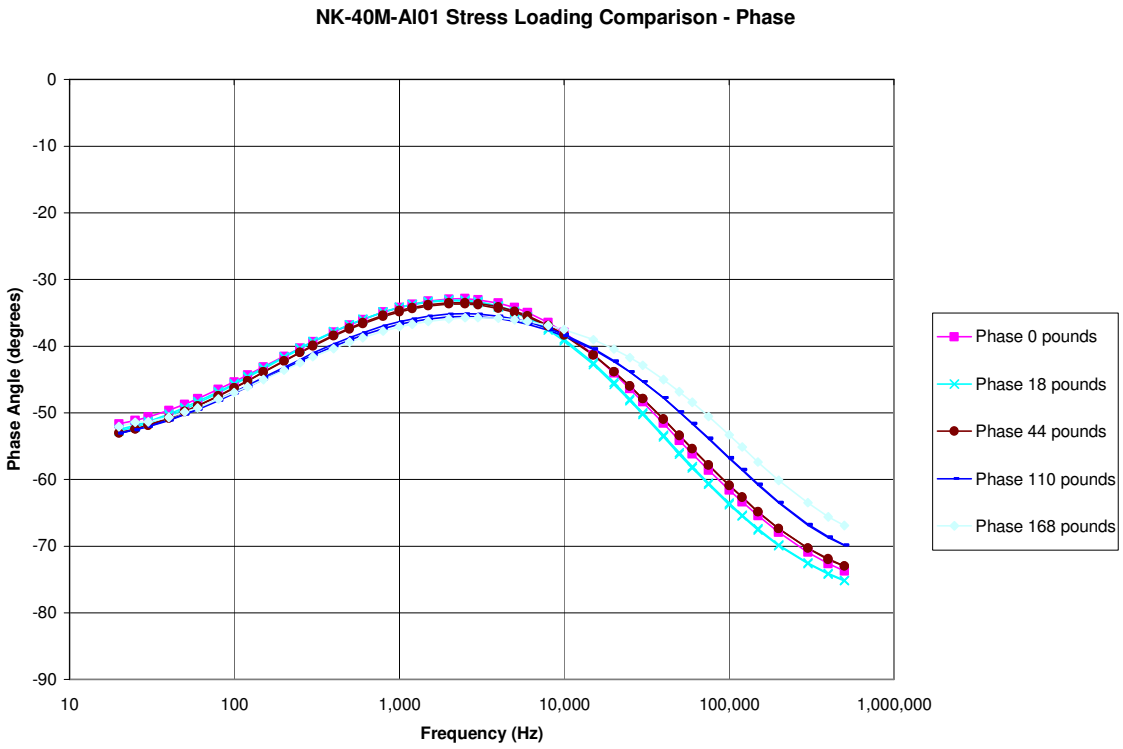



Figure 45. Aluminum Fractor stress loading comparison – phase plot.

An aluminum Fractor was subjected to loading in various steps from 0 pounds to 168 pounds and its electronic response to the stress variation was noted.

Figure 45 shows the variation in the phase angle on loading the Fractor at different frequencies. The 0 pounds phase is the initial phase before loading. On applying load, there is very slight difference in the phase till 100 Hz, after which the phase falls

below the initial till about 100 kHz. Near the electronic frequency range of 10 kHz the phase crosses over.

Largely, this trend is followed by the phase lines under increasing load in which the phase keep on falling below the initial one till around 20 kHz to 100 kHz and rises above it at higher frequencies displaying the crossover effect. Thus, at 20 Hz, the 0 pounds phase is the highest and 168 pounds the lowest. At 500 kHz, the 168 pounds phase is the highest and the 0 pounds phase is last but one.

Figure 46 shows the variation in the impedance upon application of increasing load at various frequencies. The highest impedance is the initial impedance or at 0 pounds stress. On application of load the impedance linearly drops on the logarithmic plot. This trend is followed by all impedances from 0 pounds to 168 pounds. The total impedance drop at lower frequencies is about 60,000 ohms while at the higher frequencies it is about 275 ohms. This shows that the impedance of the aluminum Fractor drops on the application of stress.

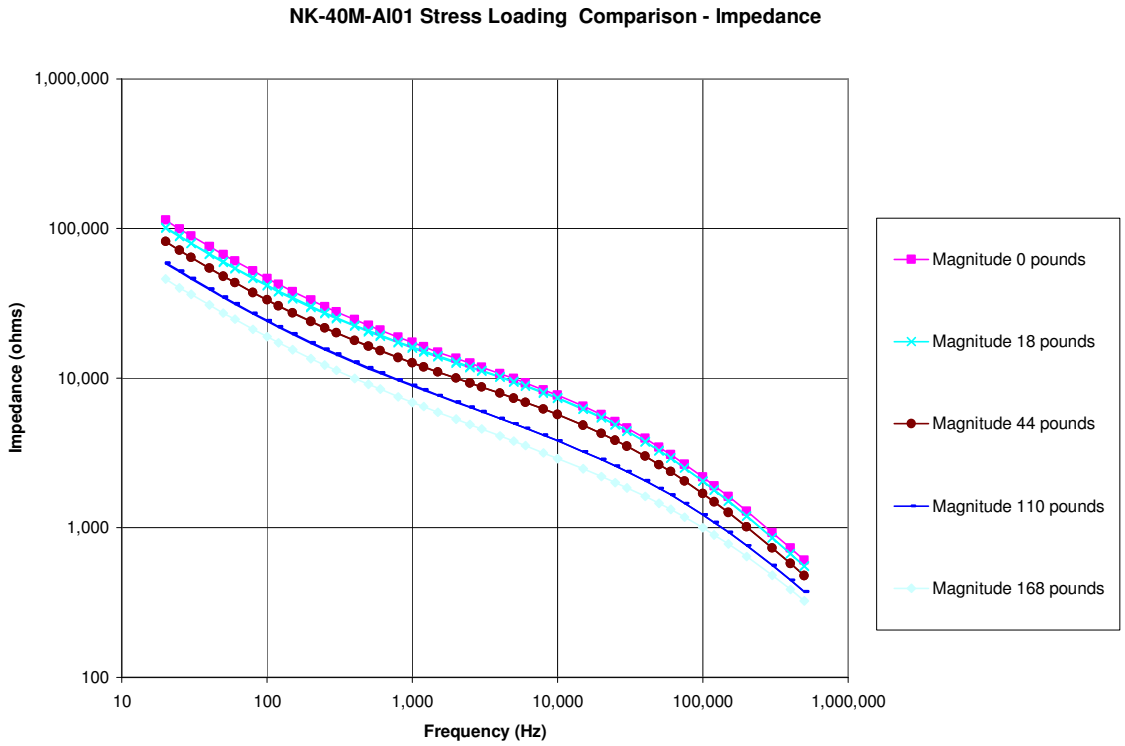
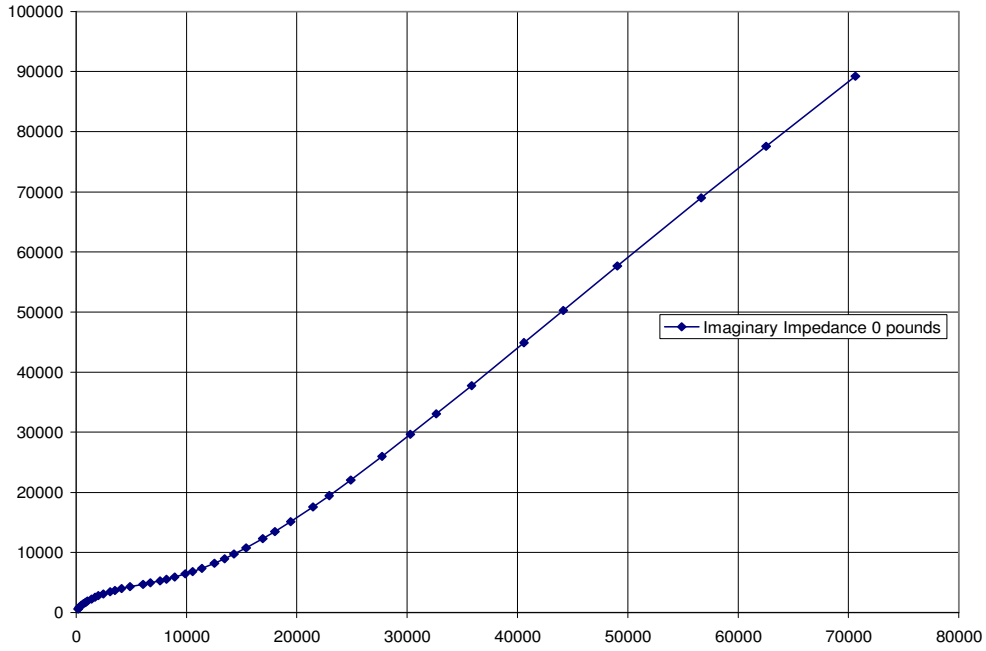


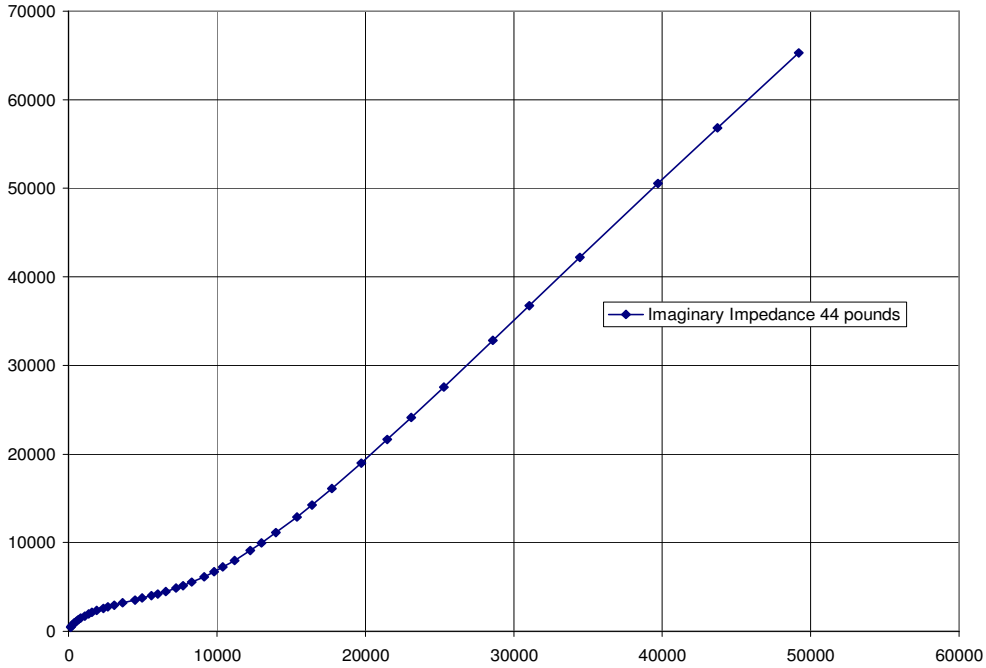

Figure 46. Aluminum Fractor stress loading comparison – impedance plot.

Figure 47 shows the Nyquist plots at different loading of 0 pounds, 44 pounds and 168 pounds. As mentioned before the Nyquist plots show the relative contributions of the real and imaginary impedances. The slope of the line on the Nyquist plot lie between 0.45 and 0.65 range indicating that the generalized Warburg impedance is being displayed. We fall back on these plots just to ensure the validity of our "concept" theory which states that the magnitude of the impedance lowers on increasing the load.

**NK-40M-Al04 0 pounds Nyquist**




**NK-40M-Al01 44 pounds Nyquist**



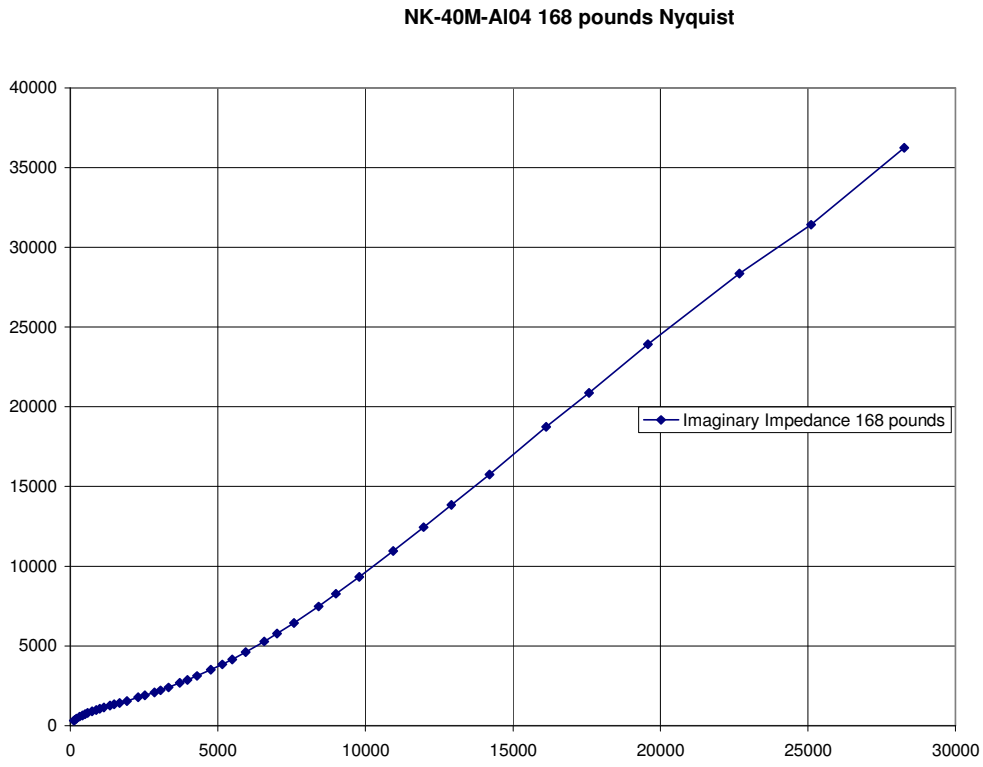



Figure 47. Nyquist plots at different loading.

As can be seen from the plots, the increase in loading is causing reduction in the impedance but the relative contributions from the two components are falling down equally i.e. there is no change in the inclination angle with respect to any graph. Thus we can conclude that our conceptual theory that capacitive impedance decreases due to decrease in the distance and resistive impedance decreases due to more exposed area (lesser hurdle to the ionic flow) seems to be working right.

## Aluminum Fractor Unloading

The aluminum Fractor was then tested for recovery by unloading it step by step from 167 pounds to 0 pounds. The electronic response was noted.

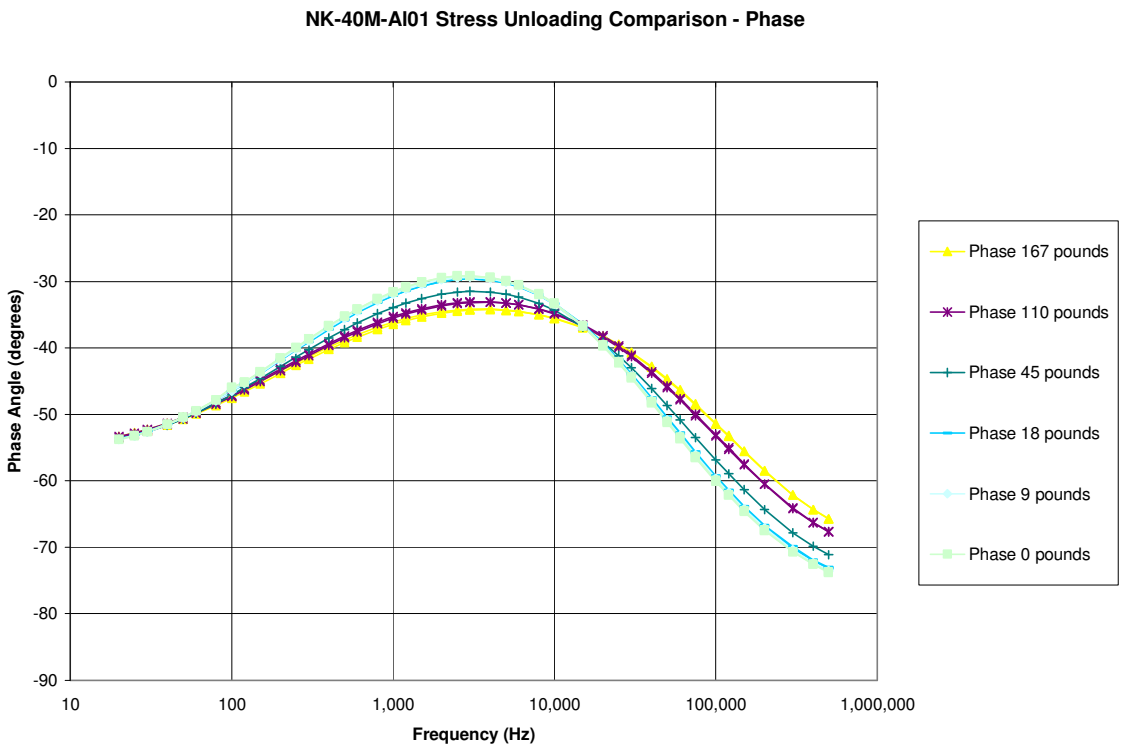



Figure 48. Aluminum Fractor stress unloading comparison – phase plot.

Figure 48 shows the phase of the aluminum Fractor on loading.

At the lower frequency of 20 Hz, there is very negligible variation in the phase angles, the 168 pounds phase being the maximum at 53.16° and the 0 pounds phase being

the least at 53.28°. The transition occurs at 200 Hz, where the 0 pound phase starts ascending and becomes the highest phase. After 15000 Hz, crossover effect takes place and the 0 pounds phase drops below all the other phases. The other phases follow the inversion. At the high frequency extreme of 500 kHz, the 168 pounds phase is the highest and the 0 pounds lowest with the difference of 5°. All the other phases lie in between with respect to their unloading stress.

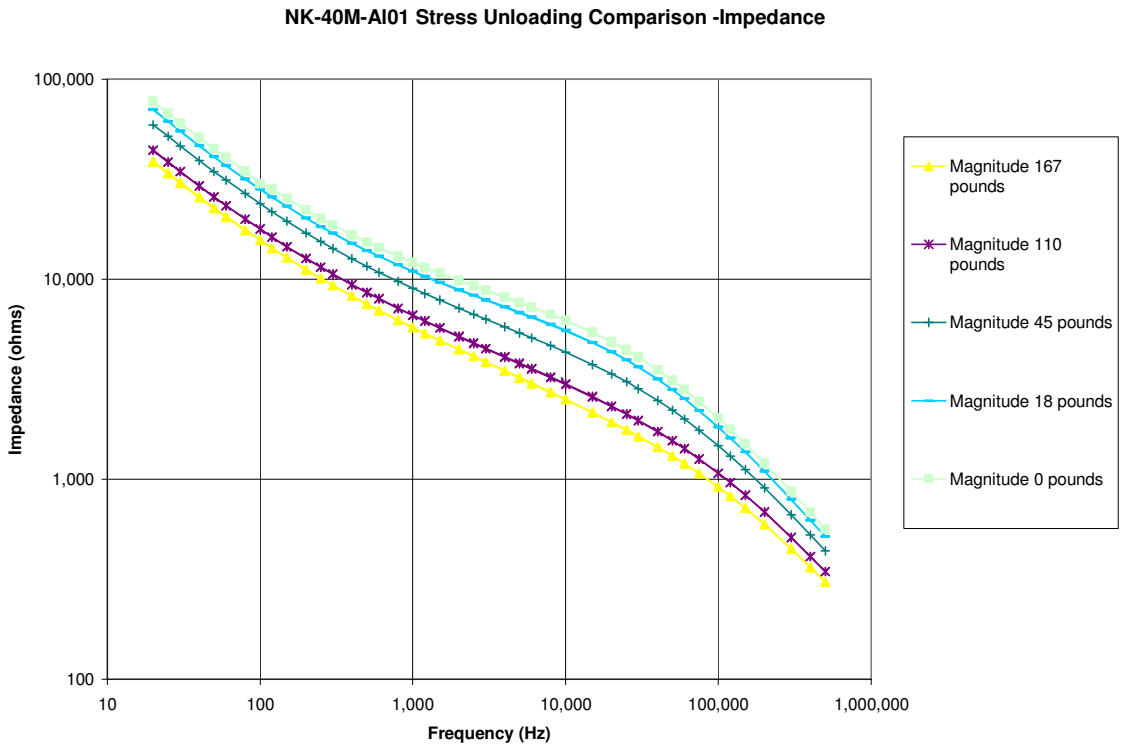
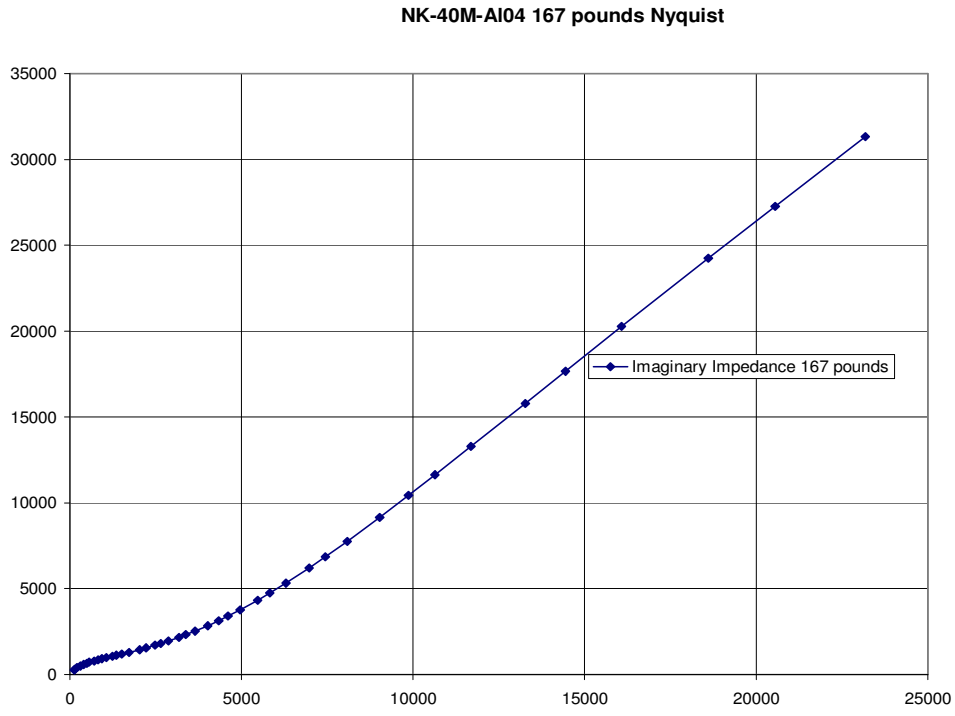


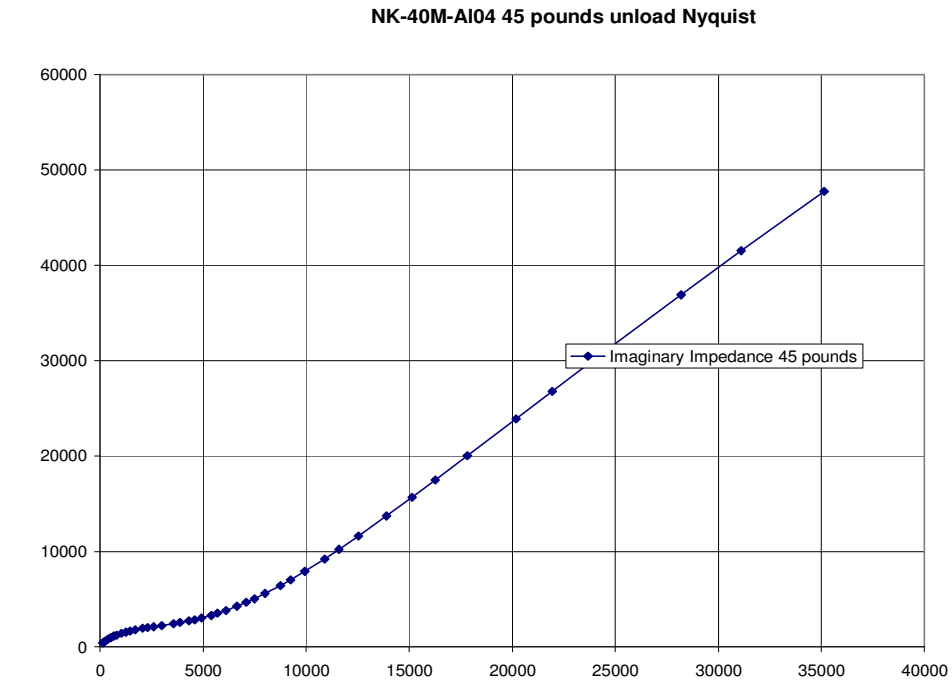

Figure 49. Aluminum Fractor stress unloading comparison – impedance plot.

Figure 49 shows the variation in the impedance upon reducing the load at various frequencies. On removal of load the impedance rises linearly on the logarithmic scale. This trend is followed by all impedances from 167 pounds to 0 pounds. The highest

impedance is the initial impedance or at 0 pounds stress. The total impedance rise at lower frequencies is about 40,000 ohms while at the higher frequencies it is about 250 ohms. This shows that the impedance of the aluminum Fractor increases on the relieval of stress.

To ensure the validity of the loading concept, the Nyquist was plotted at different loadings. The concept predicted no change in the relative contributions of the real and imaginary components of the impedance but gradual decrease in its magnitude. Figure 50 shows the Nyquist plots at different unloading from 167 pounds, 44 pounds and 0 pounds.





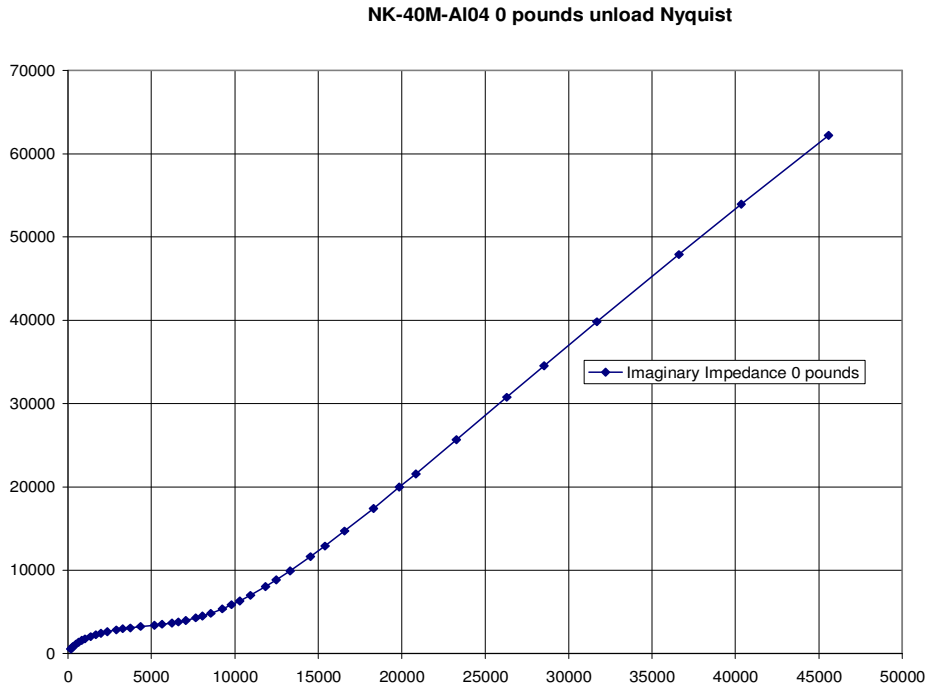




Figure 50. Nyquist plots at different unloading.

As can be observed from the plots, the decrease in loading is causing increase in the impedance and the relative contributions from the two components are rising down equally i.e. there is no change in the inclination angle with respect to any graph. Thus we can conclude that capacitive impedance increases due to increase in the interfacial distance and resistive impedance increases due to less exposed area.

Steel Fractor Loading

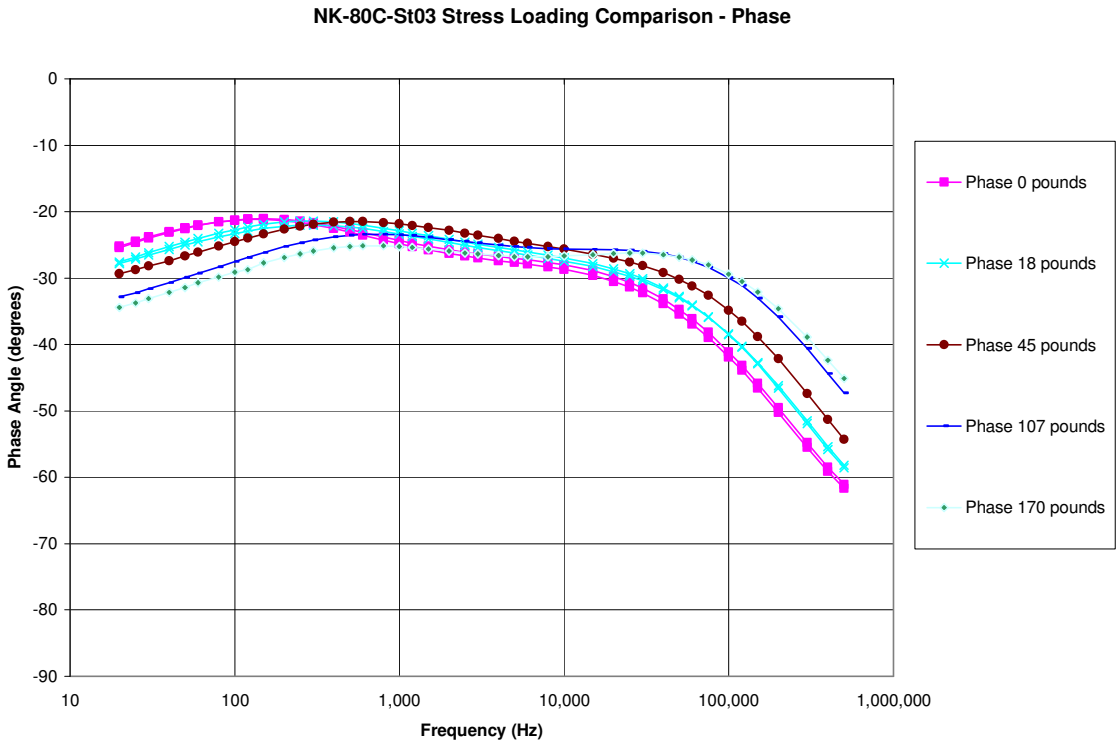



Figure 51. Steel Fractor stress loading comparison – phase plot.

Figure 51 shows the phase variation of 80C steel Fractor subjected to loading from 0 pounds to 170 pounds in the respective steps shown in the legend. The initial

phase line is the 0 pounds line. The application of stress seems to lower the phase angle initially indicating slight inclination capacitive nature. In the 1000 Hz to 10,000 Hz region though, the phase crosses over to show slight resistive nature which might lack of ionic contribution as ions do not flow at such high frequency.

An increase in the load results in increasing lifting the phase angle at the higher frequency end and lowering it at the lower frequency end. At all loads the phase angle reflects this trend. Consequently, in the more important ion dominated low frequency range the variation of phase angle is about 9° over all loads.

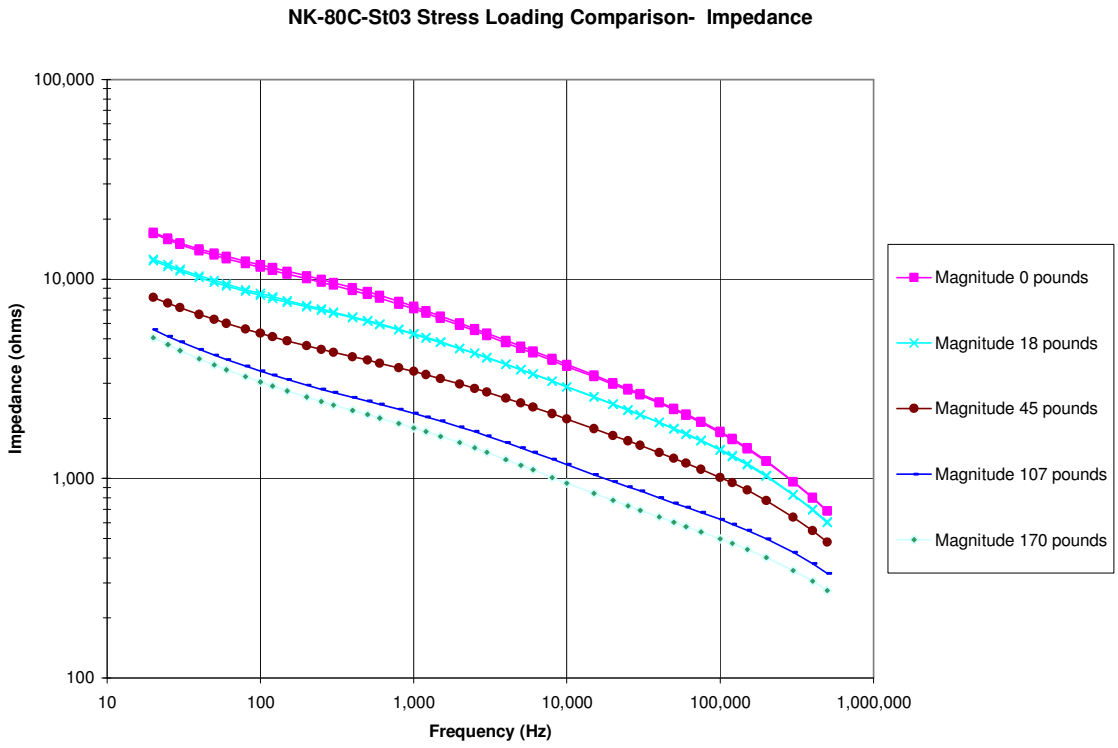



Figure 52. Steel Fractor stress loading comparison – impedance plot.

Figure 52 shows the change in the impedance with the variation in the load over the specified frequency range. The initial impedance is the 0 pounds impedance line. On the load of 18 pounds, the impedance suddenly drops below the initial by about 5,000 ohms at 20Hz and by 80 ohms at 500 kHz. This trend is followed by all the appreciating loads till the 170 pound impedance line. Thus, the 170 pounds impedance demonstrates lowest impedance at all frequencies.

Conclusively, during loading of the steel Fractor, it was noticed that the phase angle drops below the initial at lower frequencies and rises above the initial at mid and higher frequencies as the load increases. This phenomenon is called as “crossover” which takes place possibly due to stoppage of ionic charge carriers. The impedance on the other hand, drops below the initial with increasing load which matches the conceptual hypothesis made.

## Steel Fractor Unloading

Figure 53 shows the stress unloading/relieving performed on the steel Fractor. The Fractor was unloaded from 171 pounds to 0 pounds and its phase angle V/S frequency response was noted.

There is not a significant difference in the phase angle till the ionic range of about 10,000 Hz but the electronic range shows reasonable difference. In the lower frequency range as the unloading increases, the phase angle rises. In the frequency range of 1000 Hz to 10 kHz, the phases all come together with a very minimal difference.

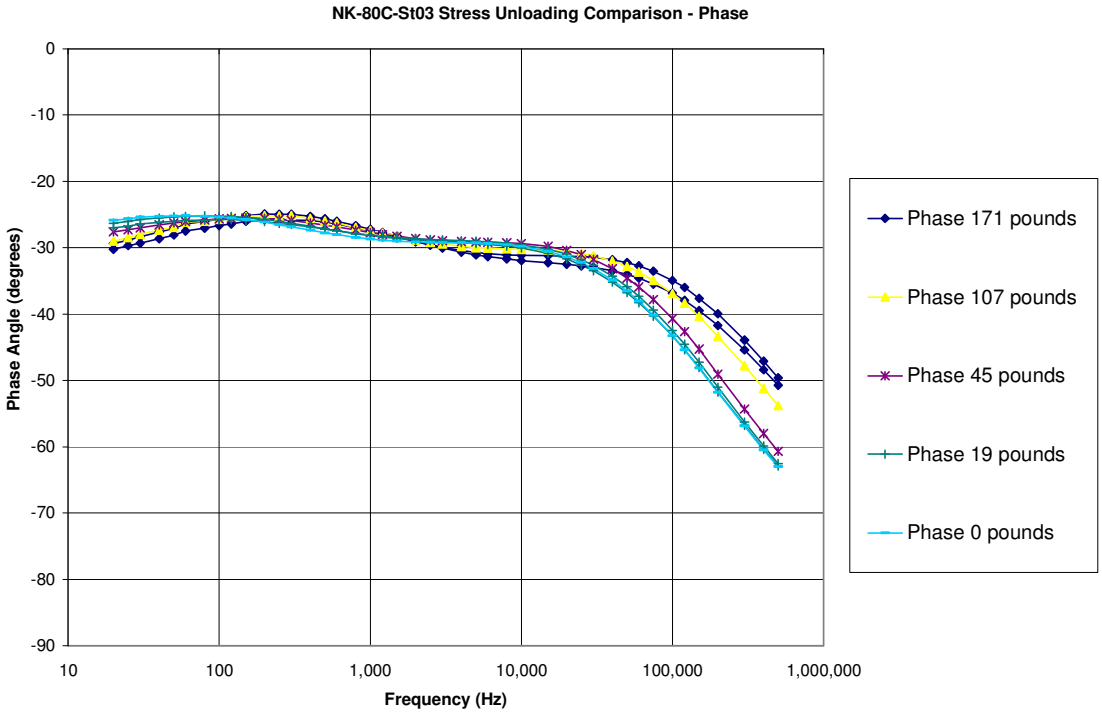



Figure 53. Steel Fractor stress unloading comparison – phase plot.

This is the crossover frequency range. In the high frequency region, the phase straightaway drops from 171 pounds to 0 pounds and each of the intermediate unloading stresses lie respectively in between.

Figure 54 shows the variation in the impedance with the lowering of the load over the frequency range. At lower frequency of about 20 Hz, the 3 pounds unloading impedance is higher than the 0 pounds impedance. This ascendancy goes on till 60 kHz where the 0 pounds unloading impedance overtakes the 3 pounds unloading impedance. Apart from this anomaly, the other unloading impedances drop linearly as the load goes on decreasing, the 171 pounds unloading impedance being the lowest.

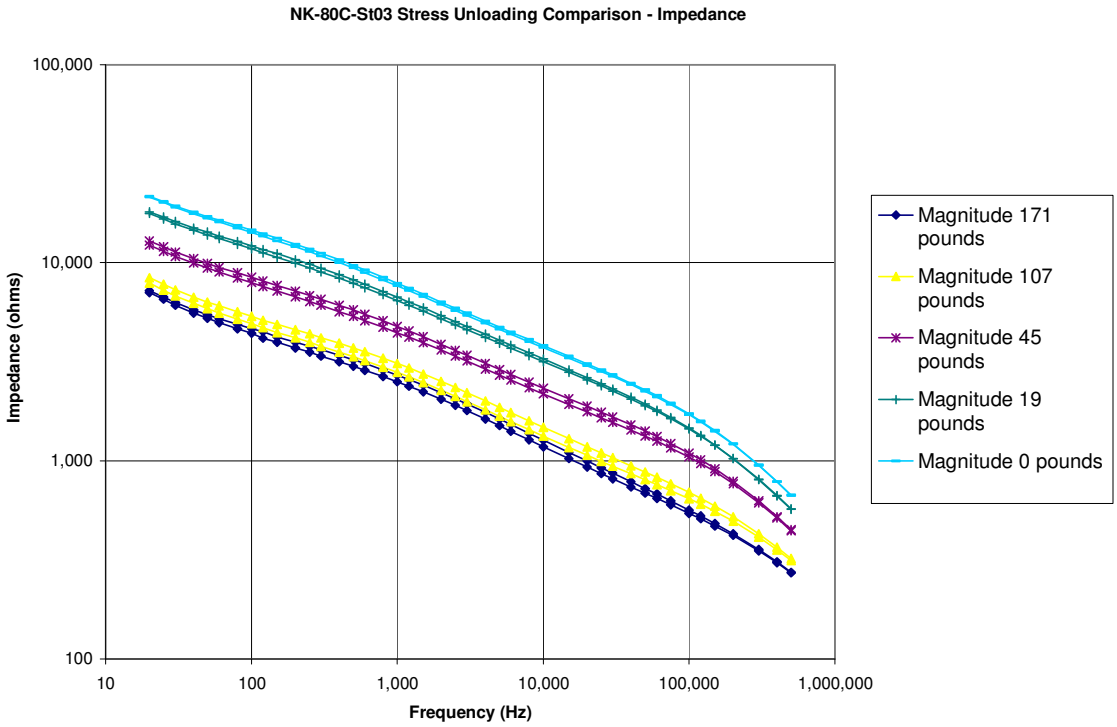



Figure 54. Steel Fractor stress unloading comparison – impedance plot.

Conclusively, for the steel Fractor we notice that the phase angle drops at lower frequency range and lifts up at higher frequency range with respect to the initial phase on the application of stress and vice versa. Thus it exhibits the cross over phenomenon. Apart from this, there is very slight change in the phase angle on stress variation. The impedance on the other hand drops gradually on increase in the stress and increase on reducing the stress. On reducing the stress to 0 pounds, the Fractor recovers but does not exactly match the initial response.

## Copper Fractor Loading

A copper Fractor was subjected to loading in various steps from 0 pounds to 171 pounds and its electronic response to the stress variation was noted.

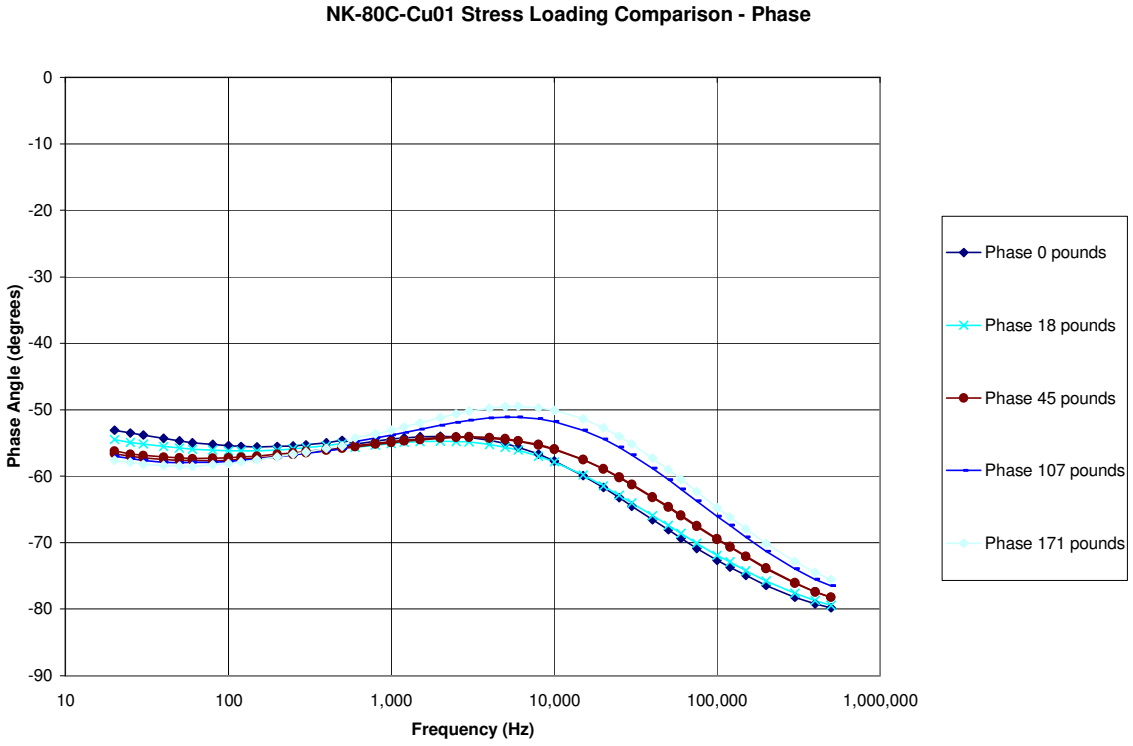



Figure 55. Copper Fractor stress loading comparison – phase plot.

Figure 55 shows the phase V/S frequency variation of an 80C copper Fractor subjected to loading from 0 pounds to 171 pounds in the respective steps shown in the legend. The initial phase is that at 0 pounds. In the graph, the phases show a minute variation under the respective loads. As the load increases the variation becomes more

pronounced. The trend exhibited by the graph is decrease in phase angle with increase in load at ionic frequencies and vice versa. The crossover takes place at about 1000Hz.

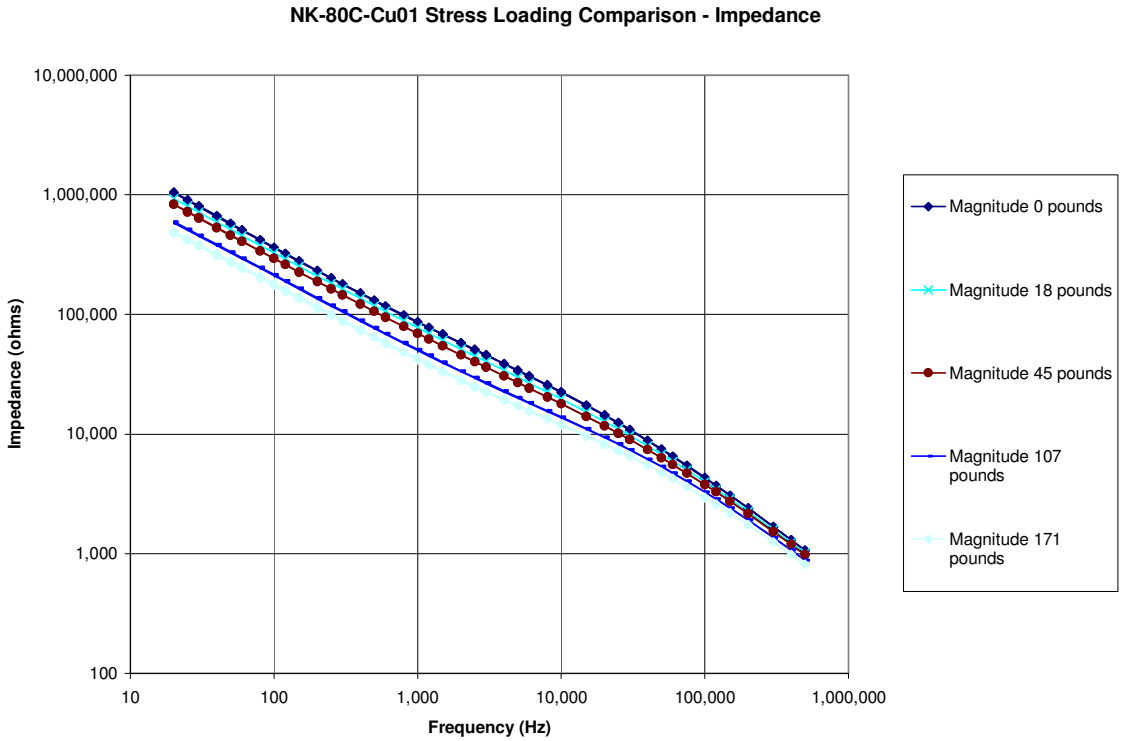



Figure 56. Copper Fractor stress loading comparison – impedance plot.

Figure 56 shows the change in the impedance with the variation in the load over the specified frequency range. The initial impedance is the 0 pounds impedance line. As per the hypothesis, impedance drops during the loading. This trend is followed by all the appreciating loads till the 171 pound impedance line in the above graph. Thus, the 171 pounds impedance demonstrates lowest impedance at all frequencies. It can be observed that the impedance drop is sizeable at lower frequency extremes than the higher ones due to the heavier charge on the ions as compared to the electrons.

Conclusively, during loading of the copper Fractor, it was noticed that the phase angle decreases as the load increases at ionic frequency range. There is crossover near 1000 Hz. The impedance on the other hand, drops below the initial with increasing load.

## Copper Fractor Unloading

The copper Fractor was unloaded from 172 pounds to 0 pounds to relieve the stress and cause recovery. The electronic properties were studied.

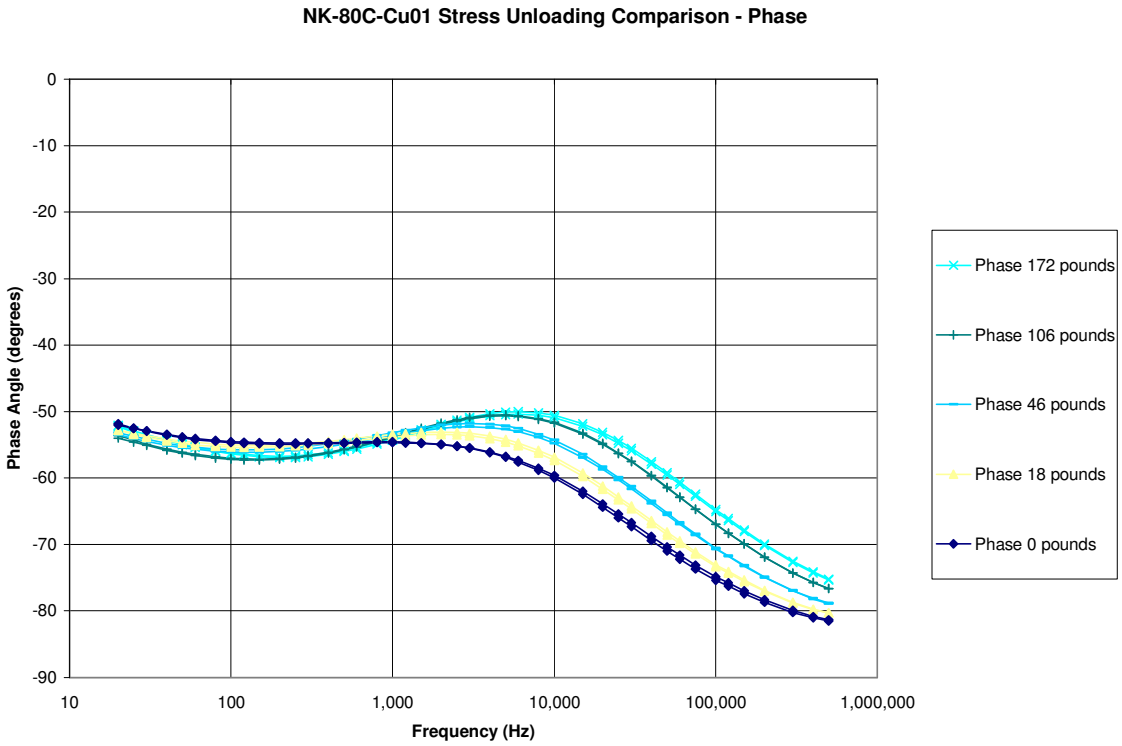



Figure 57. Copper Fractor stress unloading comparison – phase plot.

Figure 57 shows the stress unloading/relieving performed on the copper Fractor and its phase angle V/S frequency response was noted.

The unloading phase plot exhibits the same characteristics as done before by the Steel and Aluminum Fractors while unloading. There is not much difference in the phase angle initially. The difference between the lowest i.e. 172 pounds unloading phase, and the highest i.e. 0 pounds phase being about 2° at 20Hz. The crossover transition takes place at 1000 Hz where all the phases take their positions according the decreasing load. At the frequencies above 1000 Hz, the 172 pounds phase is the highest and the 0 pounds the lowest. The rest of the phases lie in between.

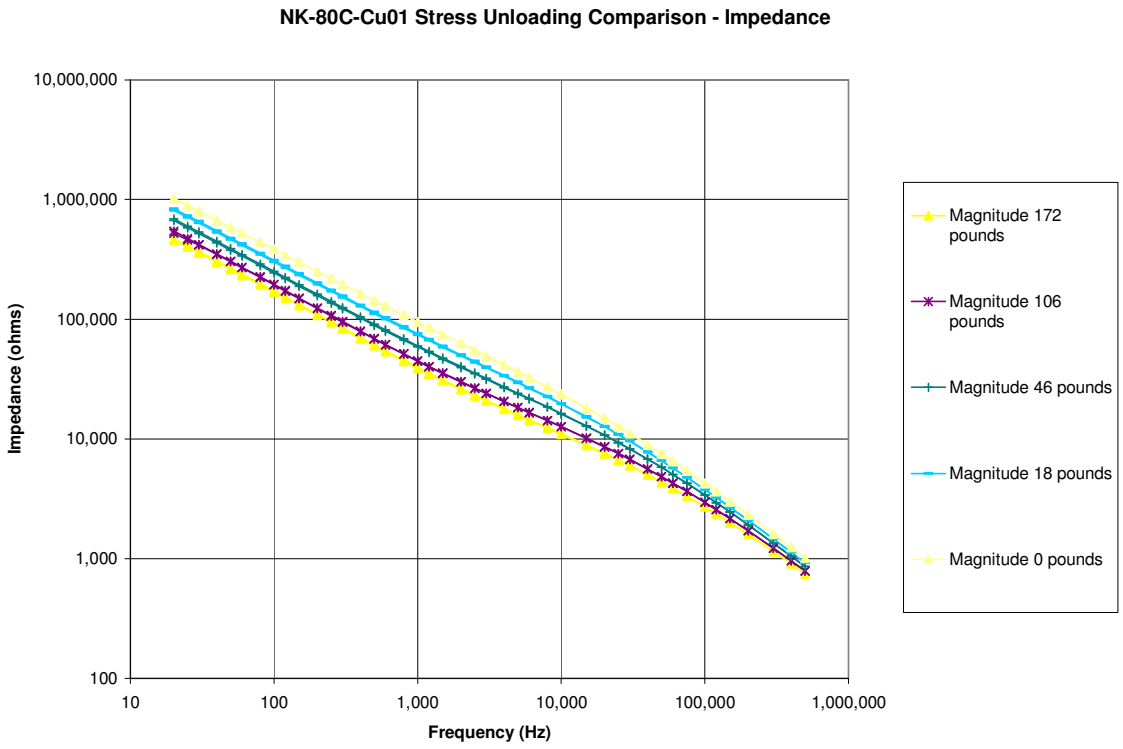



Figure 58. Copper Fractor stress unloading comparison – impedance plot.

Figure 58 shows the variation in the impedance with the lowering of the load over the frequency range. Over the whole frequency range, the 0 pounds unloading impedance

is the highest and the 172 pounds the lowest. All the other impedances lie in between according to their stress magnitude. The impedance drop is highest at 20 Hz. and measures close to 350,000 ohms. The impedance drop is lowest at 500 kHz and is about 225 ohms.

## Conclusion

On the whole, it can be noticed that there is not much variation in the phase angle especially in the ion dominated frequency range of up to 10 kHz on application or removal of compressive stress due to equal contribution from resistive and capacitive impedance. However, the impedance decreases on application of stress and increases on the removal. Thus it can be said that the impedance response of the Fractor is inversely proportional to the applied stress.

# VIBRATION RESPONSE ANALYSIS

The effect of vibration on the Fractor was studied by mounting it on a shaker and giving it a sine wave function. This was done to simulate the behaviour of the Fractor in actual real time environment function generator (Hewlett Packard, 33120A, 15MHz), oscilloscope (Tektronix, TDS 210, two channel, digital real time, 60 MHz), amplifier, Wayne Kerr impedance analyzer and computer with general purpose interface bus (GPIB).

## Concept

This experiment was performed to analyze the variation in the phase angle and impedance of the Fractor due to vibration. As explained before, the Fractor performance is due to the metal gel film interface. Even if the abraded electrode of the Fractor is screwed tightly with the other two electrodes, the vibration tends to change its orientation slightly. This has an effect on the electronic response.

## Experimental Setup

The Fractor was mounted on the shaker and was held in position by placing on a double sided sticky tape attached to the shaker surface. The function generator gave a signal via the oscilloscope to the power amplifier. The power amplifier amplified the signal and sourced it to the shaker.

The Fractor was connected to the Wayne Kerr impedance analyzer, which analyzed the impedance and phase angle at different frequencies and passed the information to the computer via the General Purpose Interface Bus (GPIB) connector. The data was stored in the computer in the format of Microsoft Excel sheet. The setup is shown in figure 59.

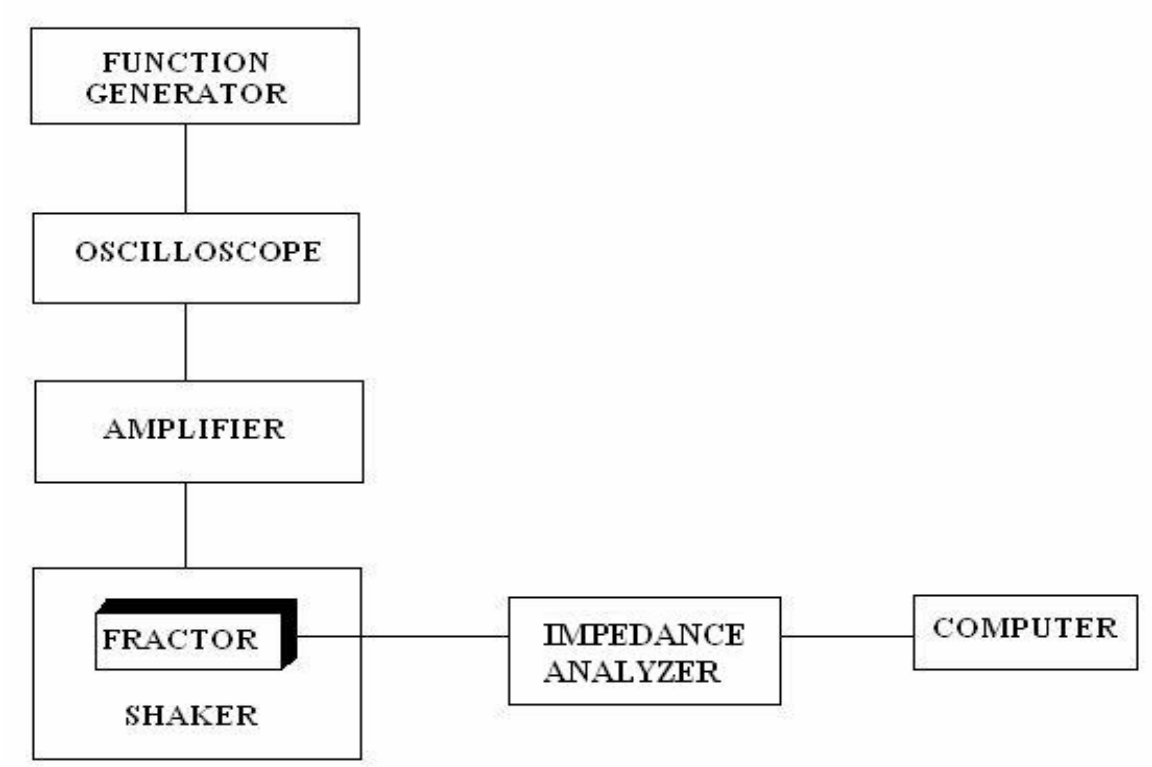



Figure 59. Block diagram of vibration setup.

## Vibration Process

The Fractor was subjected to a vibration frequency of 150 Hz, the input to the shaker being in form of a sine wave. A couple of initial Fractor readings were measured. The Fractor was then subjected to vibration and three dynamic readings taken. After the vibration, two more normal readings were taken to study the change in the Fractor response due to vibration.

Effects of vibration on several different Fractors were studied. Results of three different configuration Fractors are shown here.

## Aluminum Fractor Vibration

Figure 60 shows the difference in the phase before, during and after the vibration of the Fractor NK-80C-Al04 over the specified frequency range.

As can be observed from the graph, the phases before vibration, during vibration and after vibration overlap each other. All of them exhibit -64° at 20 Hz and 74° at 50 kHz. There is a very slight variation between the phase before vibration and other two in the frequency range of 20 kHz and 500 kHz. Other than this the vibration seems to have had no significant effect on the phase angle. The phases are unaffected especially in the ionic region from 20 Hz to 10,000 Hz.

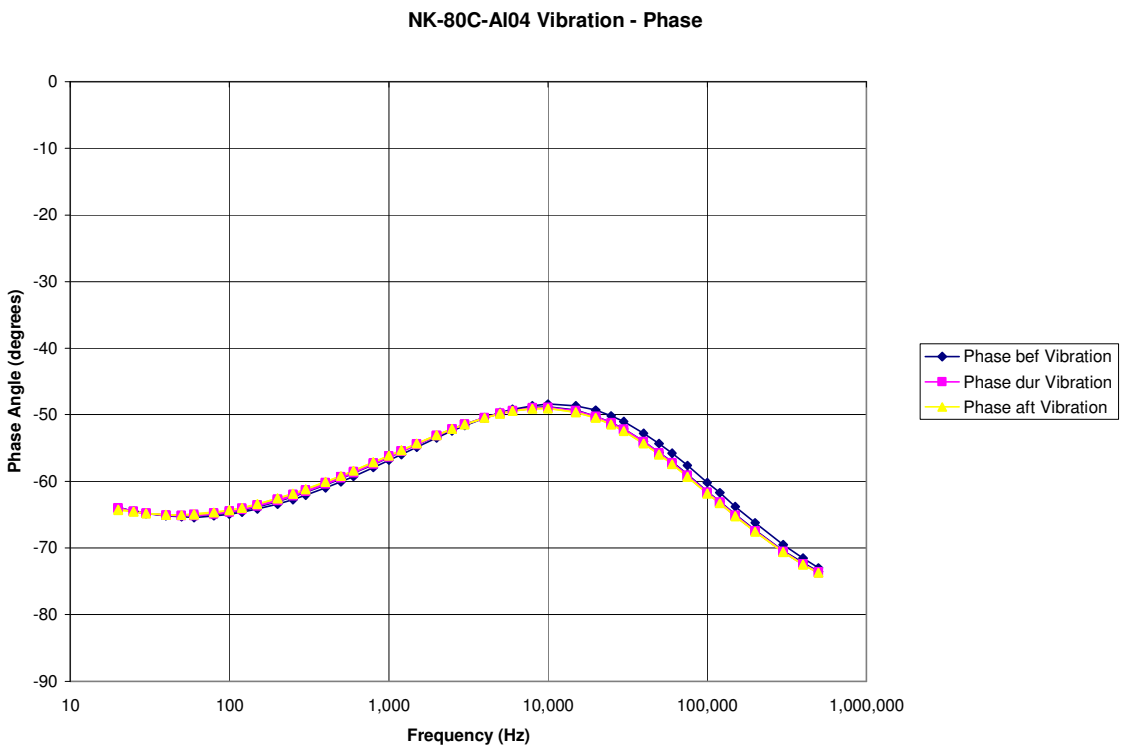



Figure 60. Aluminum Fractor vibration comparison – phase plot.

Figure 61 shows the difference in the impedance before, during and after the vibration of the Fractor NK-80C-Al04 over the specified frequency range. The impedance magnitudes before vibration, during vibration and after vibration do not display any changes. The three impedance lines overlap each other.

The vibration seems to have caused absolutely no change in the impedance. Thus vibration has had no effect on the Aluminum Fractors performance.

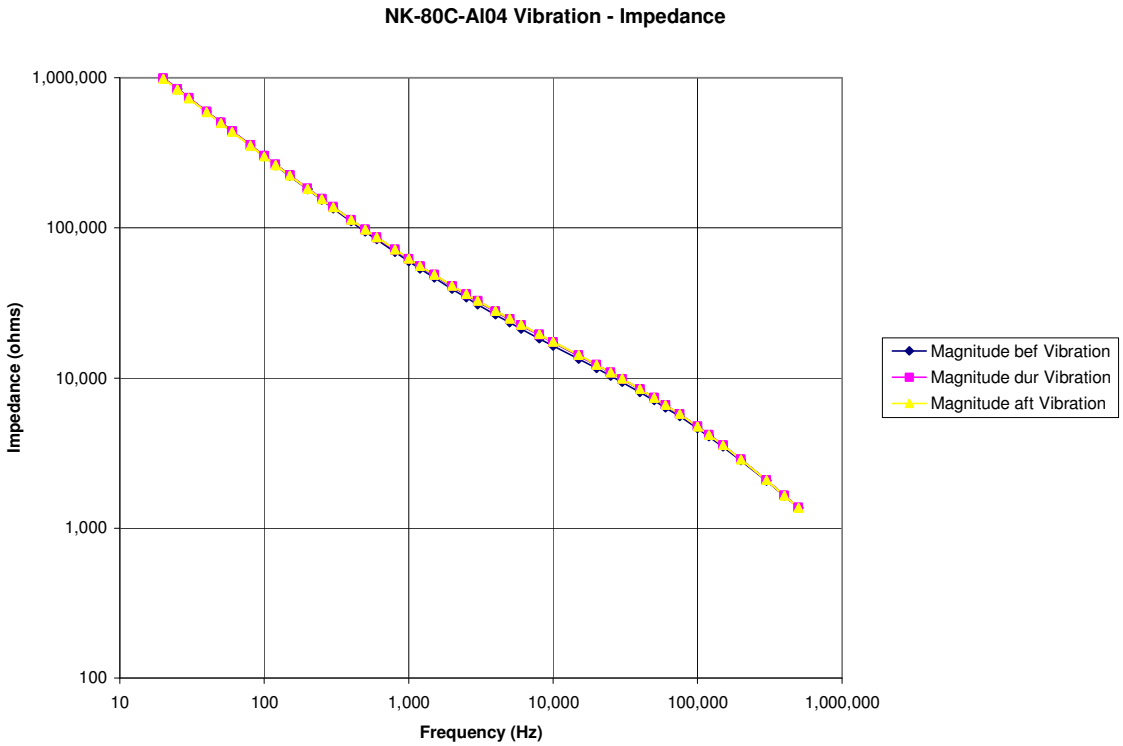



Figure 61. Aluminum Fractor vibration comparison – impedance plot.

## Steel Fractor Vibration

Figure 62 shows the difference in the phase before, during and after the vibration of the Fractor NK-80C-St01 over the specified frequency range.

The first run of NK-80C-St01 before vibration yields a slightly higher phase which seems to settle down on the second run. In the second run phase of the initial NK-80C-St01, the phase measurements during the vibration run and after the vibration run don't exactly overlap each other but follow each other with a slight difference.

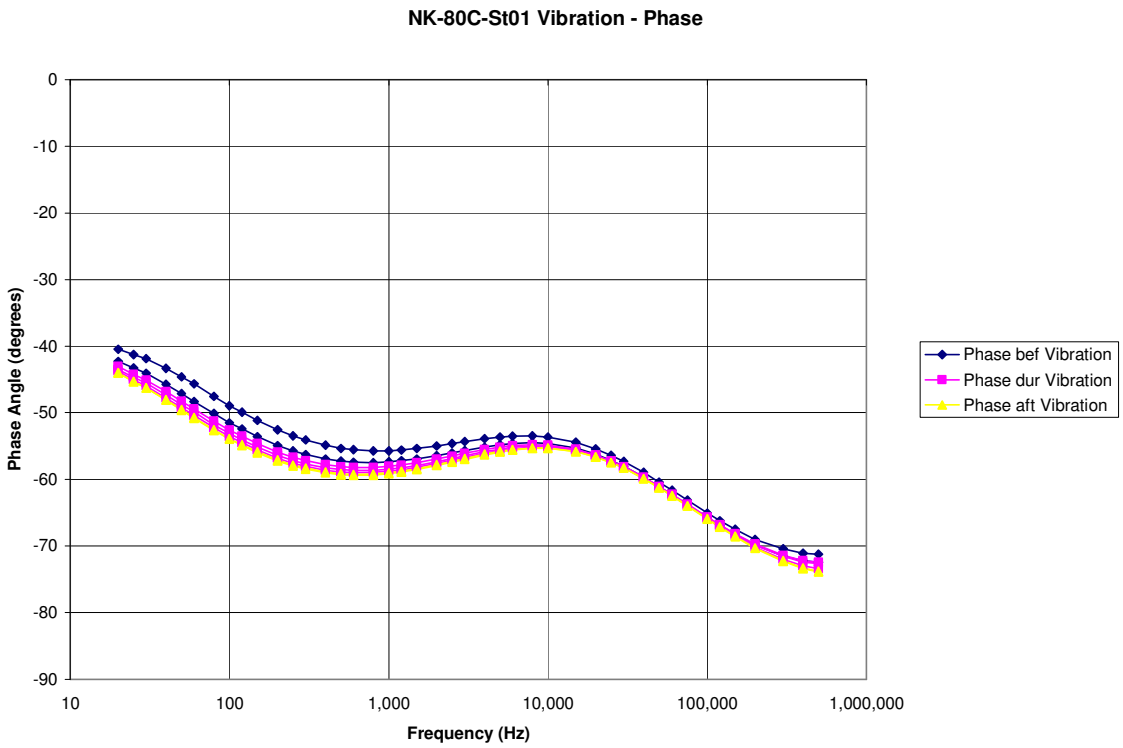



Figure 62. Steel Fractor vibration comparison – phase plot.

At 20 Hz, the difference between the phase before vibration run and phase during the vibration run is less than 0.6°, while the difference between the phase during the vibration run and after the vibration run is about 1°.

At 500 kHz, the difference between the "second run" phase before the vibration run and phase during the vibration run is 0°, while the difference between the phase during the vibration run and after the vibration run is about 1.4°.This shows that the vibration effect on the NK-80C-St01 phase is negligible.

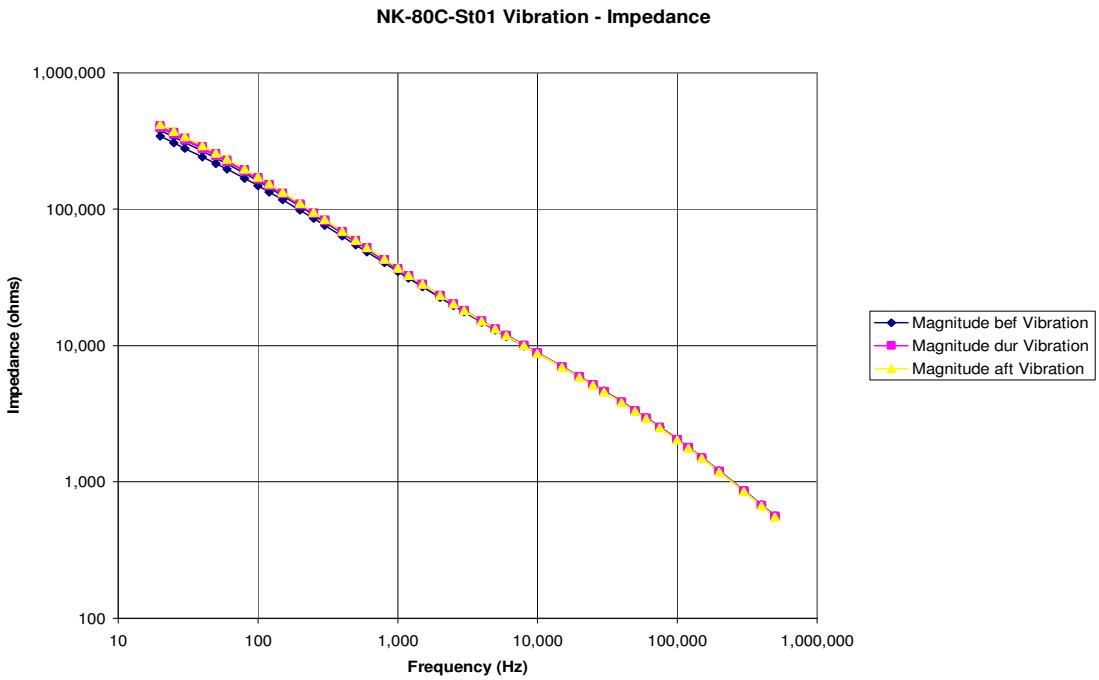



Figure 63. Steel Fractor vibration comparison – impedance plot.

Figure 63 shows the difference in the impedance before, during and after the vibration run of the Fractor NK-80C-St01 over the specified frequency range.

The impedances during the vibration run and after the vibration run are very much equal at all frequencies as can be seen from the graph. The first run impedance of NK-80C-St01 before vibration slips slightly at lower frequencies than the impedances during vibration and after vibration. But the second run impedance lies exactly upon the other two through out the frequency range.

Thus it can be inferred that vibration has had no effect on the impedance of the NK-80C-St01 Fractor.

Copper Fractor Vibration

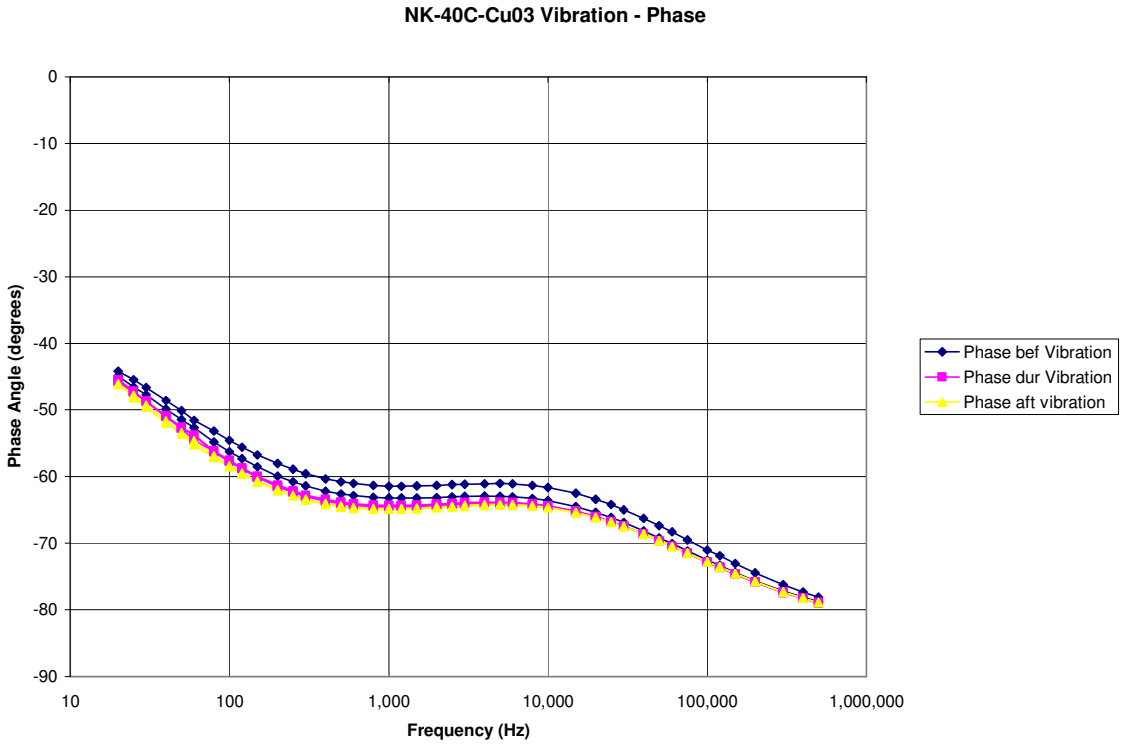



Figure 64. Copper Fractor vibration comparison – phase plot.

Figure 64 shows the difference in the phase measurements before, during and after the vibration of the Fractor NK-40C-Cu01 over the specified frequency range.

The second run of NK-40C-Cu03 before vibration yields a phase lower than the first run. This phase closely traces the phases during vibration and after vibration. The difference between this phase and the phase during vibration phase at 20 Hz is 0.5° while the difference between the phase during vibration and after vibration is also about 0.5° at 20 Hz.

At the higher frequency of 500 kHz, all the three phases merge into each other at a phase angle of 78.8°. A slight alteration is observed in the three phases between the frequency range of 100 Hz to 10 kHz.

This shows that the vibration effect on the NK-40C-Cu03 phase is negligible.

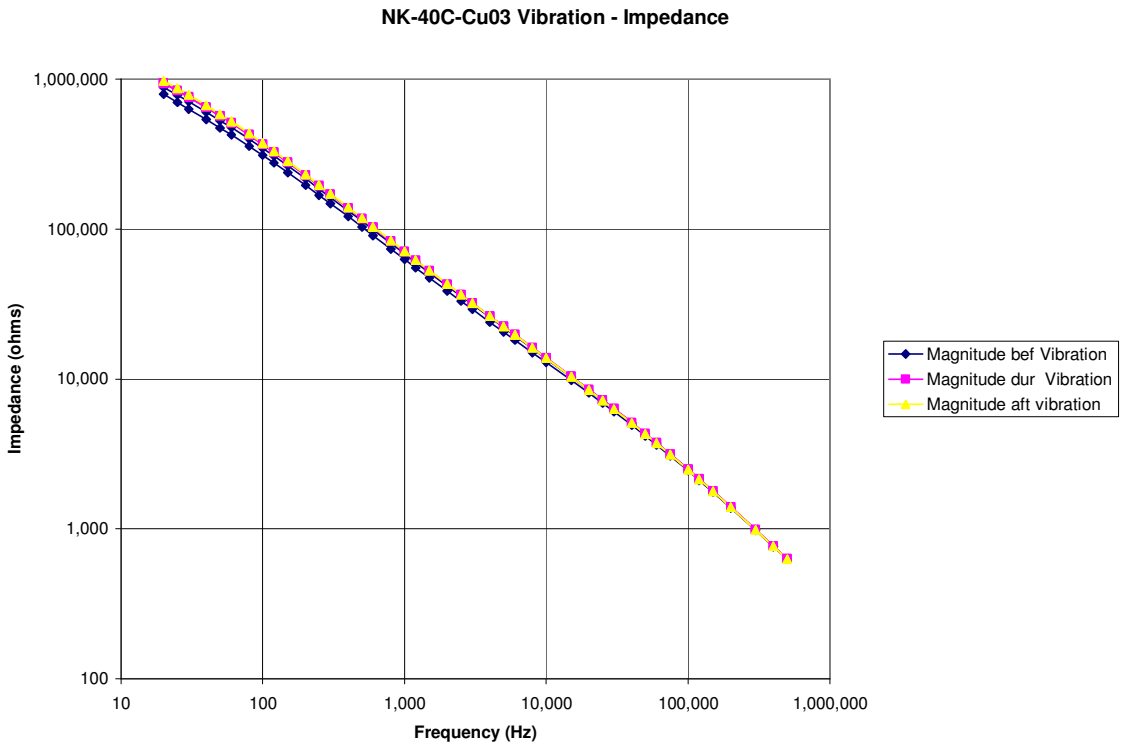



Figure 65. Copper Fractor vibration comparison – impedance plot.

Figure 65 shows the difference in the impedance before, during and after the vibration run of the Fractor NK-40C-Cu03 over the specified frequency range.

The impedances during vibration and after vibration are very much equal at all frequencies as can be seen from the graph. The first run impedance of NK-40C-Cu03 before vibration lowers slightly at lower frequencies than the impedances during

vibration and after vibration. But the second run impedance lies exactly upon the other two through out the frequency range.

Thus it can be inferred that vibration has had no effect on the impedance of the NK-40C-Cu03 Fractor.

## 24 Hour Vibration Run

Process: A Fractor was subjected to a 24 hour run at the same frequency of 133 Hz to see the effect of continuous vibration on the response. The initial response of the Fractor was noted and the dynamic vibration response was compared with it.

Figure 66 shows the variation in the phase angle of the Fractor NK-40M-Al01 over a frequency range. The readings shown above are edited to measurements before vibration and during the last few minutes of the 24 hour vibration.

It can be seen that there is a slight shift in the phase angle after 24 hours of vibration. The phase wavers about the phase before vibration, going below it till 100 Hz, then lifting up and going below again at about 200 kHz. The maximum fluctuation is about 5° at the higher frequency end.

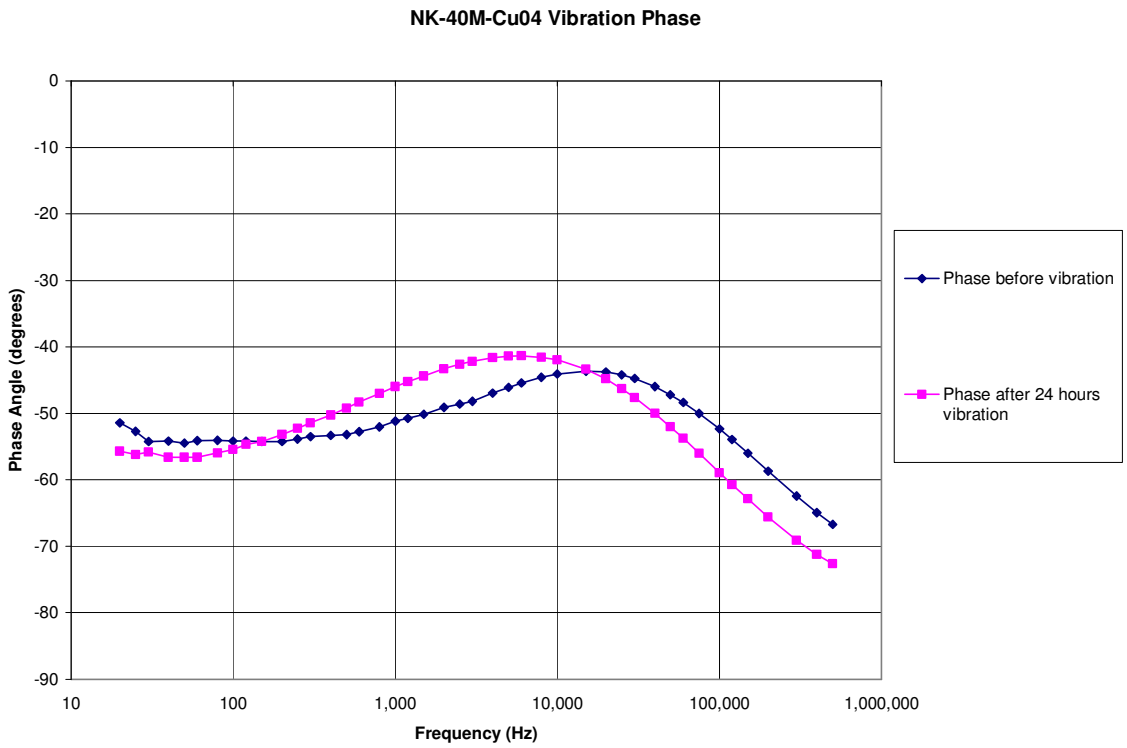



Figure 66. Copper Fractor 24 hour vibration comparison – phase plot.

Figure 67 shows the variation in the impedance of the Fractor NK-40M-Al01 over a frequency range. The readings shown above are edited to measurements before vibration and during the last few minutes of the 24 hour vibration.

It can be seen that there is not much variation in the impedance. The impedance at the higher frequency and lower frequency extreme are nearly the same with a bit of difference in the 10 kHz to 100 kHz range.

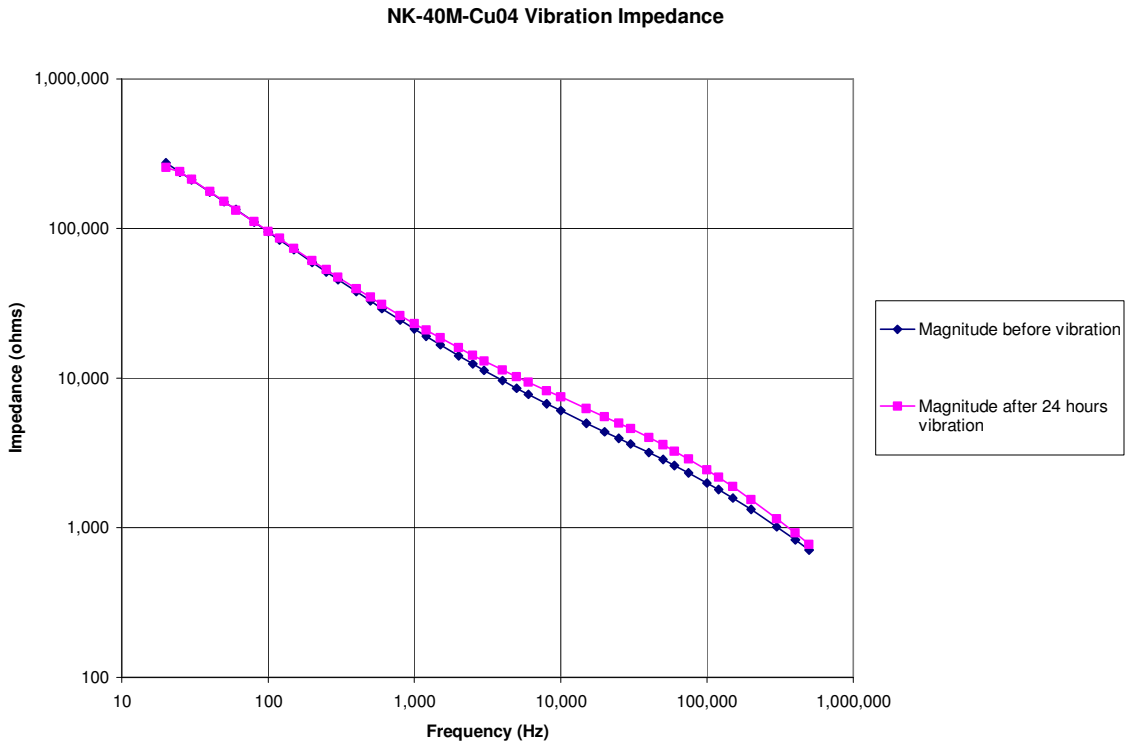



Figure 67. Copper Fractor 24 hour vibration comparison – impedance plot.

## Conclusion

From the above results we can conclude that short term vibration experiments do not have any effect on the Fractor. The long term (24 hour) run seems to change the phase angle and the impedance slightly. This might be because the vibration causes the screws on the Fractor to loosen slightly. This results in reduction in pressure on the electrodes allowing a minor displacement between the metal-gel interface. This leads to slight change in the response.

# THERMAL RESPONSE ANALYSIS

The effect of temperature on the Fractor is an important aspect in the working environment. To test the effect of the temperature variation the Fractor was tested in a Sun Systems thermal chamber and its response to the variations was noted.

## Concept

The majority of the impedance in the lower frequency range (about 10 kHz) is contributed by the lithium ions. The mobility of then ions depends upon the surrounding temperature. In an ambient environment, the ions migrate at normal mobility. On heating, the over all energy level rises and leads to increase in the mobility of the ions. Whereas cooling reduces the energy level and the ions have to de more work to displace themselves from the initial position.

Thus, increase in temperature results in higher amount of ion flow, thus reducing the impedance. The decrease in temperature on the other hand, necessitates more energy to move the ions, increasing the overall impedance.

## Experimental Setup

The Fractor under consideration was placed in the Sun System's thermal chamber which had a digital temperature controller. The leads of the Fractor were connected to the Wayne Kerr impedance analyzer though a tiny insulated outlet. A 10kΩ thermistor (WEI, Model TCS610) was connected to the upper copper electrode of the Fractor using

conductive glue. The output from this thermistor went to a voltmeter which measured its change in resistance at different temperatures. This change in resistance was converted to temperature using a WEI Steinhart-Hart equation thermistor chart. This provided us with the temperature inside the Fractor. The thermal analysis setup is shown in the figure 68.

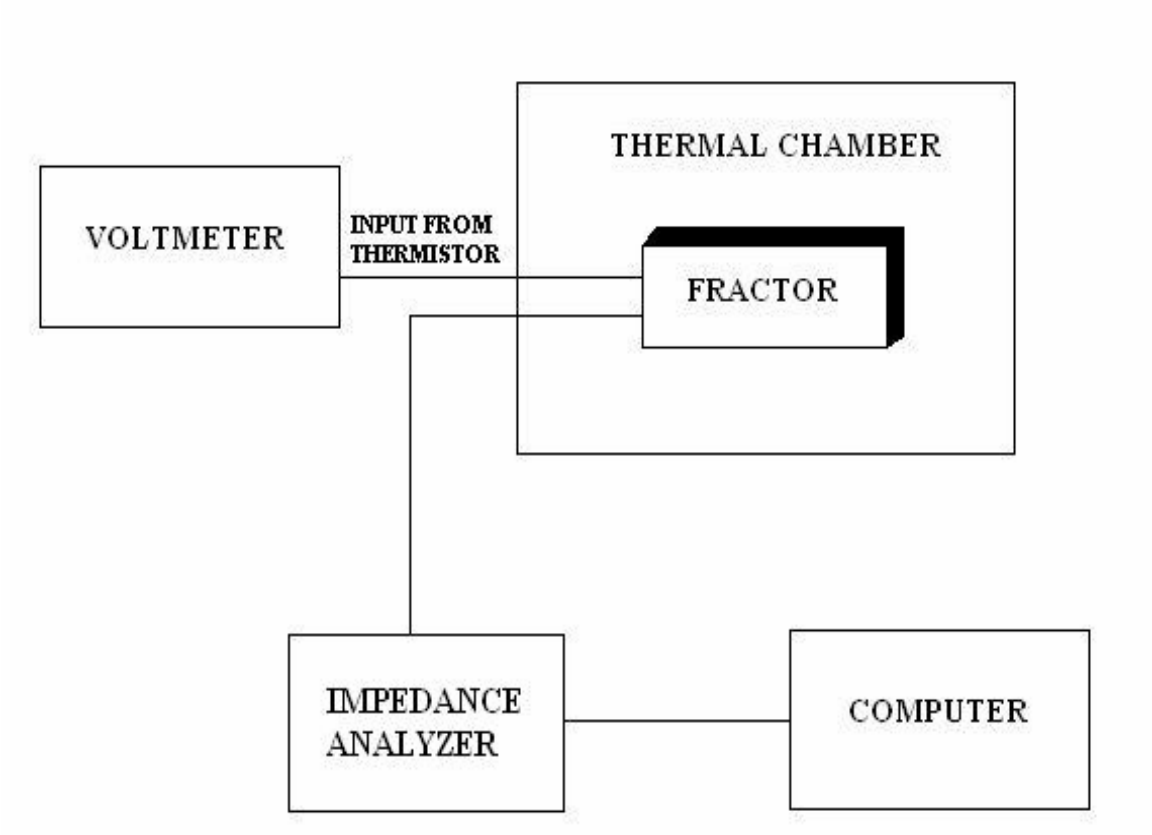



Figure 68. Thermal test setup.

Thermal Variation Process

The temperature inside the thermal chamber was varied from -40°C to 45°C in predefined steps. The variation was done as follows:

| Step No. | Temperature Variation | Process type |
|---|---|---|
| 1 | 20°C to 0°C | Cooling |
| 2 | 0°C to -20°C | Cooling |
| 3 | -20°C to -40°C | Cooling |
| 4 | -40°C to -20°C | Heating |
| 5 | -20°C to 0°C | Heating |
| 6 | 0°C to 20°C | Heating |
| 7 | 20°C to 45°C | Heating |
| 8 | 45°C to 20°C | Cooling |

Table 2: Temperature variation.

The rate of temperature variation from one point to another was 2°C per minute. So the chamber generally reached the steady state in about 12 to 14 minutes according to the digital readout while the sample took about 4 to 5 minutes more as per the thermistor reading. The readings were taken dynamically once the variation was started. Time for

which the Fractor was dynamically observed was 30 minutes. Out of the Fractors subjected to thermal variation, results of three different ones are displayed here.

The results are graphed according to thermal cooling and thermal heating response from the above table. The curves being shown are the final run reading curves at which the Fractor had reached the steady state final temperature.

## Steel Fractor Cooling

The response of a 40C steel Fractor upon cooling was noted.

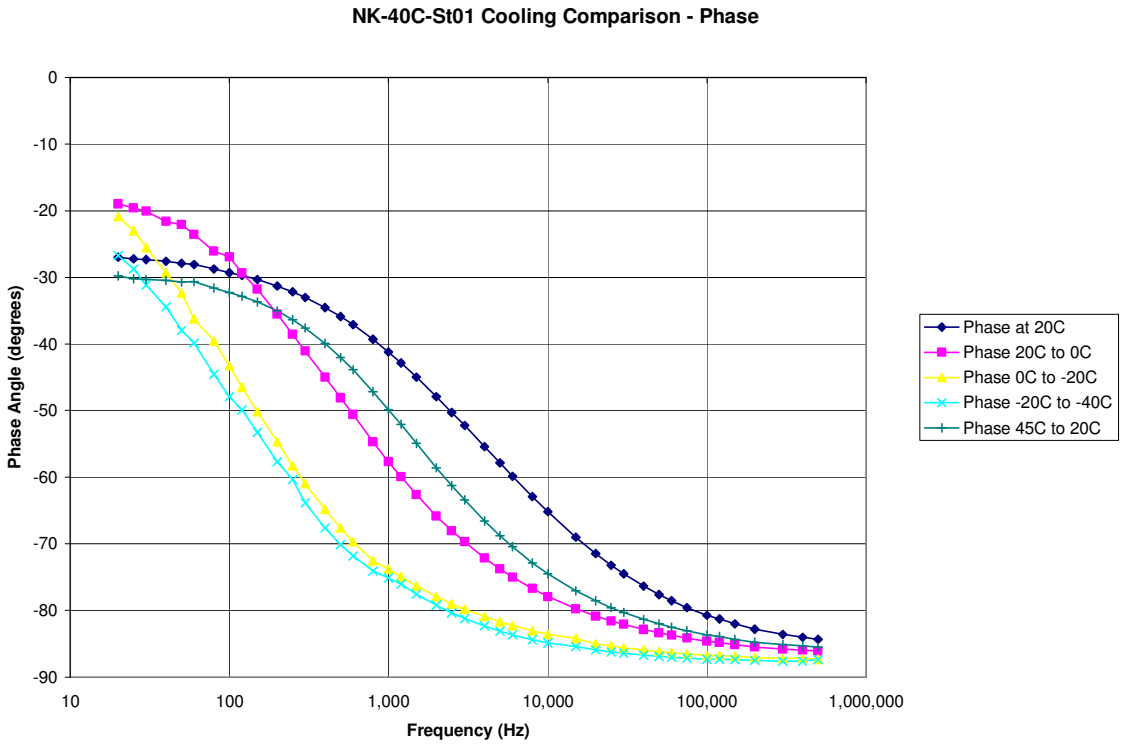



Figure 69. Steel Fractor cooling comparison – phase plot.

Figure 69 shows the variation in the phase angle of the NK-40C-St01 Fractor during cooling over a frequency range at various temperatures.

The initial phase is the one at 20°C. Upon cooling, a gradual drop in the phase can be seen especially in the 100 Hz to 10 kHz region. On cooling from 20°C to 0°C, the phase rises slightly till 100 Hz for some unknown reason and then drop down showing capacitive nature. As the temperature goes on falling, the phase starts dropping closer to 90° indicating that cooling is making the Fractor capacitive in nature.

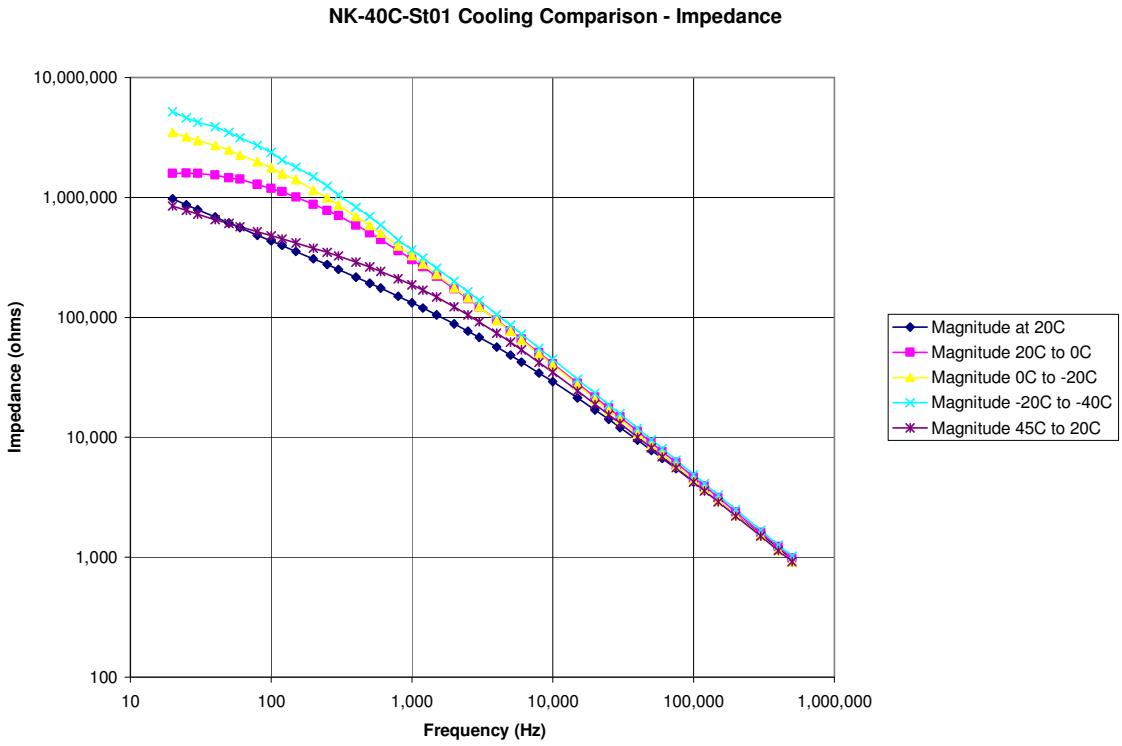



Figure 70. Steel Fractor cooling comparison – impedance plot.

Peculiarly, when the Fractor is cooled from 45°C to 20°C, it does not show

complete recovery, but a drop in phase which can be imputed to micro changes in the chemical structure due thermal variation stress.

Figure 70 shows the variation in the impedance of the NK-40C-St01 Fractor during cooling over a frequency range at various temperatures.

The magnitude at 20°C is the initial magnitude. As can be seen, there is a gradual rise in the impedance upon cooling especially in the ionic range of up to 10 kHz. The magnitude is the highest at -20°C to -40°C and the temperature during the final run is steady at -40°C. This indicates that cooling restricts the ionic movement thereby increasing the impedance. It can also be seen that on cooling from 45°C to 20°C, the impedance is nearly recovered.

Steel Fractor Heating

The response of a 40C steel Fractor upon heating is shown here.

Fgure 71 shows the variation in the phase angle of the NK-40C-St01 Fractor during heating over a frequency range at various temperatures.

On heating from -40°C to -20°C, the phase angle shows rise as compared to cooling phase from -20°C to -40°C (in the above cooling phase graph). As the temperature increases the phase starts getting closer to the initial. On heating from 0°C to 20°C, the phase more rises above the initial phase. This is possibly due to changes in the gel microstructure because of exposure to thermal variation. On heating to 45°C, the phase rises even higher showing slight resistive nature.

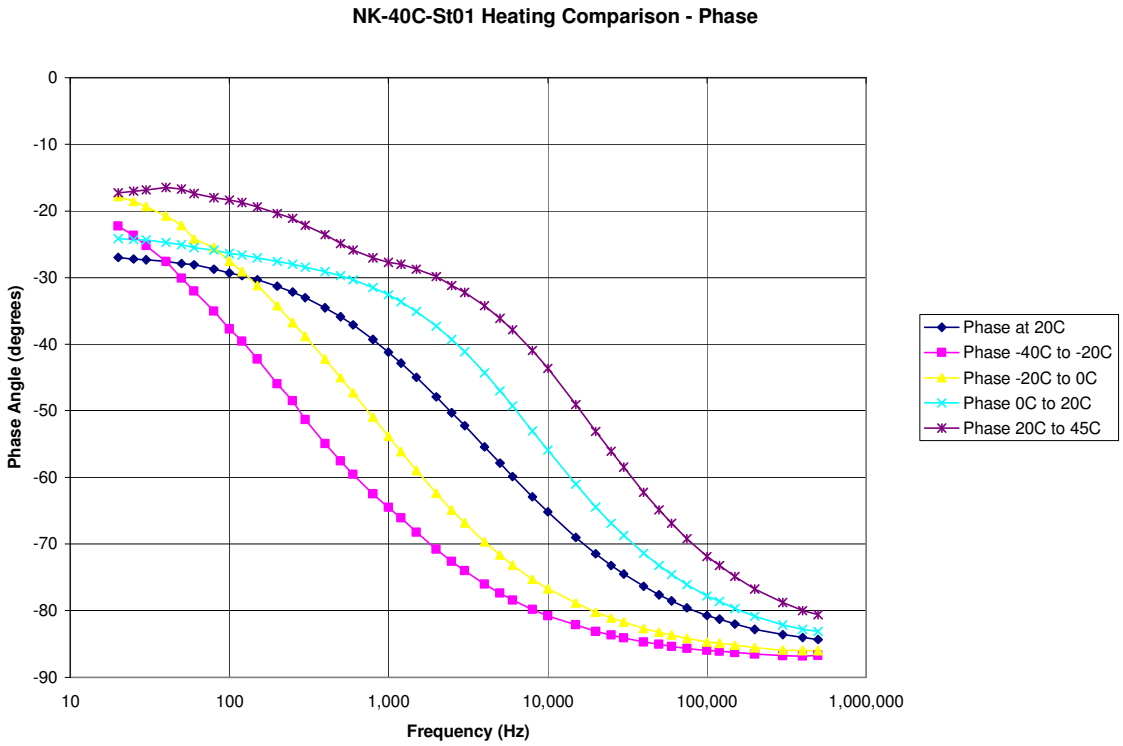



Figure 71. Steel Fractor heating comparison – phase plot.

Figure 72 shows the variation in the impedance of the NK-40C-St01 Fractor during heating over a frequency range at various temperatures.

It can be seen that the impedance drops upon heating leading to easy flow of the ions. The Fractor is heated from -40°C to 45°C in distinct step over the whole process, and a fall in the impedance is clearly noticed after each step. The recovery of the Fractor impedance when it is heated from 0°C to 20°C is very close to the initial at 20°C but not complete. This can be attributed to micro structural changes in the gel due to thermal variations

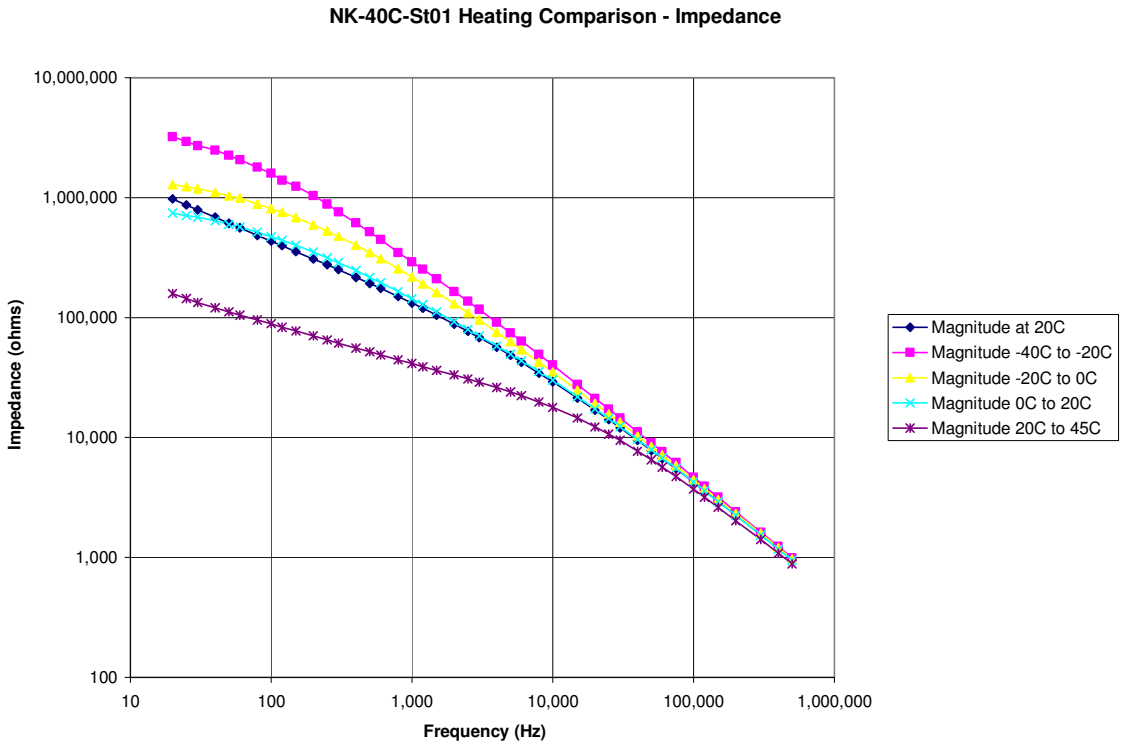



Figure 72. Steel Fractor heating comparison – impedance plot.

## Copper Fractor Cooling

The response of a 40C copper Fractor on cooling is displayed here.

Figure 73 shows the variation in the phase angle of the NK-40C-Cu02 Fractor during cooling over a frequency range at various temperatures.

The initial phase is the one at 20°C. Upon cooling, from 20°C to 0°C, there is a distinct drop in the phase over the whole frequency regime. On further cooling, the drop increases making the phase at -20°C to -40°C the most capacitive. This shows that the decrease in temperature results in decrease in phase angle.

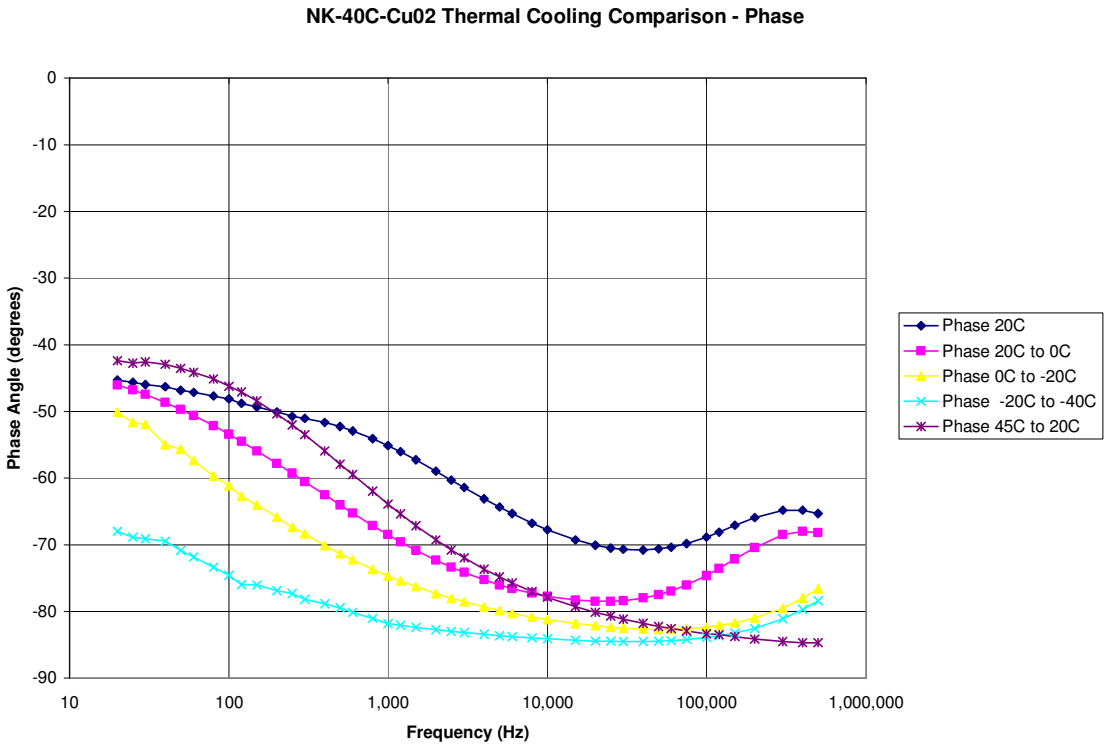



Figure 73. Copper Fractor cooling comparison – phase plot.

When the Fractor is cooled from 45°C to 20°C, it doesn't show complete recovery, but a crossover in phase at about 200 Hz, which might have resulted from the thermal stress on the metal gel interface.

Figure 74 shows the variation in the impedance of the NK-40C-Cu02 Fractor during cooling over a frequency range at various temperatures.

The magnitude at 20°C is the initial magnitude. As can be seen, there is a steady rise in the impedance upon cooling especially in the range of up to 1 kHz. The magnitude is the highest at -20°C to -40°C and the temperature during the final run is steady at -40°C.

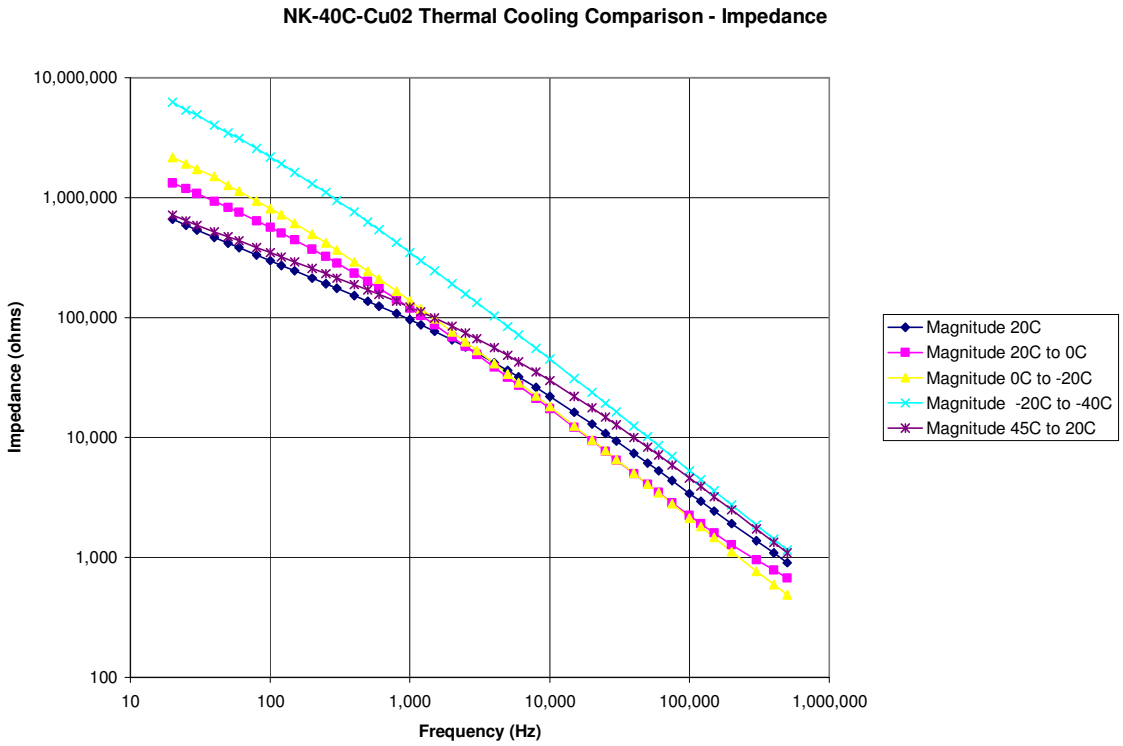



Figure 74. Copper Fractor cooling comparison – impedance plot.

There is some crossover in the impedances at 5000 Hz which might be alluding to the increase in the electronic activity. It can also be seen that on cooling from 45°C to 20°C, the impedance is nearly recovered.

## Copper Fractor Heating

The response of a 40C copper Fractor upon heating is displayed here.

Figure 75 shows the variation in the phase angle of the NK-40C-Cu02 Fractor during heating over a frequency range at various temperatures.

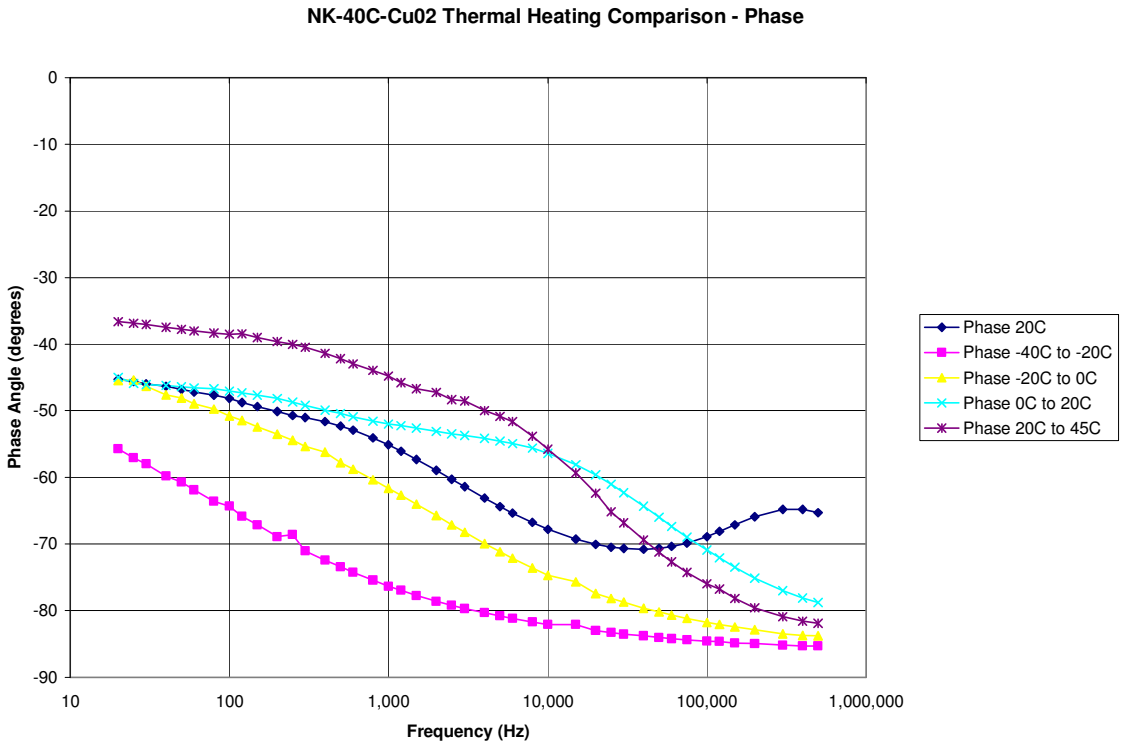



Figure 75. Copper Fractor heating comparison – phase plot.

On heating from -40°C to -20°C, the phase angle shows rise as compared to cooling phase from -20°C to -40°C (in the above cooling phase graph). As the temperature increases the phase starts getting closer to the initial. On heating from 0°C to 20°C, the phase rises above the initial phase. On heating to 45°C, the phase rises higher showing slight resistive nature. Thus heating results in overall phase uplift.

Figure 76 shows the variation in the impedance of the NK-40C-Cu02 Fractor during heating over a frequency range at various temperatures.

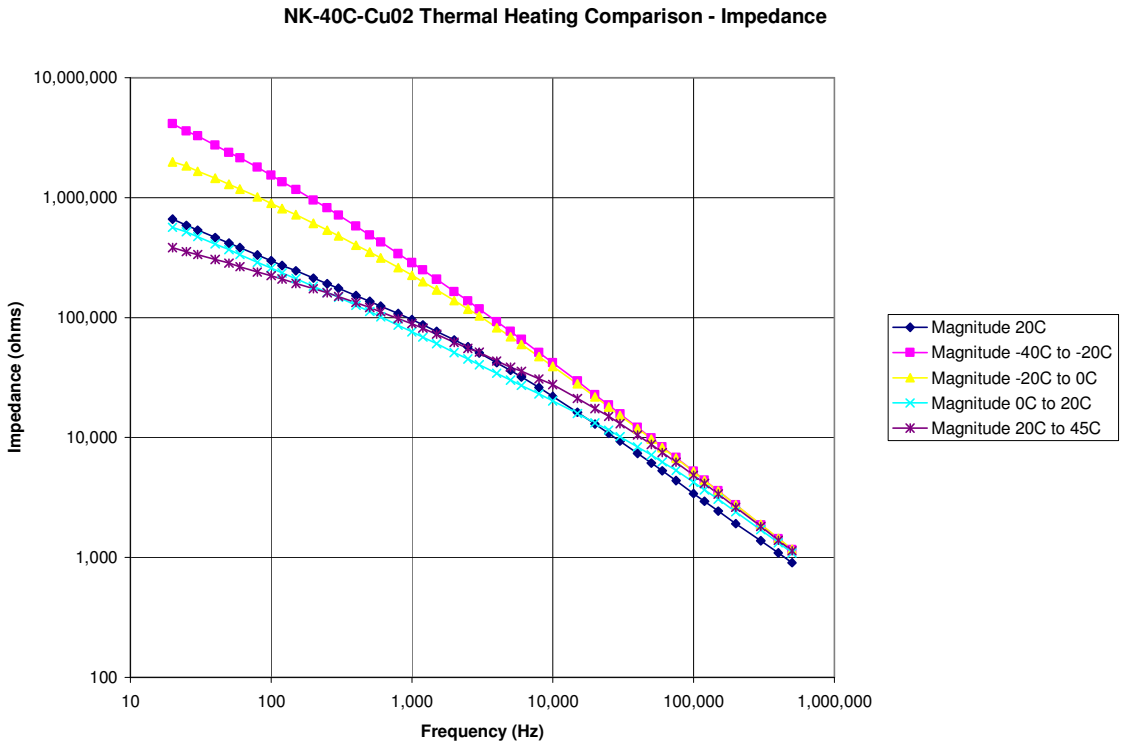



Figure 76. Copper Fractor heating comparison – impedance plot.

On the whole it can be seen that the impedance drops upon heating. There is a significant drop in the impedances between -20°C to 0°C and 0°C to 20°C. The recovery of the Fractor impedance when it's heated from 0°C to 20°C is very close to the initial. On being subjected to more heating, from 20°C to 45°C, the impedance drops to the lowest.

Thus the decrease in temperature makes the copper Fractor more capacitive in nature and increases its impedance while increase in temperature makes the copper Fractor more resistive and reduces its impedance.

## Aluminum Fractor Cooling

The resulting responses on cooling a 40C aluminum Fractor are exhibited below.

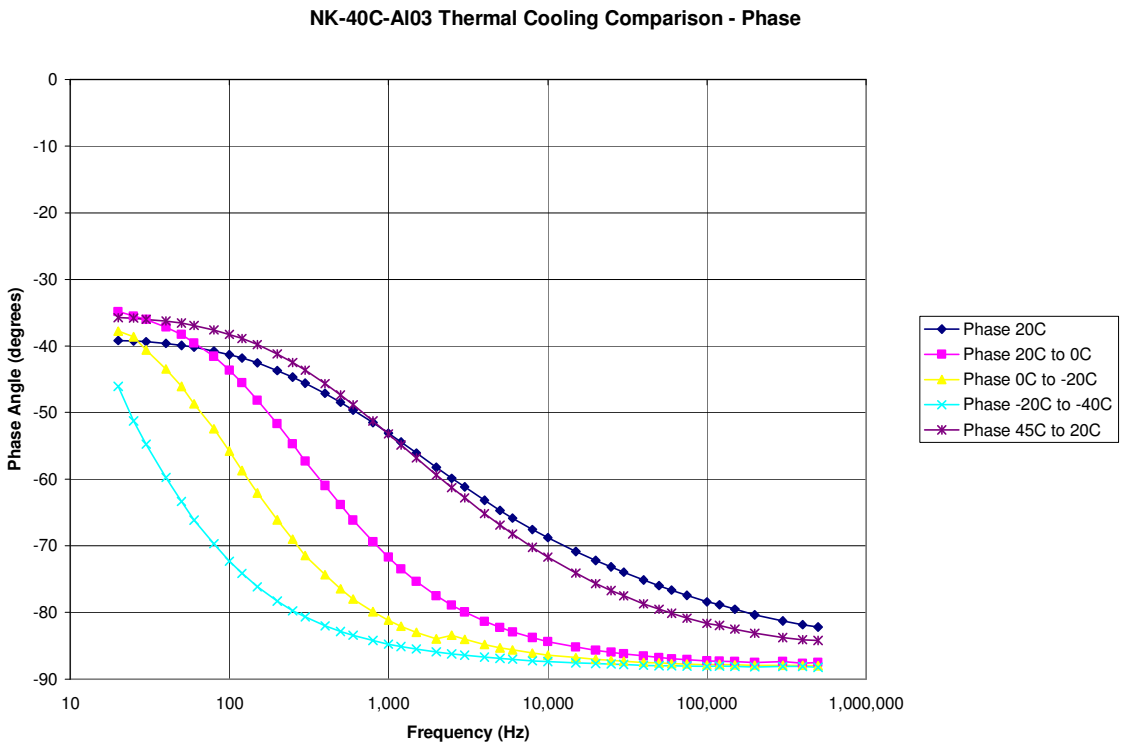



Figure 77. Aluminum Fractor cooling comparison – phase plot.

Figure 77 shows the variation in the phase angle of the NK-40C-Al03 Fractor during cooling over a frequency range at various temperatures.

The initial phase is the one at 20°C. Upon cooling from 20°C to 0°C, a sharp drop in the phase can be observed throughout the frequency range apart from 20Hz to 100 Hz where it drifts above the initial phase. From thereon, the phase drops steadily with

decrease in temperature. As the temperature goes on falling, the phase starts dropping closer to 90° making the Fractor capacitive in nature. The cooling recovery from 45°C to 20°C seems to be reasonably good.

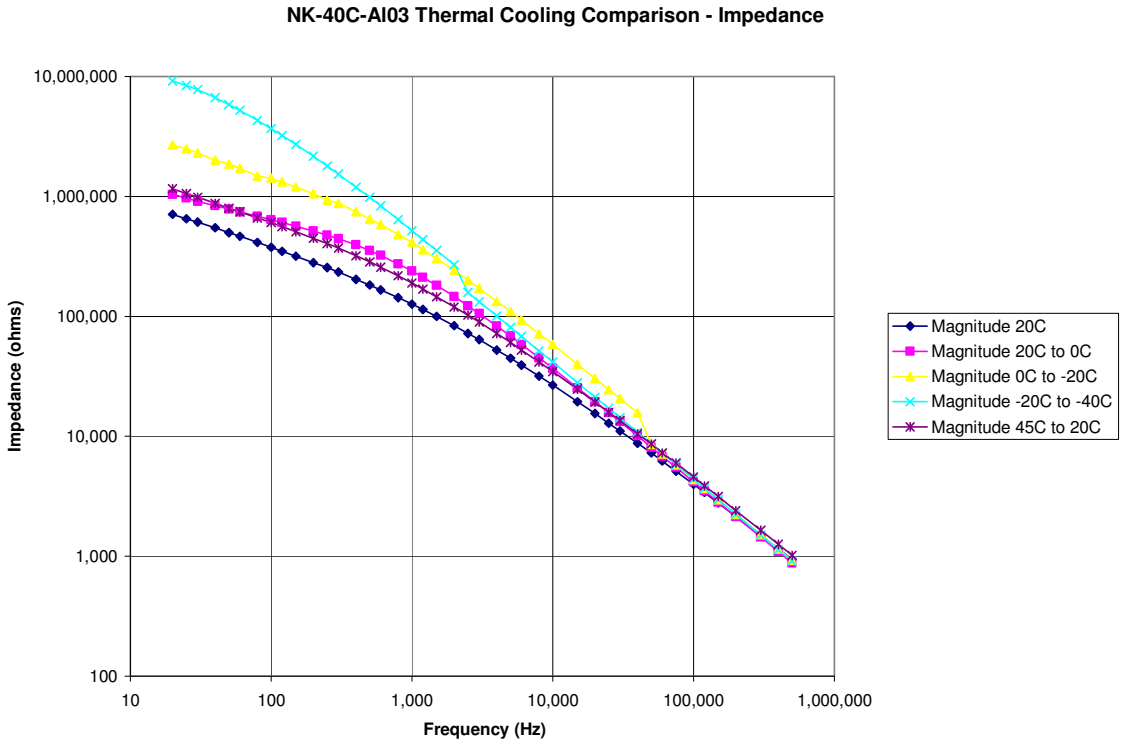



Figure 78. Aluminum Fractor cooling comparison – impedance plot.

Figure 78 shows the variation in the impedance of the NK-40C-Al03 Fractor during cooling over a frequency range at various temperatures.

The magnitude at 20°C is the initial magnitude. As can be noticed, the magnitude is the highest at -20°C to -40°C when the temperature at steady state is -40°C. This rise is significant above the impedance from 0°C to -20°C. The recovery from 45°C to 20°C is not very good and nearly matches the impedance from 20°C to 0°C.

But on the whole it can be concluded that the impedance rises on reducing the temperature.

## Aluminum Fractor Heating

Response of a 40C aluminum Fractor upon heating is shown here.

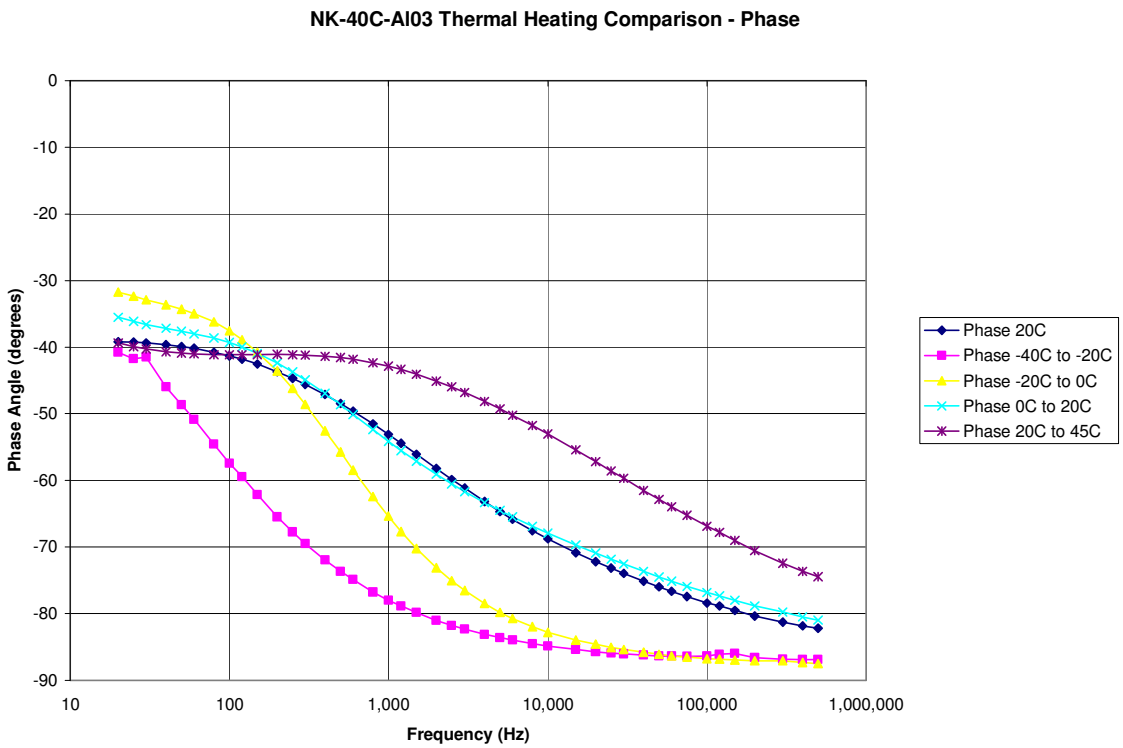



Figure 79. Aluminum Fractor heating comparison – phase plot.

Figure 79 shows the variation in the phase angle of the NK-40C-Al03 Fractor during heating over a frequency range at various temperatures.

On heating from -40°C to -20°C, the phase angle shows rise as compared to cooling phase from -20°C to -40°C (in the above cooling phase graph).On further heating

from -20°C to 0°C the phase displays sudden lift up and even goes above the initial phase over the 20 Hz to 200 Hz range. Upon further heating from 0°C to 20°C though, the phase drops down in the 20 Hz to 200 Hz range and rises up in the rest of range to closely follow the initial phase. This can be attributed to the micro structural changes in the gel interface due to thermal stress. On heating to 45°C, the phase rises even more in the higher frequency range, showing slight resistive nature. Thus heating results in overall uplift of the phase angle.

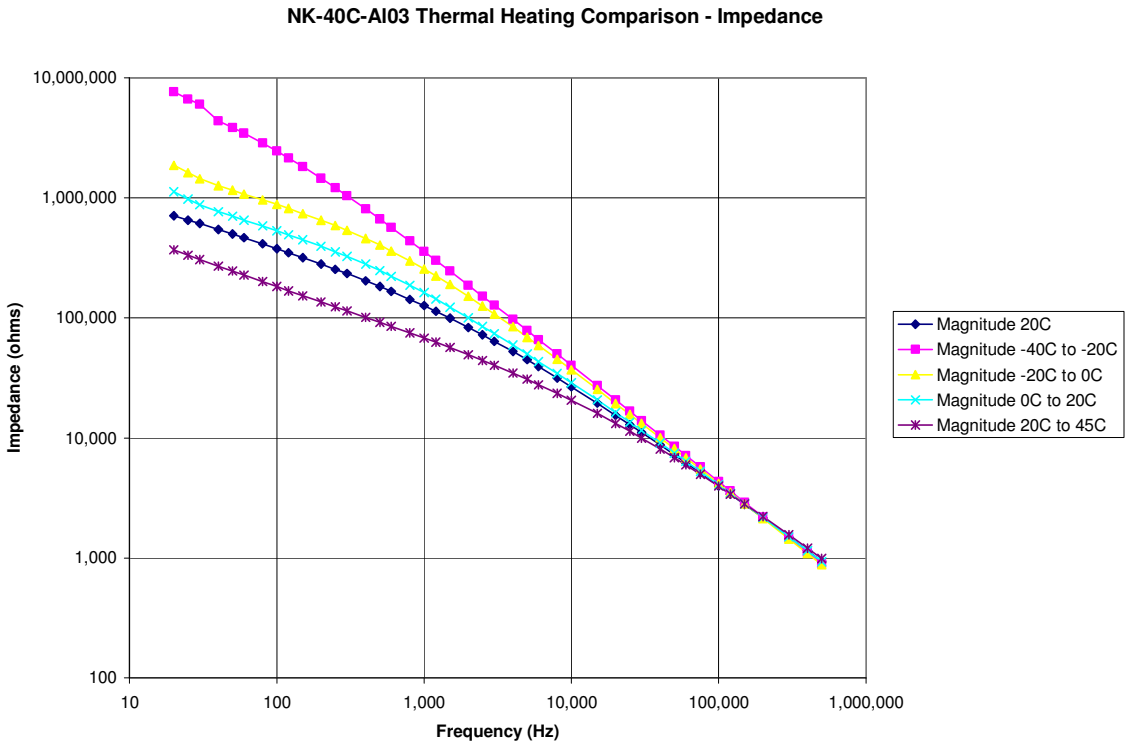



Figure 80. Aluminum Fractor heating comparison – impedance plot.

Figure 80 shows the variation in the impedance of the NK-40C-Al03 Fractor during heating over a frequency range at various temperatures.

On the whole it can be seen that the impedance drops upon heating. There is a significant drop in the impedances between -40°C to -20°C and -20°C to 0°C. The recovery of the Fractor impedance when it's heated from 0°C to 20°C is reasonably close to the initial. On being subjected to more heating, from 20°C to 45°C, the impedance drops to the lowest.

## Conclusion

On the whole we can conclude that despite using different metals the temperature variation has similar effect on all Fractors.

1) The impedance rises on lowering the temperature.
2) The phase angle lowers on lowering the temperature.
3) The impedance lowers on increasing the temperature.
4) The phase angle lifts up on increasing the temperature.

It can also be seen in most of the cases that on heating or cooling back to the room temperature, the phase and impedance come close to the initial.

There is some variation unexpected in the impedance and phase like drifting above or below the initial response during recovery but this can be due to changes in the gel microstructure due to the thermal variation stress.

# HUMIDITY RESPONSE ANALYSIS

Fractors were subjected to variation in the humidity and the effect on their response was noted.

## Concept

An aqueous environment facilitates ease of ionic flow. By increase in the humidity, the ionic charge carriers face lesser opposition to the flow while decrease in the humidity (dehumidification) increases resistance to the ion flow. Hence we expect higher impedance on dehumidification and lower impedance on humidification at any specific frequency for a given Fractor.

## Experimental Setup

Humidification:

The Fractor was placed in a plastic petri dish which in turn was placed in a container. The container contained sufficient water to immerse half of the petri dish in it. An opening was provided in the container to insert the connections, which went to the impedance analyzer, and a probe, for measuring the change in the humidity, which was linked to a humidity analyzer with digital display.

Dehumidification:

The Fractor was placed in a dehumidification chamber containing potassium sulphate. These chemicals have the nature of absorbing the humidity from the ambient atmosphere.

Connections from the impedance analyzer and probe for humidity measurement were introduced in the chamber. Figure 81 shows the humidity analysis setup. The humidity analyzer was home designed.

The circuit board was manufactured by Cygnal Integrated Products, Inc and the assembly was done at Wavelength Electronics by Dr.Gary Bohannan.

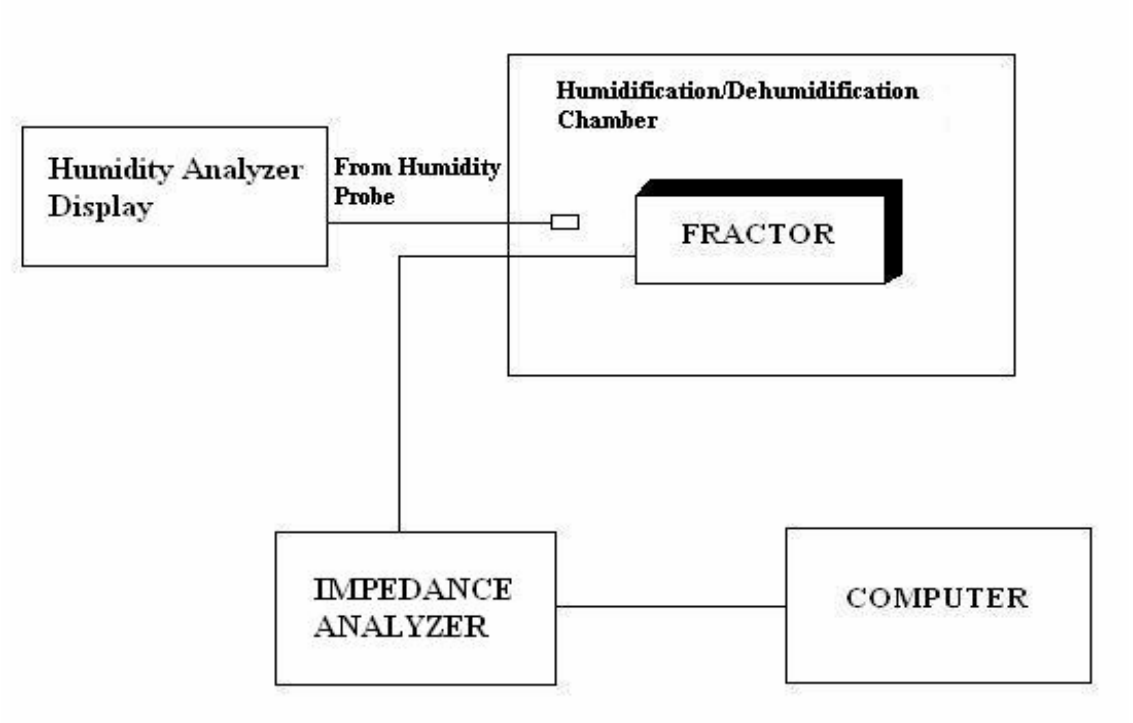



Figure 81. Humidity analysis setup.

## Process

The humidity response was measured in the following steps.

1) Normal run at ambient humidity – 30 minutes
2) Humidification dynamic run – 1 day (3% final humidity)
3) Normal run (humidification normalizing) at ambient humidity – 1 day
4) Dehumidification dynamic run – 1 day (89% final humidity)
5) Normal run (dehumidification normalizing) at ambient humidity – 1 day

The response was continuously monitored during the experiments. The final few runs were plotted to clearly exhibit the resulting response.

## 40C Steel Fractor - Humidity Variation

The humidification and dehumidification test was performed on a 40C steel Fractor and its response was noted.

Figure 82 shows the phase angle on variation of humidity over a frequency range for a 40C steel Fractor.

On humidification, the humidity inside the container reaches to about 89%, this results in the phase angle during humidification dropping below the initial in the ionic range of 10,000 Hz and lifting above the initial in the electronic range of 10000 Hz to 500 kHz.

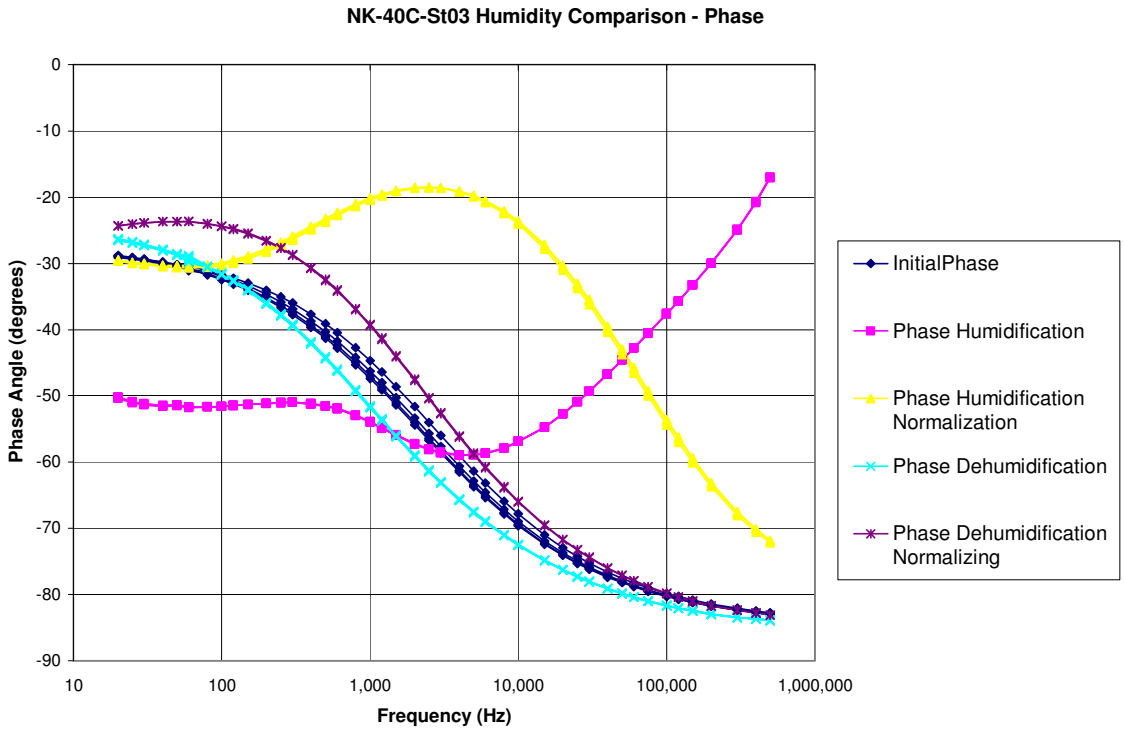



Figure 82. Steel Fractor (40C) humidity variation comparison – phase plot.

On normalizing in ambient humidity, the phase lifts up significantly above the initial phase. On dehumidification, the phase drops near the original. On normalizing in ambient humidity after dehumidification, the phase shows relative recovery and approaches close to the initial phase.

Figure 83 shows the impedance on variation of humidity over a frequency range for a 40C steel Fractor.

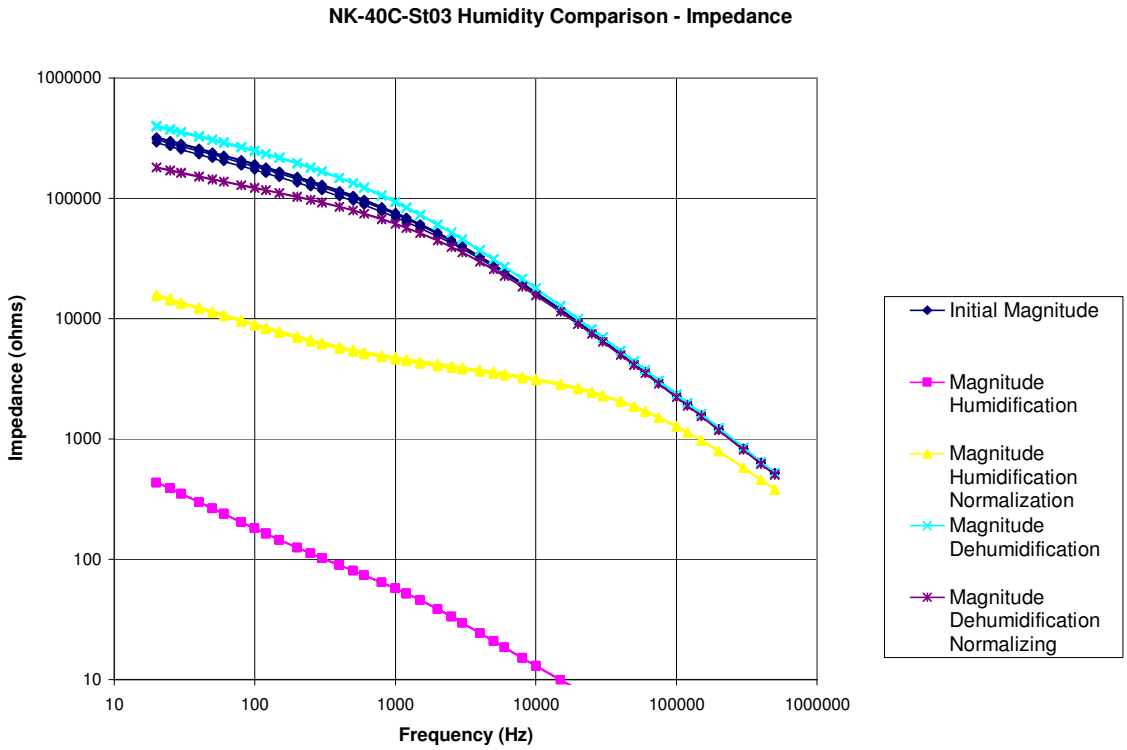



Figure 83. Steel Fractor (40C) humidity variation comparison – impedance plot.

On humidification, the impedance drops drastically below the initial indicating ease in ionic flow. On normalizing in ambient humidity after humidification, the impedance starts to creep back to the initial. On dehumidification, the impedance rises above the initial indicating opposition to the ionic flow. On normalizing after dehumidification, the impedance drops slightly below the initial, indicating some amount of recovery. This recovery matched the initial impedance response of the Fractor very closely but showed variations in the phase.

## 80C Steel Fractor – Humidity Variation

The humidification and dehumidification test was performed on a 40C steel Fractor and its response was noted.

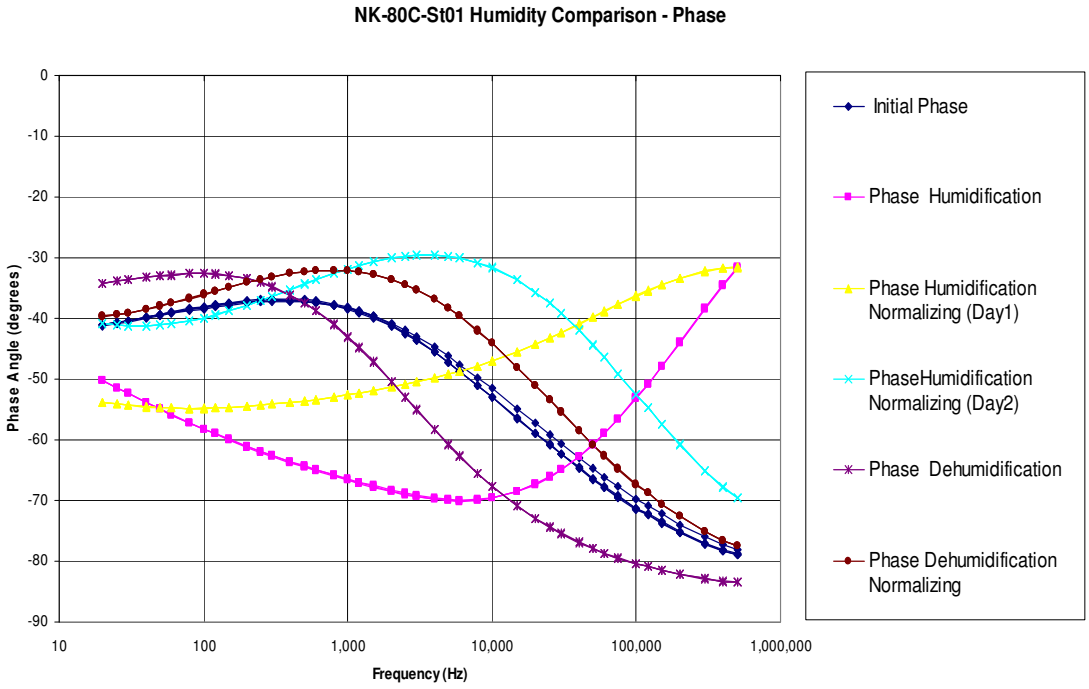



Figure 84. Steel Fractor (80C) humidity variation comparison – phase plot.

Figure 84 shows the phase angle on variation of humidity over a frequency range for a 80C steel Fractor. The variation is much similar to the 40C steel Fractor shown above.

On humidification, the phase drops below the initial in the ionic range and jumps above the initial in the electronic higher frequency range. On normalizing in ambient humidity after humidification, the phase jumps up above the initial one. On

dehumidification, there is a sudden drop in the phase whereas after normalization there is a fair amount of recovery towards initial.

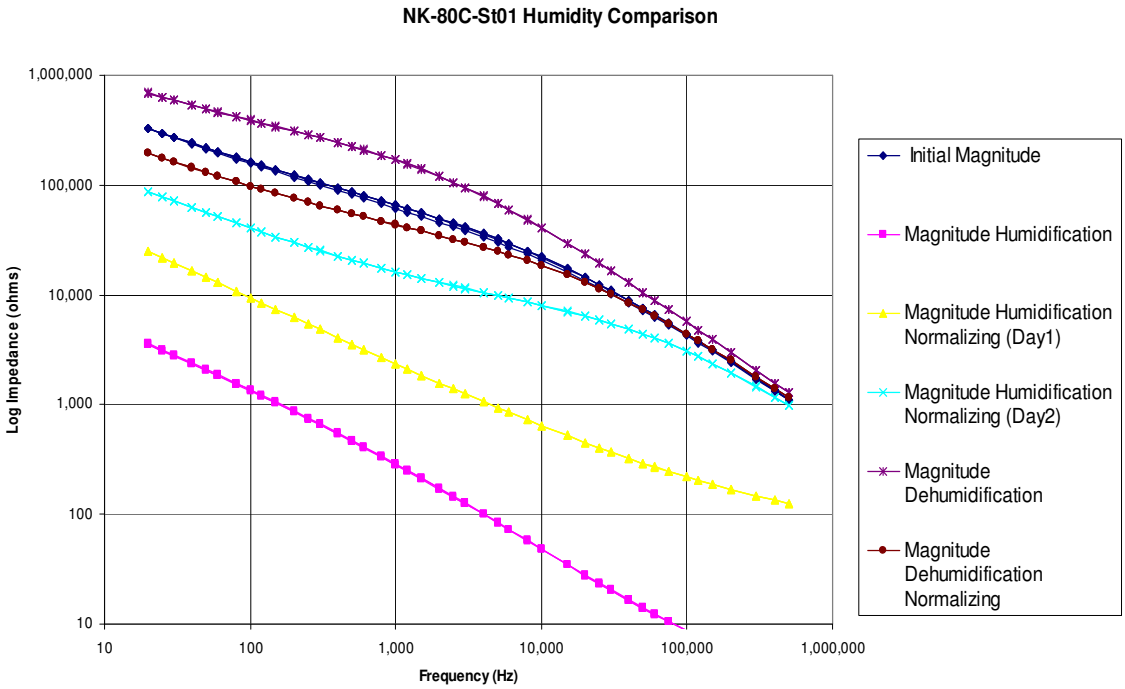



Figure 85. Steel Fractor (80C) humidity variation comparison – impedance plot.

Figure 85 shows the impedance on variation of humidity over a frequency range for a 80C steel Fractor.

It can be observed on humidification, the impedance drops significantly below the initial indicating ease in ionic flow. On normalizing in ambient humidity after humidification, the impedance starts to creep back to the initial. On dehumidification, the impedance rises above the initial indicating opposition to the ionic flow. On normalizing

after dehumidification, the impedance drops slightly below the initial, indicating that there is partial recovery.

## Conclusion

From the above results we can conclude that phase of the Fractor keeps changing due to variation in humidity. There is a drop in the phase in the ionic range on humidification with respect to the initial phase. Dehumidification shows slight variation in phase with respect to the initial.

The variation in the impedance on the other hand clearly suggest, on increase in humidity the impedance decreases as aqueous environment aid in facilitating the ionic flow. On decreasing the humidity, the impedance increases indicating that non aqueous environment deters the flow of ions.

Thus it is concluded that the Fractor response varies with change in the humidity.

# FINAL CONCLUSION

Manufacturing parameters:

It can be observed from the impedance analysis of the manufactured Fractors that the variations in the metal electrodes or the blasting pressures make no difference to the Fractor response. But the fine grit (80 micron) SiC fails to make sufficiently deep indentations in the metal surface during grit blasting and results in conductive breakthrough on encapsulation.

Stress Variation:

It can be observed from the stress response analysis that the Fractor phase and hence the CPE is insensitive to stress but the impedance decreases on increasing the stress. This must be happening due to the ease in the ionic flow on loading.

Vibration:

Short term vibrations do not affect the Fractor response. Long term vibration results in slight change in the response possibly due to loosening of screws on the Fractor device. The phase is not significantly changed and the CPE does not vary much.

Thermal Variations:

Thermal variations cause change in the impedance as well as the phase of the Fractor. On cooling, the impedance increases while the phase becomes capacitive. On

heating, the impedance decreases and the phase becomes resistive. The CPE is largely affected.

Humidity Variations:

Variations in the humidity affect the impedance as well as the phase of the Fractor. Humidification lowers the phase in the ionic region and overall impedance. Dehumidification increases the overall impedance and the phase in the ionic region. The CPE is significantly affected.

CPE:

It was noticed that the CPE does not depend only on the fractal geometry or the roughness of the electrode surface but also on the gel chemistry which changes during the thermal and humidity variations.

For the Fractor to operate with consistent response, an encapsulation must be developed that will keep the Fractor under steady unvarying stress allowing no relaxation. This will take care of the vibration and relaxation aging variations. The encapsulation should also ensure that if any pressure is applied to it, then it should not fall on the Fractor but should be diverted to some other part of the enclosure. This will account for stress loading variations. The material used for the encapsulation should be highly insulating and insensitive to heat variations. This will ensure that the Fractor inside will not be subjected to thermal variations.

# RECOMMENDATIONS FOR FUTURE WORK

The electrochemical behaviour of the Fractor is still a mystery. Identification of the following will help in understanding the Fractor mechanisms well.

1) Investigation of the relative contribution of the electrons and ions in the initial 10 kHz of the frequency spectrum by varying the ionic chemicals in the gel. The changes in the ionic gel will provide ions with different mobility and thus noticeable variations can be observed.

2) Cyclic loading – unloading of the Fractor should be performed to evaluate its effect on the Fractor response. This will confirm if the Fractor is fatigue sensitive.

3) Actual working of the relation of the fractal dimension and gel chemistry with the CPE can be found out by conducting experiments with electrodes of different roughness and different ionic gels under varying conditions. Surface profile of the electrode should also be measured during every experiment to provide the fractal dimensionality.

## REFERENCES CITED

[1] Banerjee S, Chakravorty D, J. Appl. Phys., Vol 36 (1997) ,7329 – 7333

[2] Wang et al, J. Appl. Phys. A 63 (1996), 481 – 486

[3] Bohannan GW, Analog Fraction Order Controller in Temperature Control Application. (Yet to be submitted)

[4] Madou MJ, Cardan F, Gomes WP, J. Electrochem. Soc. Vol. 131(1984), 1623

[5] Oskam G et al, J. Electroanal. Chem. Vol. 315(1991), 65.

[6] Bockris JO, Reddy KN, Modern Electrochemistry, Plenum, New York (1977), Ch 7, pages therein.

[7] Mandelbrot BB, The Fractal Geometry of Nature, Freeman, New York (1983), pages therein.

[8] Hurst SK, Preparation of Improved Indian Sandwich Materials.

[9] Liu SH, Phys.Rev. Lett. Vol.55, 529 (1988)

[10] Sapoval B, Phys.Rev. Lett. Vol.73, 33314 (1994)